Formation of stimuli responsive supramolecular materials using molecular recognition and its functionalization

A Doctoral Thesis

by

Kazuhisa Iwaso

Submitted to

The Graduate School of Science, Osaka University

February, 2016

Acknowledgements

This work was carried out from 2013 to 2015 under the supervision of Professor Dr. Akira Harada and Professor Dr. Hiroyasu Yamaguchi at the Department of Macromolecular Science, Graduate School of Science, Osaka University. The author would like to express his sincere gratitude to Professor Dr. Akira Harada for his guidance and assistance throughout this study. Grateful acknowledgements are made to Dr. Akihito Hashidzume, Professor Dr. Sadahito Aoshima, and Professor Dr. Tadashi Inoue for their continuing help. The author is also grateful to Assistant Professor Dr. Yoshinori Takashima, Assistant Professor Dr. Takuya Katashima, Dr. Yuichiro Kobayashi, Dr. Takashi Nakamura, Dr. Takahiro Kakuta, Dr. Masaki Nakahata, Dr. Tomoko Sekine, Mr. Kohei Koyanagi, Mr. Shogo Hatanaka, Mr. Suguru Nomimura, Mr. Issac Eng Ting Lee, Mr. Yuki Sawa, Mr. Yuki Hayashi, Mrs. Miyuki Otsubo, for their helpful suggestion and all the members of Harada laboratory for their cooperation and friendship. Grateful acknowledgements are also made to Mr. Seiji Adachi, Dr. Naoya Inadumi, and Dr. Yasuto Todokoro for NMR measurement, and Dr. Akihiro Ito for SEM experiments. The author appreciates the financial support from JST-CREST (Japan Science Technology, Core Research of Excellence Science Technology) (May, 2010-present).

Finally, the author would also like to express his heartfelt thanks to his parents, for their help and encouragements.

February, 2016

Kazuhisa Iwaso

Contents

Chapter 1

General Introduction.

Supramolecular chemistry based on molecular recognition

Various kinds of body tissue, such as epidermis, gene, and muscle are highly organized by biological molecules. Organizational structures are derived from non-covalently molecular recognitions such as hydrogen bond, coordination bond and hydrophobic interaction. The mechanism of molecular recognitions should be cleared to understand for not only for materials science but also for biochemistry. Science of molecular recognitions led to Supramolecualr chemistry in material science. Supramolecular chemistry was defined by Lehn as "a chemistry beyond molecules". After that, Cram,[1–3] Lehn,[4–10] and Pedersen,[11, 12] who won the Nobel Prize for their works in the division of chemistry in 1987. The field of supramolecular chemistry started from the concept of "receptor" and "lock and key".[13] In supramolecular chemistry, study the interactions between cyclic host molecule and guest molecule was called "host–guest chemistry". Crown ethers and cryptands selectively include alkali metal cations (Figure 1-1). Calixarenes[14–17] and cavidands[18–22] form inclusion complexes with aliphatic guest molecules such as adamantane and fullerene C_{60}. The formation of inclusion complexes based on the molecular recognition. Recently, supramolecular chemistry has become a tool to introduce function into polymers and biomaterials.

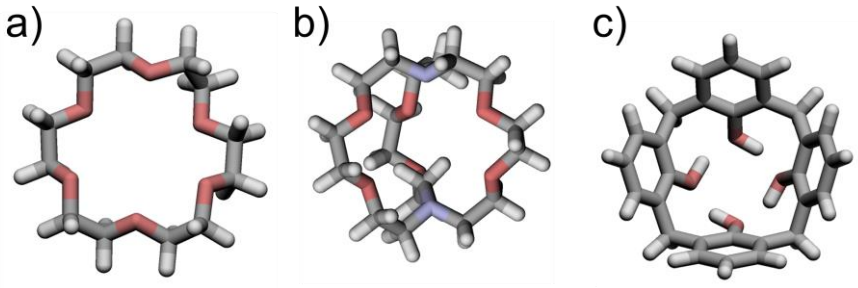

Figure 1-1. Structures of **a)** crown ether, **b)** cryptand and **c)** calixarene.

Cyclodextrines

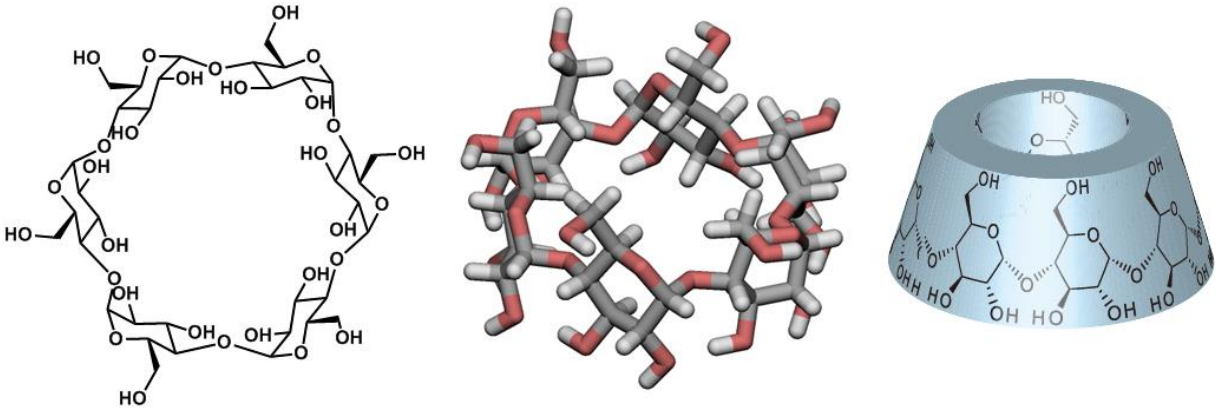

	αCD	βCD	γCD
No. of Glucose Units	6	7	8
Diameter of Cavity (nm)	0.47	0.60	0.75
Height of Torus (nm)	0.79	0.79	0.79

Figure 1-2. Properties and chemical structures of cyclodextrins.

Cyclodextrins (CDs, Figure 1-2)[23–28] are cyclic oligosaccharides comprising d-glucose units, linked by a 1,4-glycosidic bond. The three most important members of CD family are αCD, βCD, and γCD, which possess, respectively, six, seven, and eight glucose units, respectively. CDs take torus cone shape due to the hydrogen bonds among hydroxyl groups. Therefore, CDs have two different faces, one is the hydrophilic outer surface of the cavity and the other is the hydrophobic cavity. In aqueous media, CDs selectively form inclusion complexes with hydrophobic guest compounds that match the hydrophobic cavity sizes. Cramer[29–30] and Bender[31, 32] reported that CDs form inclusion complexes with various kinds of molecules with different molecular weights in water. Later, Breslow[33–36] utilized CDs as artificial hydrolysis enzymes for activated esters.

Supramolecular polymers

Many supramolecular polymers have been prepared using noncovalent interactions such as hydrogen bonding,[37–39] metal-coordination,[40] π–π interaction[41–43] electrostatic interactions,[44] and hydrophobic interaction[45, 46] (Figure 1-3a–c). Harada *et al.* reported linear,[47–49] helical polymer[50] and interlocked poly-[2]rotaxane[51] based on aliphatic moiety modified CDs (Figure 1-3d, e). Recently, supramolecular polymerization with living mechanism has been reported.[52]

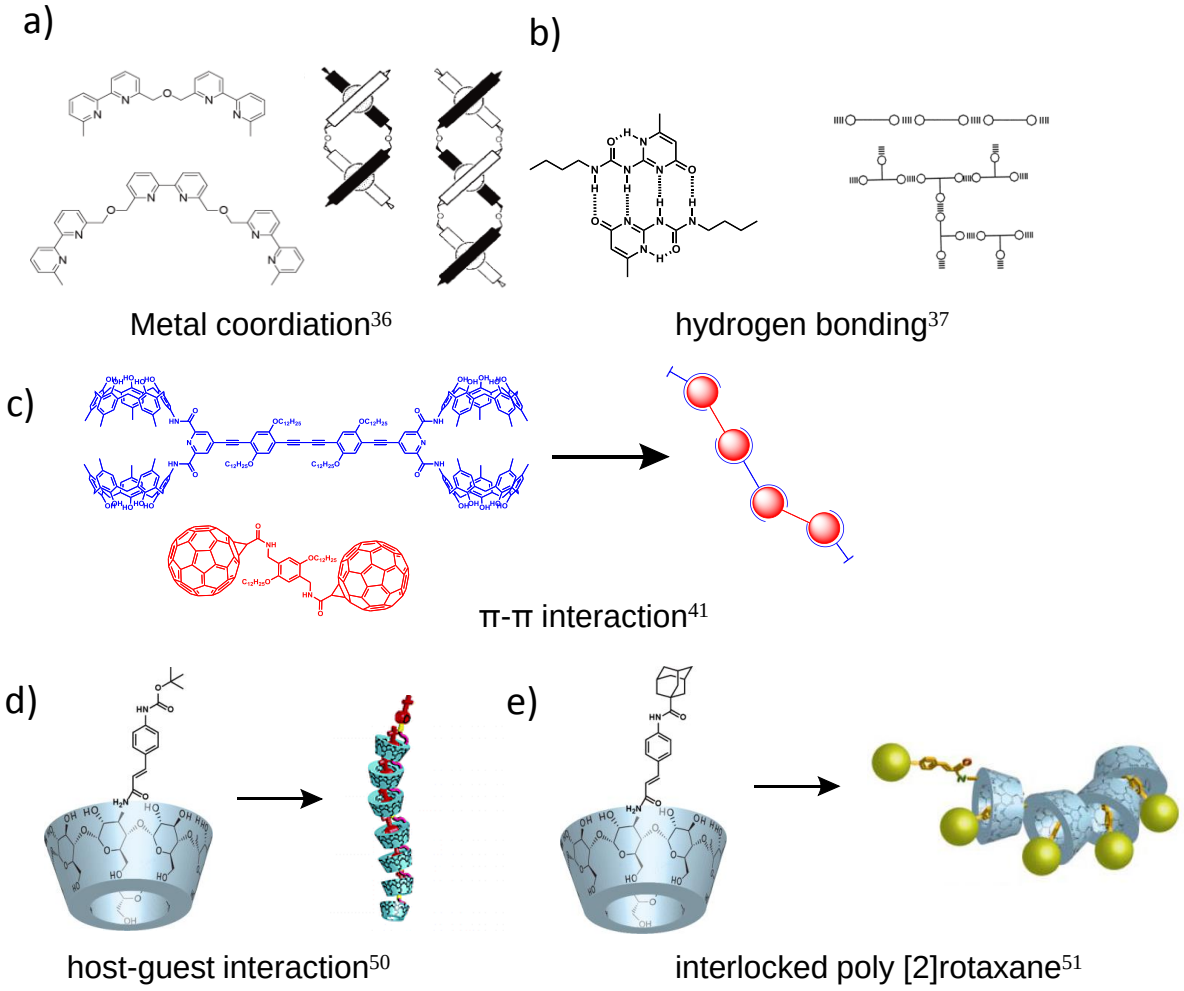

Figure 1-3. Molecular structure and formation of supramolecular polymers generated by **a)** metal coordination, **b)** hydrogen bonding, **c)** π–π interaction, **d)** host–guest interaction and **e)** mechanically inter locked supramolecular polymer.

Molecular topology; Rotaxanes, catenanes and knots

Rotaxanes (Figure 1-4a) and catenanes (Figure 1-4b) are mechanically interlocked molecular architecture consisting of two or more interlocked ring and axis components. The interlocked components cannot be dissociated without breaking covalent bonds of molecules. Names of structure were derived from Latin words: *rota* = ring, *axis* = axle, and *catena* = chain. Molecular knots are globular shape interlocked architecture consisting of only one linear molecule (Figure 1-4c).

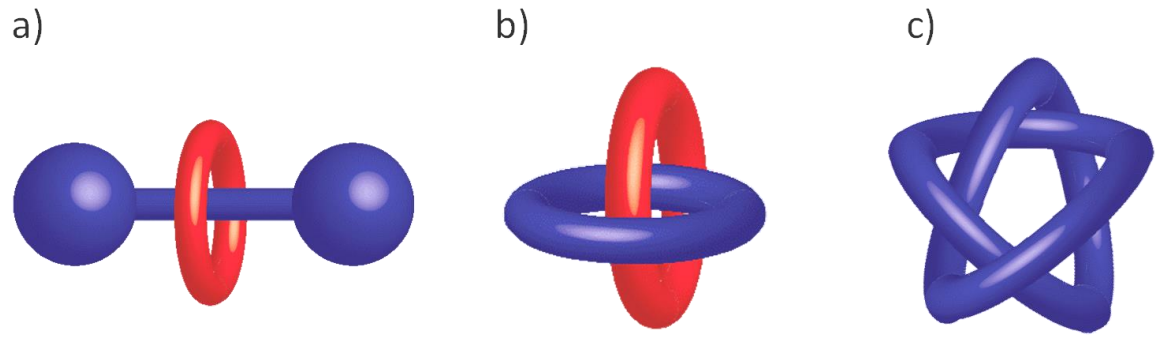

Figure 1-4. Structure images of **a)** rotaxane, **b)** catenane and **c)** knot.

First synthesis of rotaxane was reported by Harrison[53] in 1967. They premeditate to obtain the axle introduced macrocycle. After that, preparation methods of rotaxanes in high yield were reported by using hydrogen bonding,[54–56] π–π interaction,[57–59] coordination bonding[60, 61] and hydrophobic interaction. Ogino[62] prepared a rotaxane containing CD and alkyl chain which was stabilized by bulky metal crathlate stoppers (Figure 1-5a). Kaifer[63] reported the rotaxane stabilized by ammonium cation stopper (Figure 1-5b). Harada[64] used 2,4,6-trinitrobenzenesulfonic acid as a stopper (Figure 1-5c).

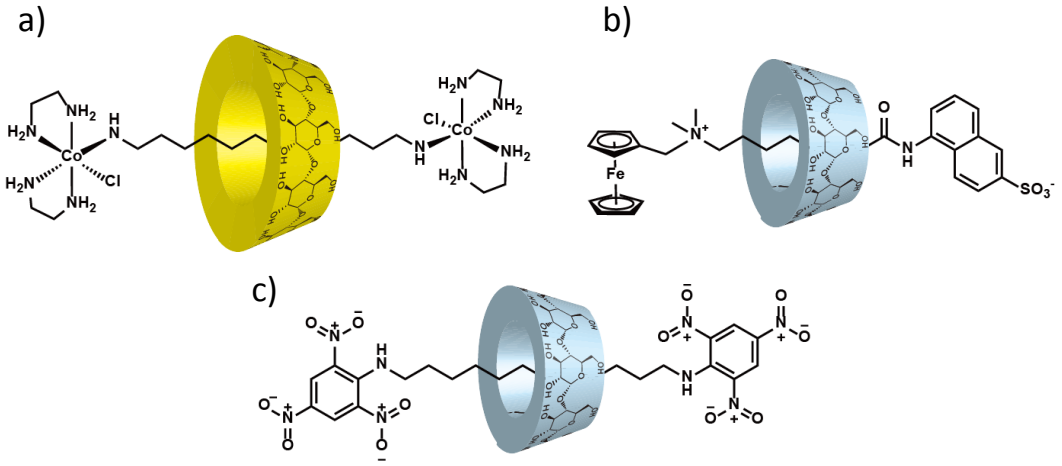

Figure 1-5. Structures of **a)** Ogino,[62] **b)** Kaifer[63] and **c)** Harada[64]'s rotaxane containing CDs.

In 1992, Harada and Kamachi[65–68] first reported polyrotaxane with polyethylene glycol threaded by many αCD units. Moreover, they obtained a tubular polymer called molecular tube derived from polyrotaxane by cross-linking hydroxyl groups of CDs using epichlorohydrin (Figure 1-6).

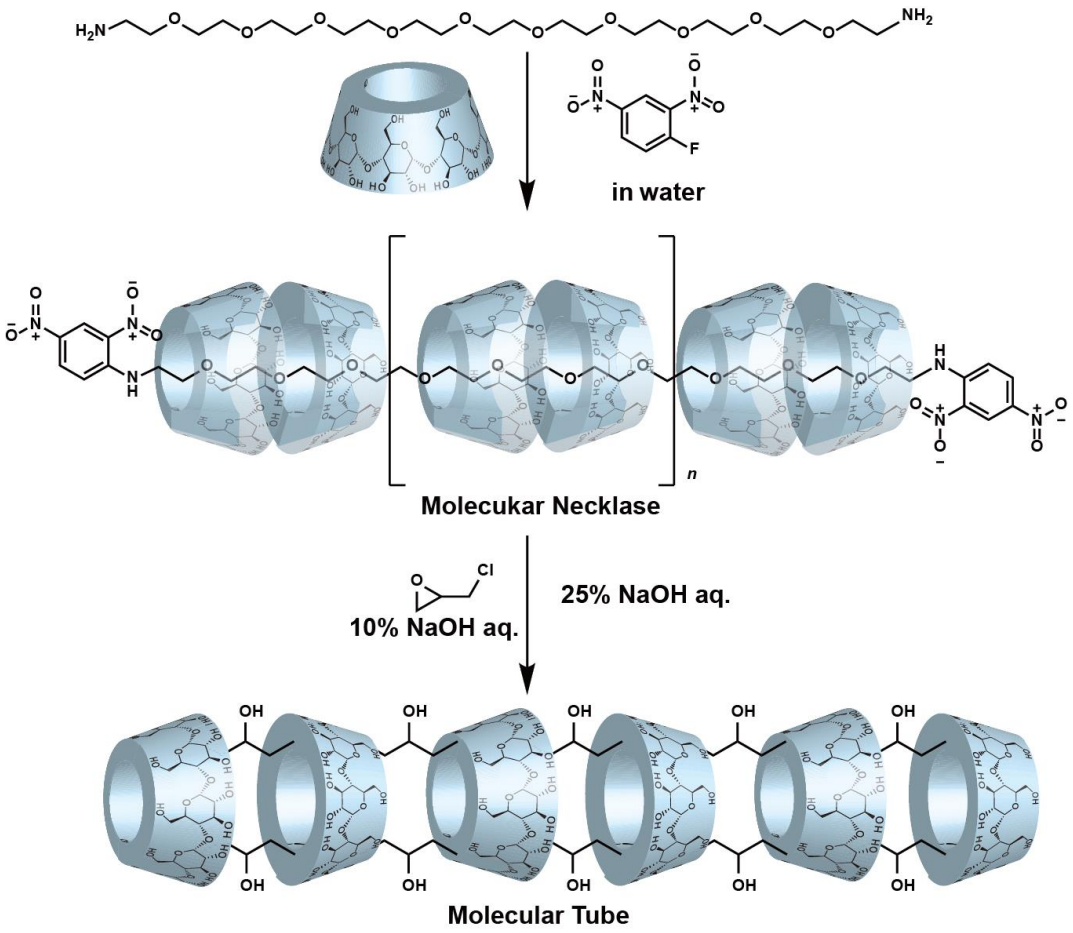

Figure 1-6. Synthetic route of polyrotaxane[66, 67] and molecular tube.

Catenanes were first synthesized by Wasserman[69] in 1960. To increase the isolated yield of catenans, Sauvage used coordination complexes as a template[70] (Figure 1-7a). Stoddart reported using donner–acceptor interaction between bipyridinium cation and dioxynaphthalene for temporary joint of two rings before final closing reaction[71] (Figure 1-7b). Borromean links[72] was a kind of catenanes which rings were interlocked each other.

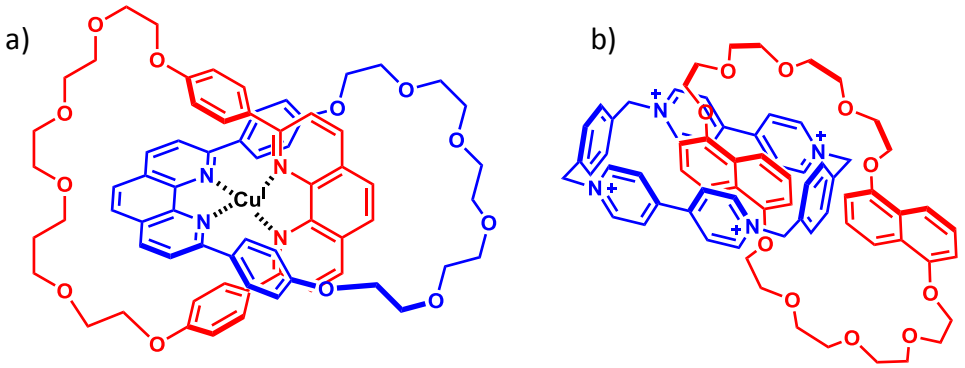

Figure 1-7. Structures of catenane which was reported by **a)** Sauvage[70] and **b)** Stoddart.[71]

Molecular knots with coordination complex consisting of cupper (I) and phenanthroline as a template were synthesized by Sauvage in 1999.[73] The trefoil knot has chirality (Figure 1-8a). Later, Leigh[74] used two types of metal complex as template to prepare the molecular knot (Figure 1-8b)

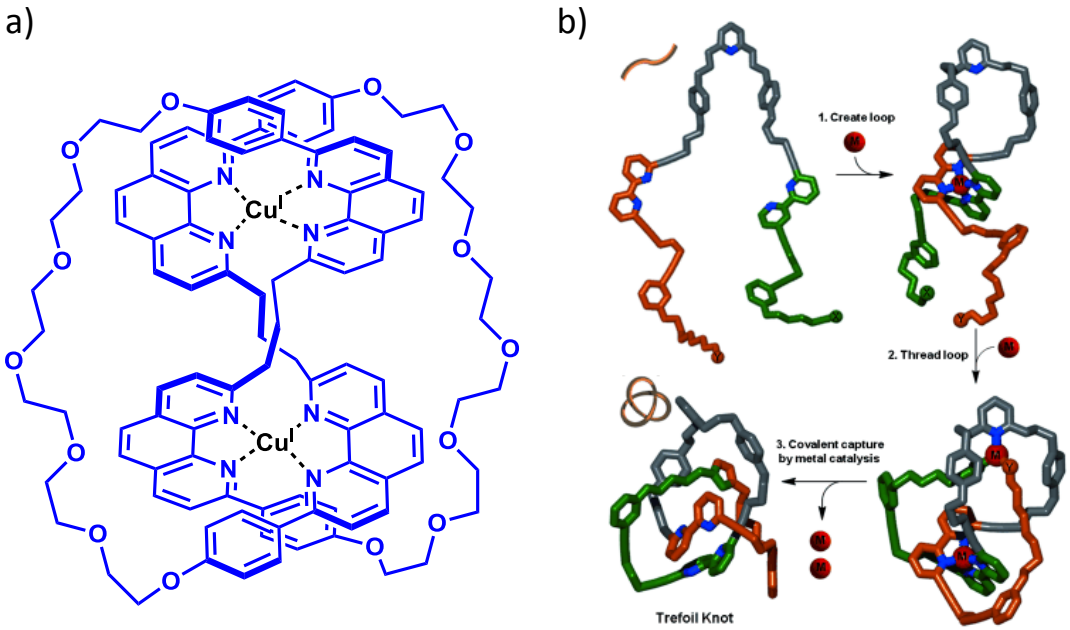

Figure 1-8. Structure of **a)** Sauvage's trefoil knot[73] and **b)** Leigh's trefoil knot by using metal template.[74]

Molecular machines

Molecular motors in biological systems are roughly distinguished between linear molecular motors, such as myosin, kinesin and dynein[75–78] from rotary motors, such as F_0F_1-ATP synthase and F_1-ATPase.[79–81] Rotaxanes are considered to be a good example of controlled molecular movement in both linear and rotary molecular motor systems. Recently, studies on controlled synthetic linear[82, 83] and rotary molecular motors have been reported by using rotaxane as building blocks, which have achieved by controlling rotary movement.[84–87] Harada *et al.* have previously reported that the linear movement of α-cyclodextrin (α-CD) in *pseudo*-[2]rotaxane with dicationic axle molecules should be controlled by the terminal group of axle molecules.[88, 89] Various biological molecular motors, such as myosin, kinesin, and dynein, can convert energy from ATP hydrolysis into a linear motion. Myosin and actin filaments in muscle cells insert into each other to form an alternating layered structure and slide to demonstrate contraction and expansion behaviour in the power stroke process.[90–92] The sliding of myosin and actin filaments has inspired the realization development of artificial linear motors using supramolecular complexes (Figure 1-9).

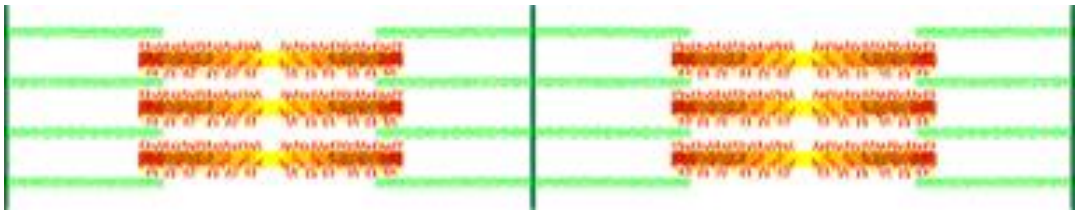

Figure 1-9. Illustration of biological molecular motor green line is actin, and orange line is myosin.

The concept of artificial molecular machines was proposed in historic lecture "There's Plenty of Room at the Bottom" by Feynman in 1959. General preparation method of molecular machines is the introducing residues responsive to external stimuli. Aida *et al.* reported photo-generated molecular pedal driven by photo-isomerization of azobenzene.[93] The molecular pedal shows mechanical twist of the second molecule in a controlled and

reversible manner (Figure 1-10a). Kelly[94] and Feringa[95, 96] reported that molecular motors showed photo and thermal responsive rotary motion (Figure 1-10b, c).

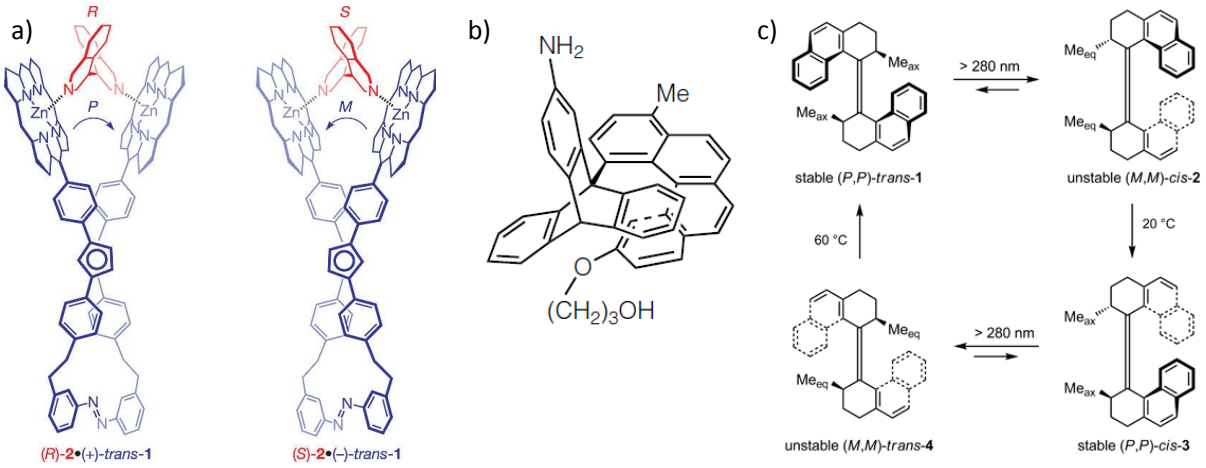

Figure 1-10. Examples of molecular machine generated by external stimuli. **a)** Aida's molecular pedal[93], **b)** Kelly's[94] and **c)** Feringa's[95] molecular motors.

Mechanically interlocked molecules are used transduction of micro-Brownian motion to linear motion. Molecular shuttles are rotaxanes in which the ring component moves from are position to another axis and *vice versa*. Stoddart[97, 98] reported stimuli responsive molecular shuttles (Figure 1-11a). Sauvage[99] and Leigh[100] manipulated the orbit of motion of cyclic molecules in catenane systems (Figure 1-11b, c).

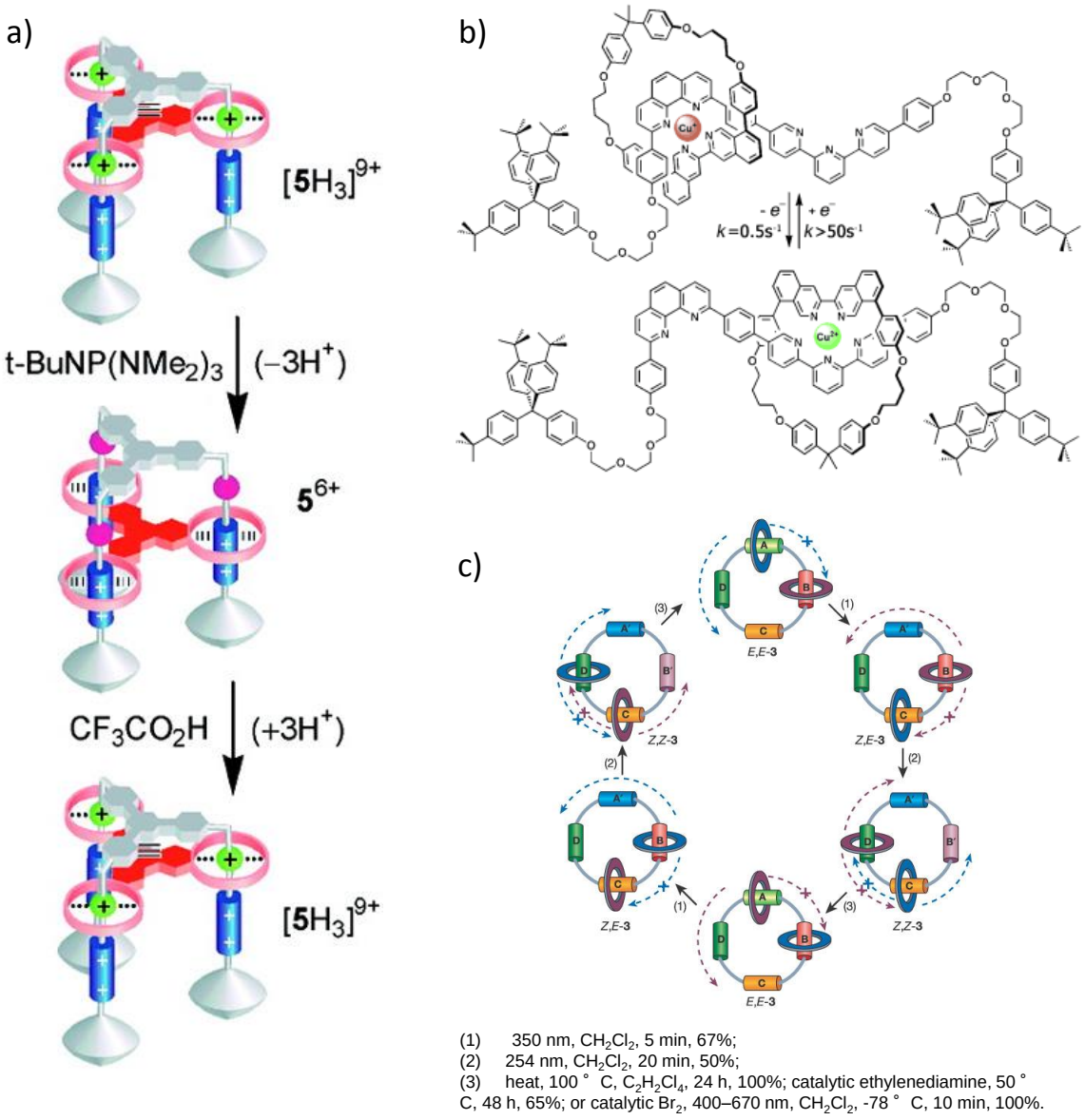

Figure 1-11. **a)** Supramolecular elevator reported by Stoddart[97] and **b)** molecular shuttle reported by Sauvage.[99] **c)** Rotating catenane in one direction reported by Leigh.[100]

[c2]Daisy chains

[c2]Daisy chains (doubly-threaded rotaxane) incorporated two cyclic and axis components are one of mechanically interlocked molecules (Figure 1-12). The doubly-threaded rotaxane shows the contraction and expansion behaviour through sliding motion by changing affinity between ring and axis components by external stimuli. The sliding motion reminds supramolecular chemists the motion of muscle fibril. In the field of supramolecular chemistry, [c2]daisy chains are important components to realize artificial molecular muscles.[101] The specific sliding actuation of [c2]daisy chains based on host–guest conjugates is controlled by external stimuli, e.g., chemicals,[102, 103] pH,[104, 105] redox[106] and light.[107–110]

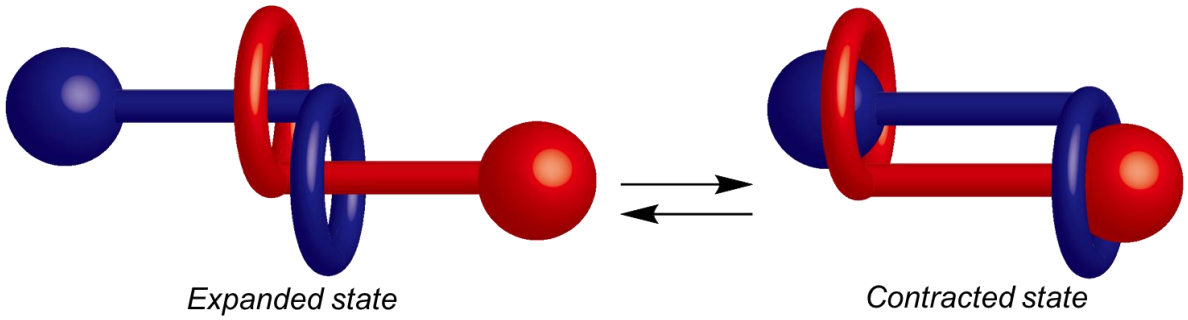

Figure 1-12. Schematic illustration of expansion and contraction of [c2]daisy chain.

Previously, Harada developed the [c2]daisy chain formed from αCD and an axis component, i.e., cinnamic acid residue modified with an oligomethylene chain.[111] Position of αCD units in [c2]daisy chain is controlled by solvent polarity. In DMSO solution, [c2]daisy chain takes an expanded state via the formation of the inclusion complex of αCD with cinnamic acid. Increasing the water volume % of solvent, [c2]daisy chain takes contracted because of the hydrophobic oligomethylene chain (Figure 1-13a). Furthermore, to realize larger contraction and expansion property, poly(ethylene glycol) (PEG) chain is used in photo-responsive [c2]daisy chain (Figure 1-13b).[112] The heptamethylene chain at the

end of PEG chain functions as the second station for αCD units. The association constant (*K*) of αCD with *trans*-azobenzene (2000 M^{-1}) is larger than that with *cis*-azobenzene (50 M^{-1}). On the other hand, *K* with heptane is 630 M^{-1}. The [c2]daisy chain takes an expanded state due to the formation of inclusion complex between αCD and *trans*-azobenzene. After UV (λ = 365 nm) light irradiation, *trans*-azobenzene isomerizes to *cis*-form. The αCD unit includes the heptamethylene chain more preferably than the *cis*-azobenzene unit.

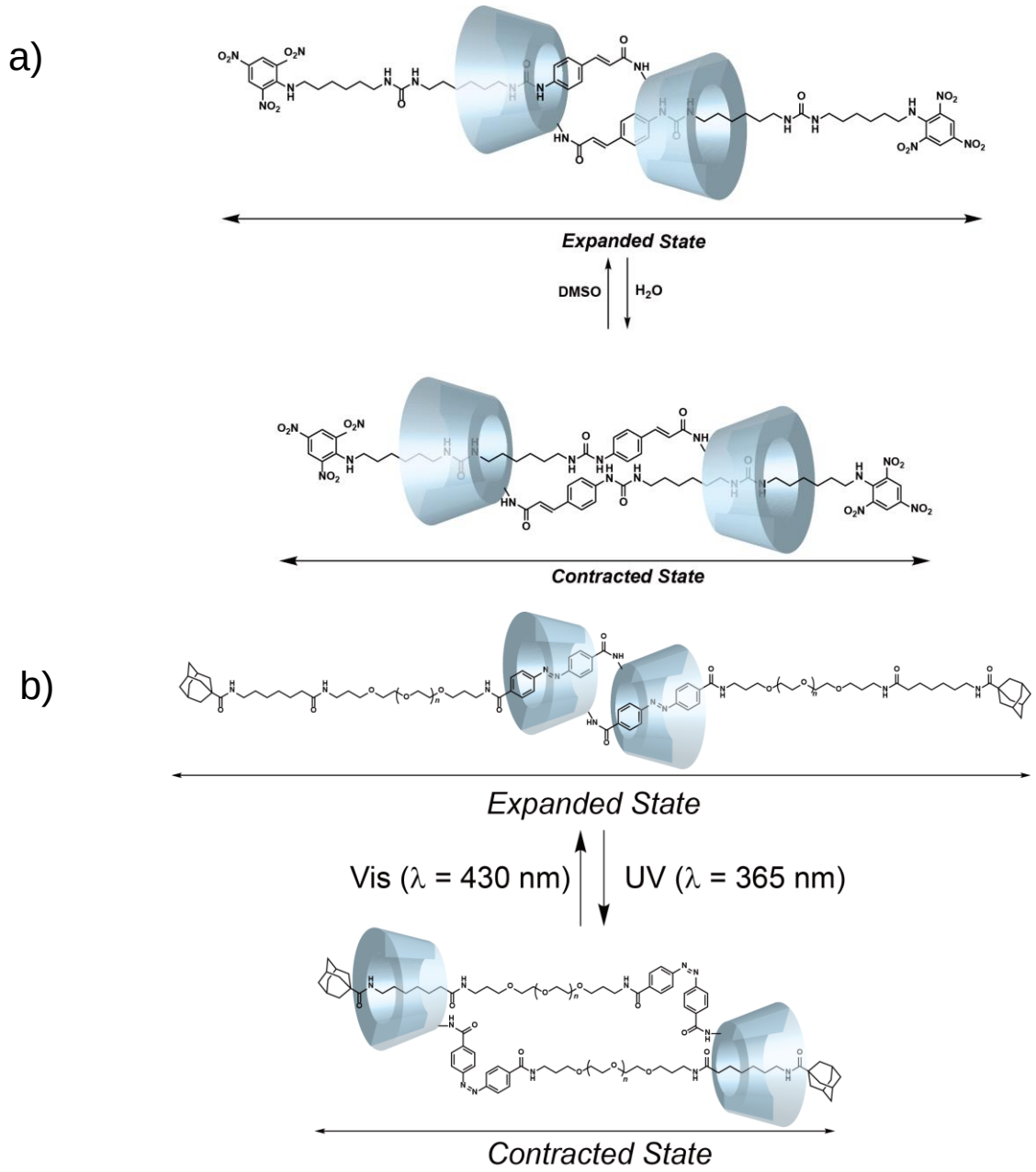

Figure 1-13. [c2]Daisy chain based on αCD and hydrophobic guest molecules. **a)** Change in the water proportion in the medium using cinnamic acid as guest molecule.[110] **b)** Association and dissociation of αCD with azobenzene by light irradiation system.[112]

Sauvage[111] reported "molecular muscle" formed from crown ether containing phenanthroline components and terpyridine components. The exchange of transition-metals triggered the contraction and expansion properties (Figure 1-14).

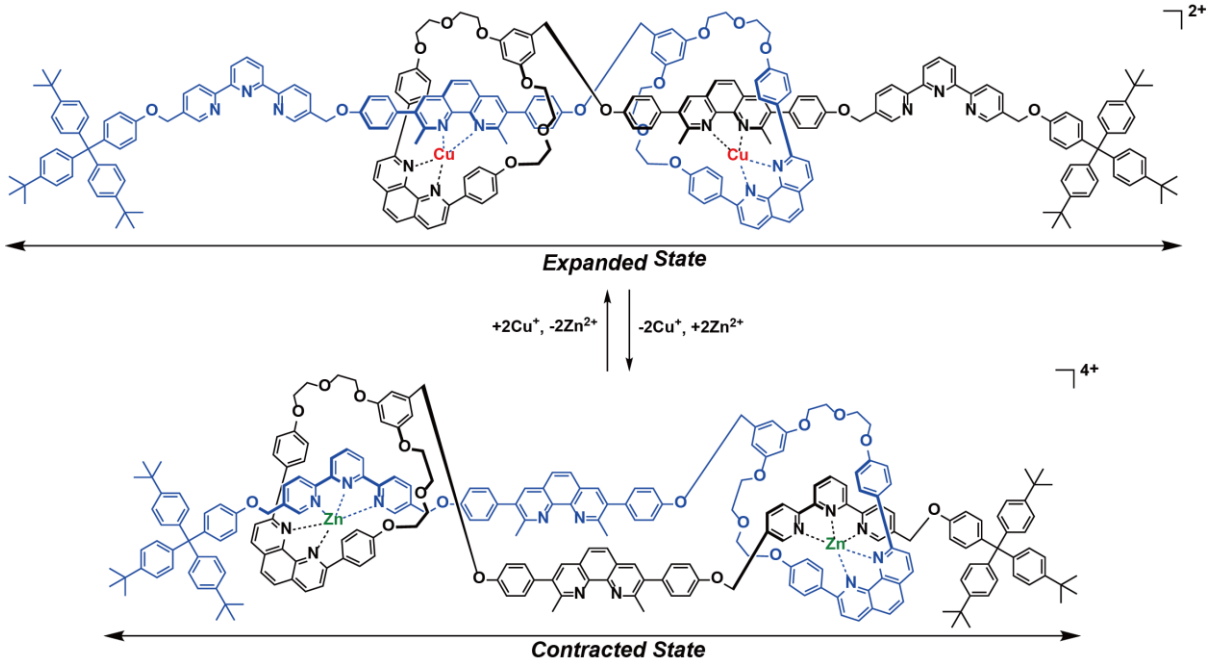

Figure 1-14. Sauvage[111]'s molecular muscle. The interconversion between contraction and expansion states was induced by the exchange of metal ion.

Easton also reported a photo-responsive [c2]daisy chain based on αCD and a stilbene derivative.[113] *trans*-Stilbene forms the inclusion complex with αCD in aqueous solution. After UV (λ = 340 nm) irradiation, the inclusion complex dissociates due to the low affinity for *cis*-stilbene. The change in the length of the [c2]daisy chain is triggered by association and dissociation of the inclusion complex between the stilbene unit and αCD (Figure 1-15).

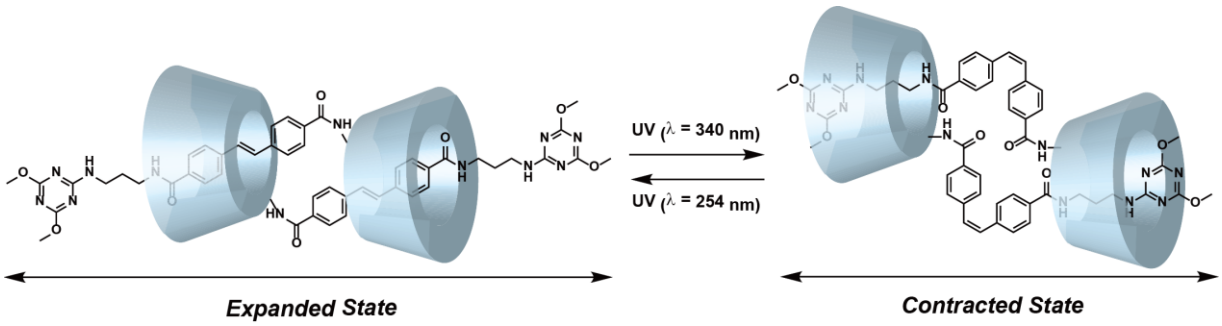

Figure 1-15. The two state of the [c2]daisy chain elaborated and studied by Easton *et al.*[113]

Kaneda prepared αCD and azobenzene based on oligo-[c2]daisy chain by cross-linking with α,α'-dibromo-*p*-xylene.[107] Under UV (λ = 365 nm) irradiation, *trans*-azobenzene isomerizes to *cis*-azobenzene and the obtained oligomer contracts due to dissociation of the inclusion complex of αCD with azobenzene residues. Under continuous Vis (λ = 430 nm) light irradiation, the contracted oligomer is restored to the initial form. After that, Stoddart reported a polymer of pH-responsive [c2]daisy chain consisting of crown ether and ammonium cation. The [c2]daisy chains in polymer takes an expanded state in organic media due to high affinity between crown ether and ammonium cation. When the ammonium units are deprotonated, the crown ether includes the bipyridinium units more favorably than the amine units. Because an affinity of crown ether and bipyridinium is higher than that crown ether and nonionic amino group. Upon addition of an acid, the length of polymer restores to initial state again (Figure 1-16).[114] These structural change causes the contraction of polymers. However there is no report of the materials based on the [c2]daisy chain polymers.

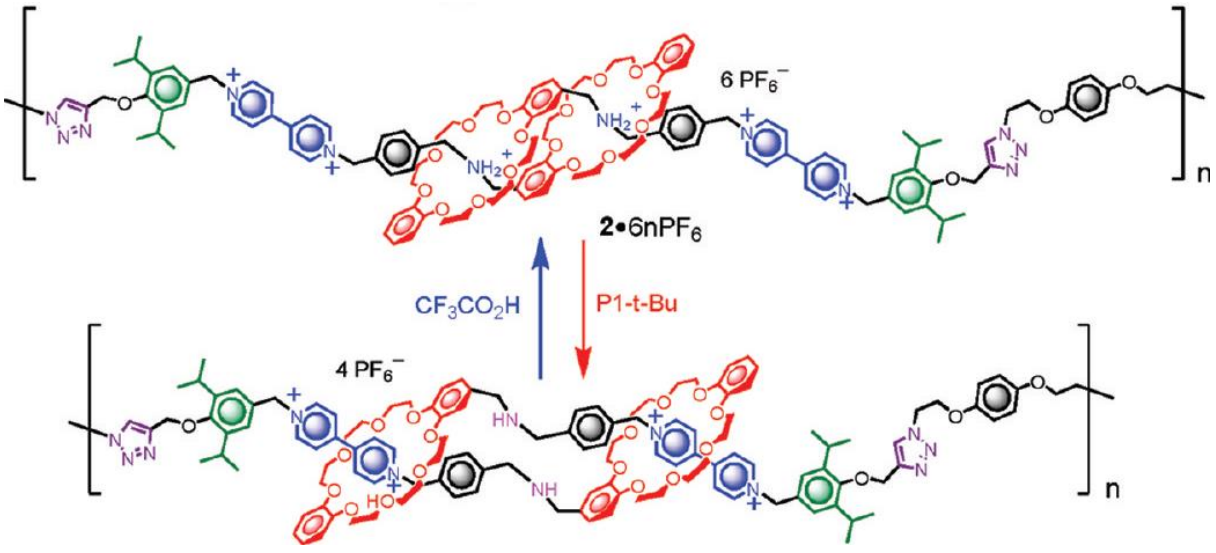

Figure 1-16. Contraction and expansion of [c2]daisy chain polymer based on the non-covalent interaction between crown ether and ammonium cation units.[114]

Actuation of materials caused by structural change of polymers

The expansion of artificial molecular machines in the field of nanotechnology into macroscopic scale is an important research subject. Researchers in supramolecular chemistry have been tried to introduce the molecular machines into polymer networks. Stoddart reported a [3]rotaxane which were connected on the gold surface (Figure 1-17a).[115] The gold substrate was bent by the sliding motion of [3]rotaxanes according responsive to redox stimulus. Leigh reported movement of drops on the glass substrate driven by the structural change of [2]rotaxanes (Figure 1-17b).[116] Recently, Giussepone *et al.* showed the contraction of organogel caused by rotating motion of molecular motor inspired by Feringa (Figure 1-17c).[117]

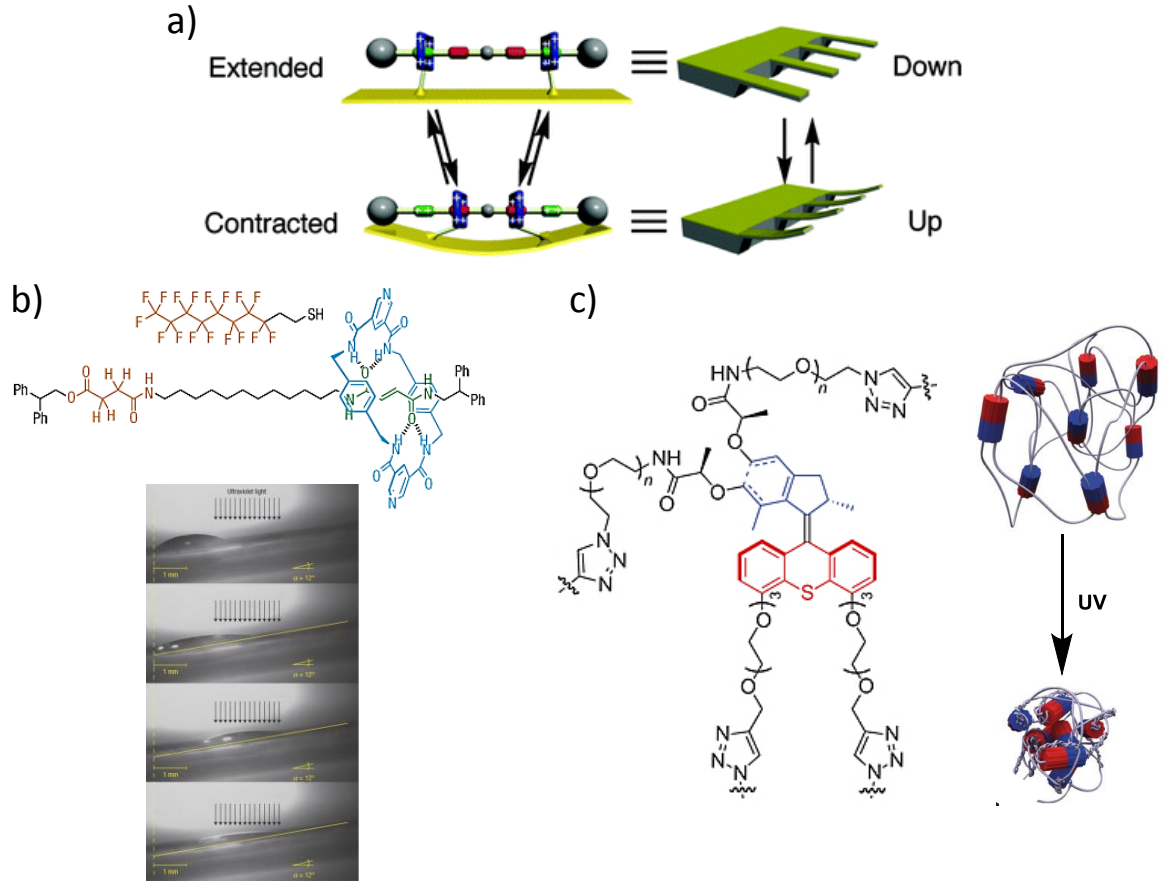

Figure 1-17. **a)** Gold surface actuation caused by shuttling of [3]rotaxane.[115] **b)** Photo-induced transport of diodemethane drop.[116] **c)** Macroscopic contraction of gel caused by rotation of molecular motor.[117]

Macroscopic self-assembly though molecular recognition

Molecular recognition properties in macroscopic scale is reported by Harada in 2011 (Figure 1-18a).[118–120] They prepared host gels (CD gels) and guest gels by modification of polyacrylamide-based gel with CD and guest residues, respectively. When both gel were through in contact under wet conditions, αCD gel adhered to *n*-butyl gel. βCD gel adhered to adamantane gel (Ad gel). These selectivities depend on the association constant of CD with guest molecules. The association constant of αCD with *n*-butyl group higher than that of the Ad group. βCD shows a high affinity for the Ad group. External stimuli such as photo,[121] chemical,[122–124] temperature,[125] pH[126] and hydrogen bonding[127] controlled the formation of macroscopic assemblies through molecular recognition. When *trans*-azobenzene modified hydrogel (Azo gel) was shaken with αCD gel and βCD gel on water, Azo gel selectively adhered to αCD gel (Figure 1-18b). Because the affinity of αCD with *trans*-Azo is higher than that of βCD. In contrast, after UV light irradiation, Azo gel selectivity adhered to βCD gel due to the high affinity between βCD and *cis*-Azo.

In the previous works, host and guest molecules were introduced into the different polymer scaffold. CDs recognize guest molecules on the hydrogel surfaces. The complex formation produces the selective adhesion properties like cell adhesion and cell-sorting systems. If host and guest units are introduced into the same hydrogel, the complex formation inside the host–guest gel will realizes functional properties, such as, highly elastic, tough, and self-healing through the molecular recognition. In particular, host–guest interactions are advantageous due to their reversibility and responsiveness to various external stimuli. Harada *et al.* have developed self-healing supramolecular hydrogels based on host–guest interactions at the side chain of water-soluble polymers. Harada *et al.* have proposed two different effective approaches to prepare supramolecular self-healable materials through host–guest interactions: (1) from a mixture of host and guest polymers and (2) from polymerization of host and guest monomers. The self-healing ability of supramolecular

hydrogels based on poly(acrylic acid) modified host and guest molecules (βCD polymer and ferrocene (Fc) polymer exhibits a redox responsive sol–gel transition.[128] Even if the gel is cut in two using a razor, the cut surface disappears and self-healing is completed in several hours. After 24 hours, the gel recovers 85% of the initial strength (Figure 1-18c).[129] To obtain effective self-healing materials, the complex with the βCD monomer and the Ad monomer can be copolymerized with acrylamide to give a self-healable hydrogel. When two freshly cut surfaces come into contact, the two pieces adhere to form a single gel, and the initial gel strength is almost completely recovered after 24 hours (Figure 1-18d).[130] In contrast, when lower molar contents of βCD and Ad (< 1mol%) gave a high elastic hydrogel (Figure 1-18e).[130] Moreover, βCD-Ad gel which is prepared under over 2 mol/kg, showed high stretching properties (more than 1000%) (Figure 1-18f).[131] The tough and flexible hydrogel can be used to a scratch coat.

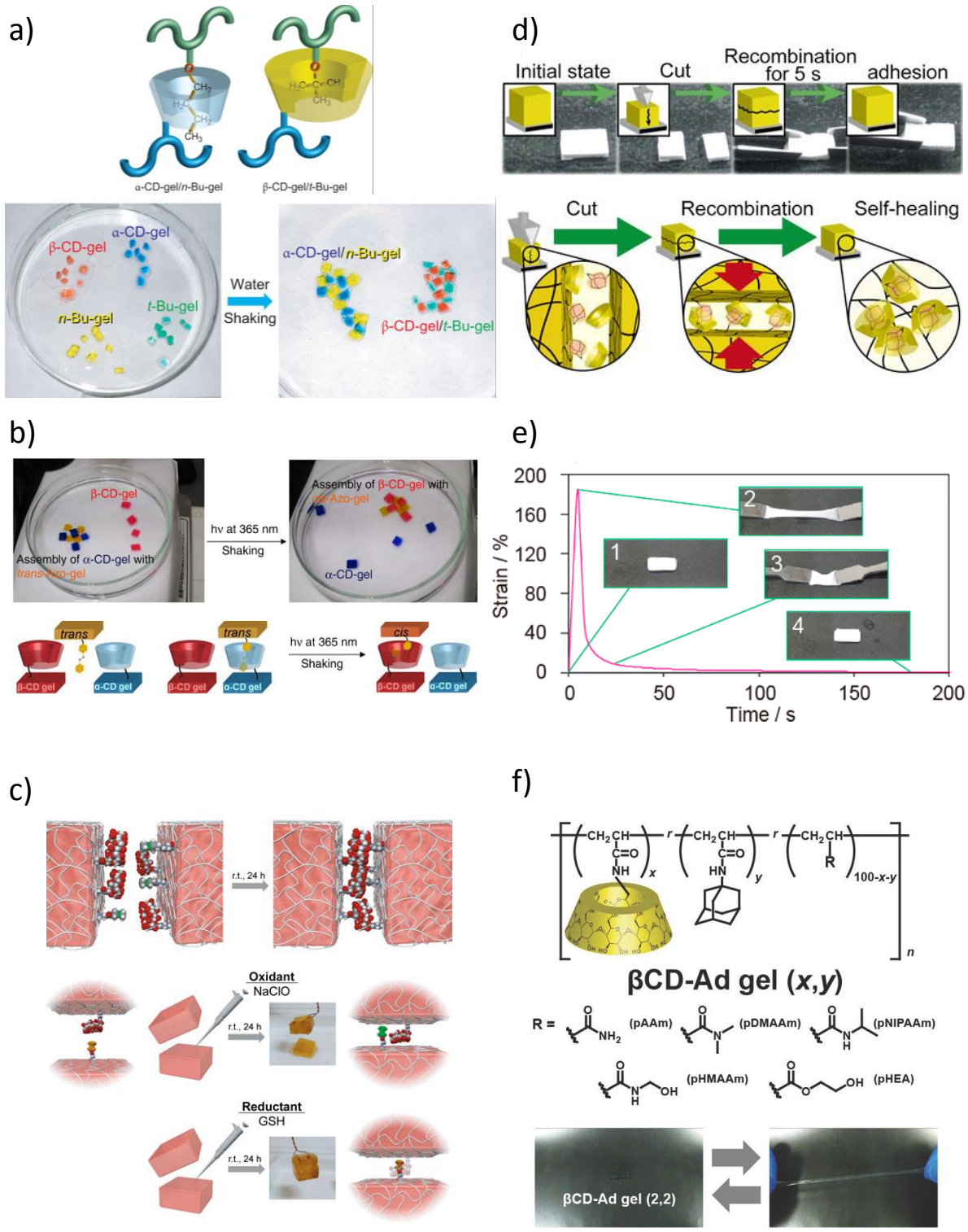

Figure 1-18. **a)** Visualization of selective molecular recognition on a macroscopic scale.[118] **b)** Photo-switchable gel assembly through isomerization of Azo.[127] **c)** Redox generated self-healing gel through change of oxidation state of Fc.[128] **d)** Self-healing gel through formation of inclusion complex between βCD and Ad.[129] **e)** Highly stretchable hydrogel consisting of βCD and Ad.[130] **f)** Tough and flexible hydrogel prepared from high molar content of monomers.[131]

Supramolecular hydrogels cross-linked by host guest inclusion complex

The supramolecular hydrogels were formed by mixing of CD polymer and guest polymer in aqueous media. The mixture of Azo modified poly(acrylic acid) and αCD modified curdlan formed a photo-responsive sol–gel switching system (Figure 1-19a).[132] Before UV light irradiation, the αCD unit recognizes the Azo unit to form an inclusion complex which functions as a reversible cross-linker. Irradiating with UV light converts the gel into a sol. However, visible light or heating (60 °C) induces back isomerization of the *cis*-Azo group to the *trans*-Azo group. The viscosity changes of the polymer mixture can be repeatedly induced using UV and visible lights.

Inclusion complexes act as cross-linking points between the polymers to yield supramolecular hydrogels. This material does not have any covalent cross-links. If introducing covalent cross-links partly into materials, the supramolecular materials will show an expansion–contraction behaviour by external stimuli. On the basis of the concept, stimuli responsive contraction and expansion hydrogels are designed. The hydrogel with the contraction and expansion properties were prepared by the copolymerization of azobenzene and αCD monomers with a covalent cross-link molecule (Figure 1-19b).[133] When the αCD-Azo gel was irradiated with UV light, the volume of the hydrogel was increased. Subsequently, irradiating with Vis light restores the initial volume due to the reformation of an inclusion complex with the αCD and Azo units. The αCD-Azo gel bends in the same direction as the incident light because the volume of the surface exposed to UV light increases, while non-exposed surface remains unchanged. Hence, the strain deformation between the exposed and unexposed areas creates the flex behaviour of αCD-Azo gels. This concept can adapt other supramolecular actuator by choosing suitable stimuli-responsive molecules. When introducing βCD as a host and Fc as guest molecules, the βCD-Fc gel exhibited the contraction–expansion behaviour responsive to redox stimulus (Figure 1-19c).[134]

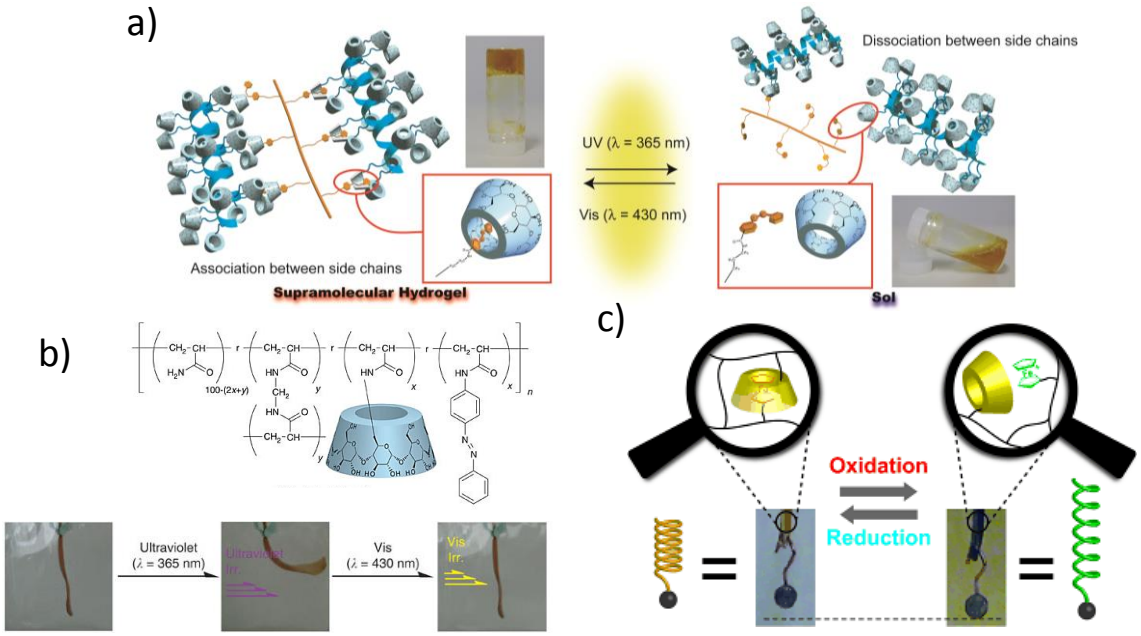

Figure 1-19. **a)** Photo-generated sol–gel transition.[132] **b)** Photo-responsive actuator consisting of αCD and Azo.[133] **c)** Redox responsive gel actuator consisting of βCD and Fc.[134]

Scope and outline of this thesis

The present thesis focuses on the preparation of supramolecular molecules and materials with the contraction and expansion properties based on photo-responsive [c2]daisy chain molecule. The sliding motion of [c2]daisy chain is caused by a change in the affinity between αCD and azobenzene via photo-isomerization. When introducing the [c2]daisy chain units in supramolecular materials, the supramolecular materials with [c2]daisy chain is expected to demonstrate the contraction and expansion properties like biological skeletal muscle. To demonstrate the actuation mechanism, the author investigates mechanical properties of the gel materials resulting from the sliding motion of [c2]daisy chain.

In Chapter 2, the [c2]daisy chain consisting of Azo and αCD ([c2]DMTAzoCD$_2$) was prepared to investigate the sliding motion and the photo-isomerization properties. [c2]DMTAzoCD$_2$ was derived from diethylene glycol (DEG) with the amino group at the end and Azo modified αCD (AmAzoCD). Under irradiation with UV (λ = 365 nm) for 60 min, the *trans*-Azo units in [c2]DMTAzoCD$_2$ is isomerized to the *cis*-isomers. In contrast, *cis*-[c2]DMTAzoCD$_2$ came back to *trans*-[c2]DMTAzoCD$_2$ within 80 s by under Vis light irradiation because the isomerization efficiency of Azo in the αCD cavity is suppressed. As a result, after UV light irradiation, the αCD unit of [c2]DMTAzoCD$_2$ move onto the azobenzene unit of the DEG chain.

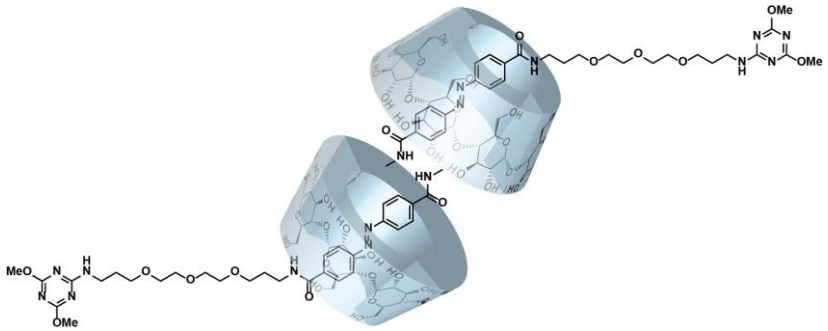

In Chapter 3, the supramolecular hydrogel was prepared by polycondensation between four-arm poly(ethylene glycol) (tetraPEG) and inclusion complex of AmAzoCD in water. The hydrogel with the [c2]daisy chain ([c2]AzoCD$_2$ hydrogel) showed the

contraction behaviour by UV light irradiation. Subsequence, Vis light irradiation, the contracted [c2]AzoCD$_2$ hydrogel was restored to the initial form. Irradiating the UV light, the plate shape [c2]AzoCD$_2$ hydrogel bent toward to the light source. In contrast, the azobenzene gel (Azo hydrogel) showed opposite behaviour to that of the [c2]AzoCD$_2$ hydrogel. Young's moduli of each hydrogels before and after UV irradiation were characterized by evaluated by tensile test. The contraction and expansion properties of the [c2]AzoCD$_2$ hydrogel was caused by the sliding motion of [c2]daisy chain. On the other hand, the expansion and contraction behaviour of the Azo hydrogel was caused by change in the cross-linking density.

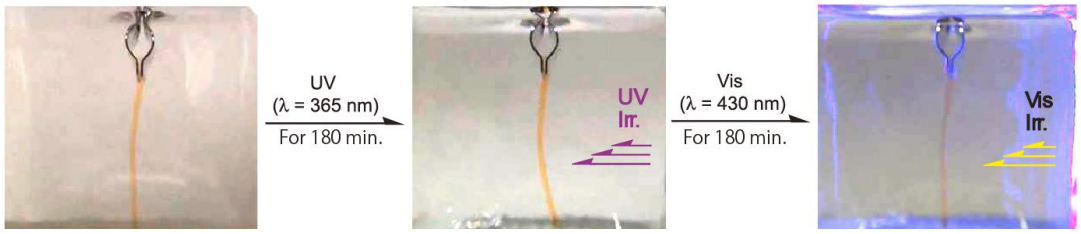

In Chapter 4, The [c2]AzoCD$_2$ xerogel lyophilized from the [c2]AzoCD$_2$ hydrogel shows rapid actuation by UV irradiation. In contrast, the Azo xerogel did not show the behaviour. The results of tensile test indicate that the [c2]AzoCD$_2$ xerogel which irradiated by UV light a higher rupture strain than non-irradiated one. In contrast, rupture strength of each xerogels did not change.

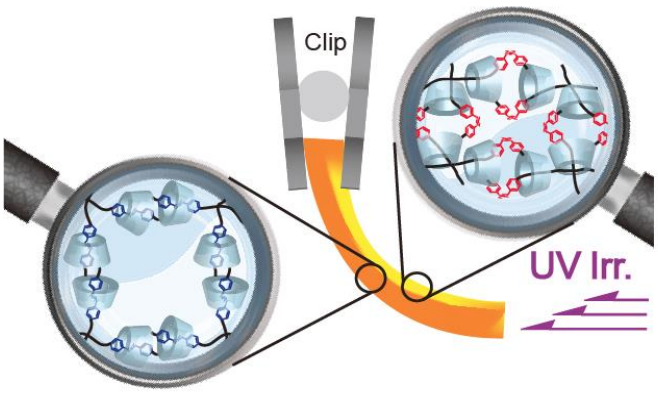

References

1. Timko, M. J., Helgeson, R. C., Newcomb, M., Gokel, G. W., Cram, D. J. Structural parameters that control association constants between polyether host and alkylammonium guest compounds. *J. Am. Chem. Soc.* **183,** 7097–7099 (1974).
2. Cram, D. J., Karbach, S., Kim, Y. H., Baczynskyj, L., Kallemeyn Cram, G. W. Shell closure of two cavitands forms carcerand complexes with components of the medium as permanent guests. *J. Am. Chem. Soc.* **219,** 2575–2576 (1983).
3. Cram, D. J. The Design of Molecular Hosts, Guests, and Their Complexes. (Nobel Lecture) *Angew. Chem., Int. Ed. Engl.* **27,** 1009–1112 (1990).
4. Lehn, J.-M. Cryptates: inclusion complexes of macropolycyclic receptor molecules. *Pure Appl. Chem.* **50,** 872–892 (1978).
5. Lehn, J.-M. Cryptates: the chemistry of macropolycyclic inclusion complexes. *Acc. Chem. Res.* **11,** 49–57 (1978).
6. Lehn, J.-M. Supramolecular Chemistry: Receptors, Catalysts, and Carriers. *Science* **227,** 849–856 (1985).
7. Lehn, J.-M. Supramolecular Chemistry- Scope and Perspectives: Molecules-Supermolecules- Molecular Devices *J. Incl. Phenom.* **6,** 351-396 (1988).
8. Lehn, J.-M. Perspectives in Supramolecular Chemistry-From Molecular Recognition towards Molecular Information Processing and Self-organization. *Angew. Chem., Int. Ed. Engl.* **27,** 1304–1319 (1990).
9. Lehn, J.-M. *Supramolecular chemistry*: *Concepts and Perspectives*; VCH: New York, (1995).
10. Lehn, J.-M. Toward complex matter: Supramolecular chemistry and self-organization. *Proc. Natl. Acad. Sci. U.S.A.* **99,** 4763–4768 (2002).
11. Pedersen, C. J. Cyclic polyethers and their complexes with metal salts. *J. Am. Chem. Soc.* **89,** 7017–7036 (1967).
12. Pedersen, C. J. The Discovery of Crown Ethers (Noble Lecture). *Angew. Chem., Int. Ed. Engl.* **27,** 1021–1027 (1988).
13. Fischer, E. Einfluss der Configuration auf die Wirkung der Enzyme. *Ber. Deutsch. Chem. Ges.* **27,** 1894, 2985–2993 (1984).
14. Gutsuche, C. D. Calixarenes. *Acc. Chem. Res.* **16,** 161–170 (1983).
15. vanDienst, E., Bakker, W. I. I. Engbersen, J. F. J., Verboom, W., Reinhoudt, D. N. Calixarenes, chemical chameleons. *Pure Apply. Chem.* **65,** 387–392 (1993).
16. Lhoták1, P., Shinkai, S. Calix[n]arenes-Powerful Building-Blocks of Supramolecular Chemistry. *Terahedron* **53,** 963–974 (1993).
17. Haino, T., Kobayashi, M., Chikaraishi M., Fukazawa, Y. A new self-assembling capsule via metal coordination. *Chem. Commun.* **18,** 2321–2323 (2005)
18. Rudkevich, D. M., Hilmersson, G., Rebek, J. Jr. Intramolecular Hydrogen Bonding

Controls the Exchange Rates of Guests in a Cavitand. *J. Am. Chem. Soc.* **41,** 9911–9912 (1997).

19. Purse, B. W., Ballester, P., Rebek, J. Jr. Reactivity and Molecular Recognition: Amine Methylation by an Introverted Ester. *J. Am. Chem. Soc.* **125,** 14682–14683 (2003).
20. Gissot, A., Rebek, J. Jr. A Functionalized, Deep Cavitand Catalyzes the Aminolysis of a Choline Derivative. *J. Am. Chem. Soc.* **126,** 7424–7425 (2004)
21. Yamanaka, M., Toyoda, N., Kobayashi, K. Hybrid Cavitand Capsule with Hydrogen Bonds and Metal−Ligand Coordination Bonds: Guest Encapsulation with Anion Assistance. *J. Am. Chem. Soc.* **131,** 9880–9881 (2009).
22. Yamanaka, M., Kawaharada, M., Nito, Y., Takaya, H., Kobayashi, K. Structural Alteration of Hybrid Supramolecular Capsule Induced by Guest Encapsulation. *J. Am. Chem. Soc.* **133,** 16650–16656 (2011).
23. Szejtli, J. *Cycrodextrins and Their inclusion complexs.* Akadémiai Kiadó: Budapest, (1982).
24. Connors, K. A. The Stability of Cyclodextrin Complexes in Solution. *Chem. Rev.* **97,** 1325–1352 (1997).
25. Szejtli, J. Introduction and general overview of cyclodextrin chemistry. *Chem. Rev.* **98,** 1743–1752 (1998).
26. Dodziuk, H., *Cyclodextrins and Their Complexes.* Wiley-VCH: Weiheim, (2006).
27. Easton, C. J.; Lincoln, S. F. *Modified cyclodextrins: scaffolds and templates for supramolecular chemistry.* Imperial College Press; Distributed by World Scientific Pub. Co.: London River Edge, NJ, (1999).
28. Cramer, F. Über Einschlußverbindungen, I. Mitteil.: Additionsverbindungen der Cycloamylosen. *Chem. Ber.* **84,** 851–851 (1951).
29. Cramer, F., Einschlußverbindungen der Cyclodextrine. *Angew. Chem.* **64,** 136 (1952**).**
30. Cramer, F., Über Einschlußverbindungen, V. Mitteil.: Basenkatalyse durch innermolekulare Hohlräume. *Chem. Ber.* **86,** 1576–1581 (1953).
31. Bender, M. L. Cycloamyloses as Catalysts. *Adv. Catal.* **23,** 209–261 (1973).
32. Bender, M. L., Komiyama, M. *Cyclodextrin Chemistry.* Springer-Verlag: Berlin; New York, (1978).
33. Breslow, R. Biomimetic control of chemical selectivity. *Acc. Chem. Res.* **13,** 170–177 (1980).
34. Breslow, R. Artificial enzymes. *Science* **218,** 532–537 (1982).
35. Breslow, R. Artificial Enzymes. *Chem. Ber. 19,* 126 (1983).
36. Breslow, R. Biomimetic Chemistry and Artificial Enzymes: Catalysis by Design. *Acc. Chem. Res.* **28,** 146–153 (1995).
37. Lehn, J.-M., Rigault, A., Siegel, J., Harrowfield, J., Chevrier, B., Moras, D. *Proc.*

Natl. Acad. Sci. USA. **84,** 2565 (1987).

38. Beijer, F. H., Kooijman, H., Spek, A. L., Sijbesma, R. P., Meijer, E. W., Self-Complementarity Achieved through Quadruple Hydrogen Bonding. *Angew. Chem. Int. Ed.* **37,** 75–78 (1998).
39. Sijbesma, R. P., Beijer, F. H., Brunsveld, L., Folmer, B. J. B., Hirschberg, J. H. K. K., Lange, R. F. M., Lowe, J. K. L., Meijer, E. W. Reversible polymers formed from self-complementary monomers using quadruple hydrogen bonding. *Science* **278,** 1601–1604 (1997).
40. Piepenbrock, M. O. M., Lloyd, G. O., Clarke, N., Steed, J. W. Metal- and Anion-Binding Supramolecular Gels. *Chem. Rev.* **110,** 1960–2004 (2010).
41. Hasegawa, M., Iyoda, M. Conducting supramolecular nanofibers and nanorods. *Chem. Soc. Rev.* **39,** 2420–2427 (2010).
42. Haino, T., Matsumoto, Y., Fukazawa, Y. Supramolecular Nano Networks Formed by Molecular-Recognition-Directed Self-Assembly of Ditopic Calix[5]arene and Dumbbell [60]Fullerene. *J. Am. Chem. Soc.* **127,** 8936–8937 (2005).
43. Haino, T., Hirai, E., Fujiwara, Y., Kashihara, K. Supramolecular Cross-Linking of [60]Fullerene-Tagged Polyphenylacetylene by the Host–Guest Interaction of Calix[5]arene and [60]Fullerene. *Angew. Chem., Int. Ed. Engl.* **49,** 7899–7903 (2010).
44. Danjo, H., Hirata, K., Yoshigai, S., Azumaya, I., Yamaguchi, K. Back to Back Twin Bowls of D_3-Symmetric Tris(spiroborate)s for Supramolecular Chain Structures. *J. Am. Chem. Soc.* **131,** 1638–1639 (2009).
45. Liu, Y., Yu, Y., Gao. J., Wabg, Z., Zhang, X., Water-Soluble Supramolecular Polymerization Driven by Multiple Host-Stabilized Charge-Transfer Interactions. *Angew. Chem. Int. Ed.* **49,** 6726–6729 (2010).
46. Zhang, Z, Luo. Y., Chen, J., Dong, S., Yu, Y., Ma, Z., Huang, F., Formation of Linear Supramolecular Polymers That Is Driven by C[BOND]H···π Interactions in Solution and in the Solid State. *Angew. Chem. Int. Ed.* 1433–1437 (2011).
47. Miyauchi, M., Harada, A. Construction of Supramolecular Polymers with Alternating α-, β-Cyclodextrin Units Using Conformational Change Induced by Competitive Guests. *J. Am. Chem. Soc.* **126,** 11418–11419 (2004).
48. Ohga, K., Takashima, Y., Takahashi, H., Kawaguchi, Y., Yamaguchi, H., Harada, A., Preparation of Supramolecular Polymers from a Cyclodextrin Dimer and Ditopic Guest Molecules: Control of Structure by Linker Flexibility. *Macromolecules.* **38,** 5897–5904 (2005).
49. Miyauchi, M., Hoshino, T., Yamaguchi, H., Kamitori, S., Harada Harada, A. A [2]Rotaxane Capped by a Cyclodextrin and a Guest: Formation of Supramolecular [2]Rotaxane Polymer. *J. Am. Chem. Soc.* **127,** 2034–2035 (2005)
50. Miyauchi, M., Takashima, Y., Yamaguchi, H., Harada, A. Chiral Supramolecular

Polymers Formed by Host−Guest Interactions. *J. Am. Chem. Soc.* **127,** 2984–2989 (2005)

51. Miyawaki, A., Miyauchi, M., Takashima, Y., Yamaguchi, H., Harada, A. Formation of supramolecular isomers; poly[2]rotaxane and supramolecular assembly. *Chem. Commun.* **4,** 456–458 (2008).
52. Kang, J., Miyajima, D., Mori, T., Inoue, Y., Itoh, Y., Aida, T. A rational strategy for the realization of chain-growth supramolecular polymerization. *Science* **347,** 646–651 (2015).
53. Harrison, I. T., Harrison, S. Synthesis of a stable complex of a macrocycle and a threaded chain. *J. Am. Chem. Soc.* **89,** 5723–5724 (1967).
54. Rowan, S. J., Cantrill, S. J., Stoddart, J. F., Triphenylphosphonium-Stoppered [2]Rotaxanes. *Org. Lett.* **1,** 129–132 (1999).
55. Andreas F. M. Kilbinger, A. F. M., Cantrill, S. J., Waltman, A. W., Day, M. W., Grubbs, R. H., Magic Ring Rotaxanes by Olefin Metathesis. *Angew. Chem. Int. Ed.* **42,** 3281–3285 (2003).
56. Langton, M. J., Robinson, S. W., Marques, I., Félix, V., Beer, P. D. Halogen bonding in water results in enhanced anion recognition in acyclic and rotaxane hosts. *Nat. Chem.* **6,** 1039–1043 (2014).
57. Anelli, P. L., Asakawa, M., Ashton, P. R., Bissell, R. A., Clavier, G., Gbrski, R., Kaifer, A. E., Langford, S. J., Mattersteig, G., Menzer, S., Philp, D., Slawin, A. M. Z., Spencer, N., Stoddart, J. F., Tolley, M. S., Williams, D. J. Toward Controllable Molecular Shuttles. *Chem. Eur. J.* **3,** 1113–1135 (1997).
58. Li, H., Fahrenbach, A. C., Dey, S. K., Basu, S., Trabolsi, A., Zhu, Z., Botros, Y. Y., Stoddart, J. F. Mechanical Bond Formation by Radical Templation. *Angew. Chem. Int. Ed.* **49,** 8260–8265 (2010).
59. Li, Z. T., Stein, P. C., Becher, J., Jensen, D. Msrk, P. Svenstrup, N. *Chem. Eur. J.* **2,** 624 (1996).
60. Mobian, P., Collin, J. P., Sauvage, J. P. Efficient synthesis of a labile copper (I)-rotaxane complex using click chemistry. *Tetrahedron Lett*. **47,** 4907–4909 (2006).
61. Aucagne, V., Berná, J., Crowley, J. D., Goldup, S. M., Hänni, K. D., Leigh, D. A., Lusby, P. J., Ronaldson, V. E., Slawin, A. M. Z., Viterisi, V., Walker, D. B. Catalytic "active-metal" template synthesis of [2] rotaxanes,[3] rotaxanes, and molecular shuttles, and some observations on the mechanism of the Cu (I)-catalyzed azide-alkyne 1, 3-cycloaddition. *J. Am. Chem. Soc.* **129,** 11950–11963 (2007).
62. Ogino, H. Relatively high-yield syntheses of rotaxanes. Syntheses and properties of compounds consisting of cyclodextrins threaded by. alpha.,. omega.-diaminoalkanes coordinated to cobalt (III) complexes. *J. Am. Chem. Soc.* **103,** 1303–1304 (1981).
63. Castro, R., Cuadrado, I., Alonso, B., Casado, C. M., Moran, M., Kaifer, A. E. Multisite Inclusion Complexation of Redox Active Dendrimer Guests. *J. Am. Chem.*

Soc. **119,** 5760–5761 (1997).

64. Harada, A. Li, J. Kamachi, M. Non-ionic [2]rotaxanes containing methylated α – cyclodextrins. *Chem. Commun.* 1413–1414 (1997).
65. Harada, A.; Kamachi, M. Complex Formation between Poly(ethylene glycol) and α – Cyclodextrin. *Macromolecules* **23,** 2821–2823 (1990).
66. Harada, A., Li, J., Kamachi, M. The molecular necklace: a rotaxane containing many threaded α-cyclodextrins. *Nature* **356,** 325–327 (1992).
67. Harada, A., Li, J., Kamachi, M. Synthesis of a tubular polymer from threaded cyclodextrins. *Nature* **364,** 516–518 (1993).
68. Harada, A., Li, J., Kamachi, M. Double-stranded inclusion complexes of cyclodextrin threaded on poly (ethylene glycol). *Nature* **370,** 126–128 (1994).
69. Wasserman, E. THE PREPARATION OF INTERLOCKING RINGS: A CATENANE1. *J. Am. Chem. Soc.* **82,** 4433–4434 (1960).
70. Dietrich-Buchecker, C., Sauvage, J. P. Templated synthesis of interlocked macrocyclic ligands, the catenands. Preparation and characterization of the prototypical bis-30 membered ring system. *Tetrahedron* **46,** 503–512 (1990).
71. Anelli, P. L., Asakawa, M., Ashton, P. R., Bissell, R. A., Clavier, G., Gbrski, R., Kaifer, A. E., Langford, S. J., Mattersteig, G., Menzer, S., Philp, D., Slawin, A. M. Z., Spencer, N., Stoddart, J. F., Tolley, M. S., Williams, D. J. Toward Controllable Molecular Shuttles. *Chem. Eur. J.* **3,** 1113–1135 (1997).
72. Chichak, K. S., Cantrill, S. J., Pease, A. R., Chiu, S. H., Cave, G. W., Atwood, J. L., Stoddart, J. F. Molecular borromean rings. *Science* **304,** 1308–1312 (2004).
73. J. –P. Sauvage., Dietrich-Buchecker, C., *Molecular Catenanes, Rotaxanes and Knots*. Wiley-VCH: Weiheim, (1999).
74. Barran, P. E., Cole, H. L., Goldup, S. M., Leigh, D. A., McGonigal, P. R., Symes, M. D.,Wu, J., Zengerle, M. *Angew. Chem. Int. Ed.* **50,** 12280–12284 (2011).
75. Goodsell, D. S. Our Molecular Nature: The Body's Motors, Machines and Messages; Copernics: New York, (1996).
76. Vale, R. D., Milligan, R. A. The way things move: looking under the hood of molecular motor proteins. *Science* **288,** 88–95 (2000).
77. Howard, J. Mechanics of Motor Proteins and the Cytoskelton; Sinauer Associates: Sunderland, MA, (2001).
78. Frey, E. Physics in cell biology: on the physics of biopolymers and molecular motors. *Chem. Phys. Chem*. **3,** 270–275 (2002).
79. Boyer, P. D. The binding change mechanism for ATP synthase—some probabilities and possibilities. *Biochimica et Biophysica Acta (BBA)-Bioenergetics*, **1140,** 215–250 (1993).
80. Boyer, P. D. Energy, life, and ATP (Nobel lecture). *Angew. Chem. Int. Ed.* **37,** 2296–2307 (1998).

81. Walker, J. E. ATP Synthesis by Rotary Catalysis. Nobel Lecture, Dec, 8 (1997).
82. Linke, M., Chambron, J. C., Heitz, V., Sauvage, J. P., Semetey, V. Complete rearrangement of a multi-porphyrinic rotaxane by metallation–demetallation of the central coordination site. *Chem. Commun.* 2469–2470 (1998).
83. Blanco, M. J., Jimenez, M. C., Chambron, J. C., Heitz, V., Linke, M., Sauvage, J. P. Rotaxanes as new architectures for photoinduced electron transfer and molecular motions. *Chem. Soc. Rev.* **28,** 293–305 (1999).
84. Shukla, R., Deetz, M. J., Smith, B. D. [2] Rotaxane with a cation-binding wheel. *Chem. Commun.* 2397–2398 (2000).
85. Koumura, N., Zijlstra, R. W., van Delden, R. A., Harada, N., Feringa, B. L. Light-driven monodirectional molecular rotor. *Nature* **401,** 152–155 (1999).
86. Koumura, N., Geertsema, E. M., Meetsma, A., Feringa, B. L. Light-Driven Molecular Rotor: Unidirectional Rotation Controlled by a Single Stereogenic Center. *J. Am. Chem. Soc.* **122,** 12005–12006 (2000).
87. Feringa, B. L. In control of motion: from molecular switches to molecular motors. *Acc. Chem. Res.* **34,** 504–513 (2001).
88. Oshikiri, T., Takashima, Y., Yamaguchi, H., Harada, A. *J. Am. Chem. Soc.* **127,** 12186–12187 (2005).
89. Oshikiri, T., Takashima, Y., Yamaguchi, H., Harada, A. Face-Selective [2] - and [3] Rotaxanes: Kinetic Control of the Threading Direction of Cyclodextrins. *Chem. Eur. J.* **13,** 7091–7098 (2008).
90. Alberts, B., Johnson, A., Lewis, J., Raff, M., Roberts, K., Walter, P. *Molecular Biology of the Cell*, 5th ed.; Garland Science: New York, (2008).
91. Yin, H., Wang, M. D., Svoboda, K., Landick, R., Block, S. M., Gelles, J. Transcription against an applied force. *Science* **270,** 1653–1657 (1995).
92. Hirokawa, N. Kinesin and dynein superfamily proteins and the mechanism of organelle transport. *Science* **279,** 519–526 (1998).
93. Muraoka, T., Kinbara, K., Aida, T. Mechanical twisting of a guest by a photoresponsive host. *Nature* **440,** 512–515 (2006).
94. Kelly, T. R., De Silva, H., Silva, R. A. Unidirectional rotary motion in a molecular system. *Nature* **401,** 150–152 (1999).
95. Koumura, N., Zijlstra, R. W., van Delden, R. A., Harada, N., Feringa, B. L. Light-driven monodirectional molecular rotor. *Nature* **401,** 152–155 (1999).
96. Fletcher, S. P., Dumur, F., Pollard, M. M., Feringa, B. L. A reversible, unidirectional molecular rotary motor driven by chemical energy. *Science* **310,** 80–82 (2005).
97. Badjić, J. D., Balzani, V., Credi, A., Silvi, S., Stoddart, J. F. A molecular elevator. *Science* **303,** 1845–1849 (2004).
98. Badjic, J. D., Ronconi, C. M., Stoddart, J. F., Balzani, V., Silvi, S., Credi, A. Operating molecular elevators. *J. Am. Chem. Soc.* **128,** 1489–1499 (2006).

99. Durola, F., Lux, J., Sauvage, J. P. A Fast-Moving Copper-Based Molecular Shuttle: Synthesis and Dynamic Properties. *Chem. Eur. J.* **15**, 4124–4134 (2009).
100. Leigh, D. A., Wong, J. K., Dehez, F., Zerbetto, F. Unidirectional rotation in a mechanically interlocked molecular rotor. *Nature* **424,** 174–179 (2003).
101. Niess, F., Duplan, V., Sauvage, J. P. Molecular Muscles: From Species in Solution to Materials and Devices. *Chem. Lett.* **43,** 964–974 (2014).
102. Amirsakis, D. G., Elizarov, A. M., Garcia-Garibay, M. A., Glink, P. T., Stoddart, J. F., White, A. J., Williams, D. J. Diastereospecific Photochemical Dimerization of a Stilbene-Containing Daisy Chain Monomer in Solution as well as in the Solid State. *Angew. Chem. Int. Ed.* **42,** 1126–1132 (2003).
103. Clark, P. G., Day, M. W., Grubbs, R. H. Switching and extension of a [c2] daisy-chain dimer polymer. *J. Am. Chem. Soc.* **131,** 13631–13633 (2009).
104. Wu, J., Leung, K. C. F., Benítez, D., Han, J. Y., Cantrill, S. J., Fang, L., Stoddart, J. F. An Acid–Base-Controllable [c2] Daisy Chain. *Angew. Chem. Int. Ed.* **47,** 7470–7474 (2008).
105. Coutrot, F., Romuald, C., Busseron, E. A new pH-switchable dimannosyl [c2] daisy chain molecular machine. *Org. Lett.* **10,** 3741–3744 (2008).
106. Bruns, C. J., Frasconi, M., Iehl, J., Hartlieb, K. J., Schneebeli, S. T., Cheng, C., Stupp, S. I., Stoddart, J. F. Redox Switchable Daisy Chain Rotaxanes Driven by Radical–Radical Interactions. *J. Am. Chem. Soc.* **136,** 4714–4723 (2014).
107. Tsuda, S., Aso, Y., Kaneda, T. Linear oligomers composed of a photochromically contractible and extendable Janus [2]rotaxane. *Chem. Commun.* 3072–3074 (2006).
108. Onagi, H., Easton, C. J., Lincoln, S. F. An hermaphrodite [2] rotaxane: Preparation and analysis of structure. *Org. Lett.* **3,** 1041–1044 (2001).
109. Yamauchi, K., Takashima, Y., Hashidzume, A., Yamaguchi, H., Harada, A. Switching between supramolecular dimer and nonthreaded supramolecular self-assembly of stilbene amide-α-cyclodextrin by photoirradiation. *J. Am. Chem. Soc.* **130,** 5024–5025 (2008).
110. Tsukagoshi, S., Miyawaki, A., Takashima, Y., Yamaguchi, H., Harada, A. Contraction of supramolecular double-threaded dimer formed by α-cyclodextrin with a long alkyl chain. *Org. Lett.* **9,** 1053–1055 (2007).
111. Jiménez, M. C., Dietrich-Buchecker, C., Sauvage, J. P. Towards synthetic molecular muscles: Contraction and stretching of a linear rotaxane dimer. *Angew. Chem. Int. Ed.* **39,** 3284–3287 (2000).
112. Li, S., Taura, D., Hashidzume, A., Harada, A. Light-switchable Janus [2] rotaxanes based on α-cyclodextrin derivatives bearing two recognition sites linked with oligo (ethylene glycol). *Chem. Asian J.* **5,** 2281–2289 (2010).

113. Dawson, R. E., Lincoln, S. F., Easton, C. J. The foundation of a light driven molecular muscle based on stilbene and α-cyclodextrin. *Chem. Commun.* 3980–3982 (2008).
114. Fang, L., Hmadeh, M., Wu, J., Olson, M. A., Spruell, J. M., Trabolsi, A., Yang, Y. W., Elhabiri, M., Gray, A. M. A., Stoddart, J. F. Acid−Base Actuation of [c 2] Daisy Chains. *J. Am. Chem. Soc.* **131,** 7126–7134 (2009).
115. Liu, Y., Flood, A. H., Bonvallet, P. A., Vignon, S. A., Northrop, B. H., Tseng, H. R., Jeppesen, J. O., Huang, T. J., Brough, B., Baller, M., Magonov, S., Solares, S. D., Goddard, W. A., Ho, C. M., Stoddart, J. F. Linear Artificial Molecular Muscles. *J. Am. Chem. Soc.* **127,** 9745–9759 (2005)
116. Bernál, J., Leigh, D. A., Lubomska, M., Mendoza, S. M., Pérez1, E. M., Rudolf, P., Teobaldi, G., Zerbetto, F. Macroscopic transport by synthetic molecular machines. *Nat. Mater.* **4,** 704–710 (2005).
117. Li, Q., Fuks, G., Moulin, E., Maaloum, M., Rawiso, M., Kulic, I., Giuseppone, N. Macroscopic contraction of a gel induced by the integrated motion of light-driven molecular motors. *Nat. Nanotechnol.* **10,** 161–165 (2015).
118. Harada, A., Kobayashi, R., Takashima, Y., Hashidzume, A., Yamaguchi, H. Macroscopic self-assembly through molecular recognition. *Nat. Chem.* **3,** 34–37(2011).
119. Yamaguchi, H., Kobayashi, R., Takashima, Y., Hashidzume, A., Harada, A. Self-assembly of gels through molecular recognition of cyclodextrins: Shape selectivity for linear and cyclic guest molecules. *Macromolecules* **44,** 2395–2399 (2011).
120. Zheng, Y., Hashidzume, A., Takashima, Y., Yamaguchi, H., Harada, A. Macroscopic observations of molecular recognition: Discrimination of the substituted position on the naphthyl group by polyacrylamide gel modified with β-cyclodextrin. *Langmuir*, **27,** 13790–13795 (2011).
121. Yamaguchi, H., Kobayashi, Y., Kobayashi, R., Takashima, Y., Hashidzume, A., Harada, A. Photoswitchable gel assembly based on molecular recognition. *Nat. Commun.* **3,** 603 (2012).
122. Zheng, Y., Hashidzume, A., Takashima, Y., Yamaguchi, H., Harada, A. Switching of macroscopic molecular recognition selectivity using a mixed solvent system. *Nat. Commun.* **3,** 831(2012).
123. Kobayashi, Y., Takashima, Y., Hashidzume, A., Yamaguchi, H., Harada, A. Reversible self-assembly of gels through metal-ligand interactions. *Sci. rep.* **3,** 1243 (2013).
124. Nakamura, T., Takashima, Y., Hashidzume, A., Yamaguchi, H., Harada, A. A metal–ion-responsive adhesive material via switching of molecular recognition properties. *Nat. Commun.* **5,** 4622 (2014).

125. Zheng, Y., Hashidzume, A., Takashima, Y., Yamaguchi, H., Harada, A. Temperature-sensitive macroscopic assembly based on molecular recognition. *ACS Macro Lett.* **1,** 1083–1085 (2012).
126. Zheng, Y., Hashidzume, A., Harada, A. pH‐Responsive Self‐Assembly by Molecular Recognition on a Macroscopic Scale. *Macromol. Rapid Commun.* **34,** 1062–1066 (2013).
127. Nakahata, M., Takashima, Y., Hashidzume, A., Harada, A. Macroscopic Self‐Assembly Based on Complementary Interactions between Nucleobase Pairs. *Chem. Eur. J.* **21,** 2770–2774 (2015).
128. Nakahata, M., Takashima, Y., Yamaguchi, H., Harada, A. Redox-responsive self-healing materials formed from host–guest polymers. *Nat. Commun.* **2,** 511 (2011).
129. Kakuta, T., Takashima, Y., Nakahata, M., Otsubo, M., Yamaguchi, H., Harada, A. Preorganized Hydrogel: Self-Healing Properties of Supramolecular Hydrogels Formed by Polymerization of Host-Guest-Monomers that Contain Cyclodextrins and Hydrophobic Guest Groups. *Adv. Mater.* **25,** 2849–2853 (2013).
130. Kakuta, T., Takashima, Y., Harada, A. Highly elastic supramolecular hydrogels using host–guest Inclusion complexes with cyclodextrins. *Macromolecules* **46,** 4575–4579 (2013).
131. Harada, A., *Macromol. Rapid Commun.* **2015,** Early View.
132. Tamesue, S., Takashima, Y., Yamaguchi, H., Shinkai, S., Harada, A. Photoswitchable supramolecular hydrogels formed by cyclodextrins and azobenzene polymers. *Angew. Chem. Int. Ed.* **122,** 7623–7626 (2010).
133. Takashima, Y., Hatanaka, S., Otsubo, M., Nakahata, M., Kakuta, T., Hashidzume, A., Yaaguchi, H., Harada, A. Expansion–contraction of photoresponsive artificial muscle regulated by host–guest interactions. *Nat. Commun.* 3, 1270 (2012).
134. Nakahata, M., Takashima, Y., Hashidzume, A., Harada, A. Redox-Generated Mechanical Motion of a Supramolecular Polymeric Actuator Based on Host‐Guest Interactions. *Angew. Chem. Int. Ed.* **52,** 5731–5735 (2013).

Chapter 2

Photo-generated [c2]daisy chain of C_2 symmetric doubly-threaded rotaxanes for contraction and expansion structures.

Introduction

Biological molecular motors such as muscle fibers, flagella and cilia[1–8] are precisely designed in nature, and are reminiscent of microscale electronic and mechanical devices The actin and myosin convert chemical energy from ATP hydrolysis to the linear movement as mechanical work, which produce contraction and expansion of sarcomar. Inspired by the linear movement of biological systems, supramolecular researchers have tried to prepare artificial molecular motors using cyclic molecules. Rotaxanes are considered to be a good example of controlled molecular movement in linear molecular motor systems. Recently, studies on controlled synthetic linear molecular motors have been reported by using rotaxane, which are achieved by controlling linear movement. Design of artificial molecular motors regards ring, axis, and bulky stopper molecules of rotaxan as myosin, actin, and Z-discs.[1, 2] Previously, there are linear type artificial molecular motors with [c2]daisy chain.[3–16] Photo-stimulus is useful energy to generate the linear motion due to tunable wavelength and switching. Photo-generated linear motion using [c2]daisy chain was developed by Kaneda *et al.*[1, 2] They introduce a long linker molecule to control the molecular motion by using the isomerization of an azobenzene (Azo) moiety in the [c2]daisy chain unit because the dissociated αCD unit from the Azo unit moves onto the linker molecule. The association constant of α-cyclodextrin (αCD) for *trans*-Azo is larger than that for *cis*-Azo (*trans*-Azo; K_a = 12,000 M^{-1}, *cis*-Azo; K_a = 4.1 M^{-1}). Harada *et al.* reported [c2]daisy chain based on αCD and Azo derivative with a poly(ethylene glycol) linker. The [c2]daisy chain shows photo-isomerization and the contraction–expansion behaviour in water.[3]

In this chapter, the author demonstrates the preparation and structural analysis of the [c2]daisy chain with αCD and Azo derivative ([c2]DMTAzoCD$_2$). [c2]DMTAzoCD$_2$ exhibits the sliding properties in response to photo-stimulus in water (Figure 2-1). The experimental procedures of AmAzoCD, [c2]DMTAzoCD$_2$ were shown at page 45–61.

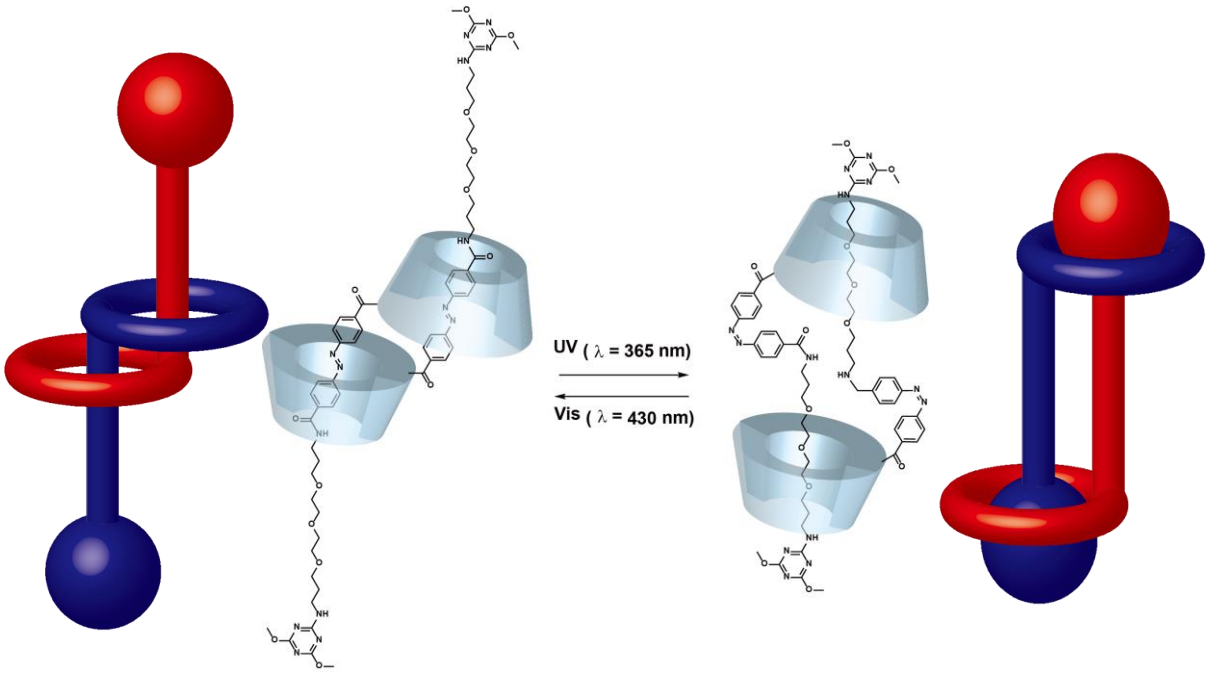

Figure 2-1. Chemical structure of [c2]DMTAzoCD$_2$

Results and discussion

Preparation and structural characterization of [c2]daisy chain

^{1}H NMR measurements of 3A-αCD with the amino-Azo derivative (AmAzoCD) determines the supramolecular structure of [c2]daisy chain in D_2O or DMSO-d_6 (2.0 mM in 700 μL). The peaks of the Azo unit split symmetrically in D_2O but asymmetrically in DMSO-d_6 (Figure 2-2). ^{1}H 2D ROESY NMR spectrum shows the correlation signals between the Azo protons and the inner protons of αCD ((C^3H, C^5H)) in D_2O (Figure 2-3). However the ROESY NMR spectrum in DMSO does not. These results indicate that the AmAzoCD forms a symmetric inclusion structure in water.

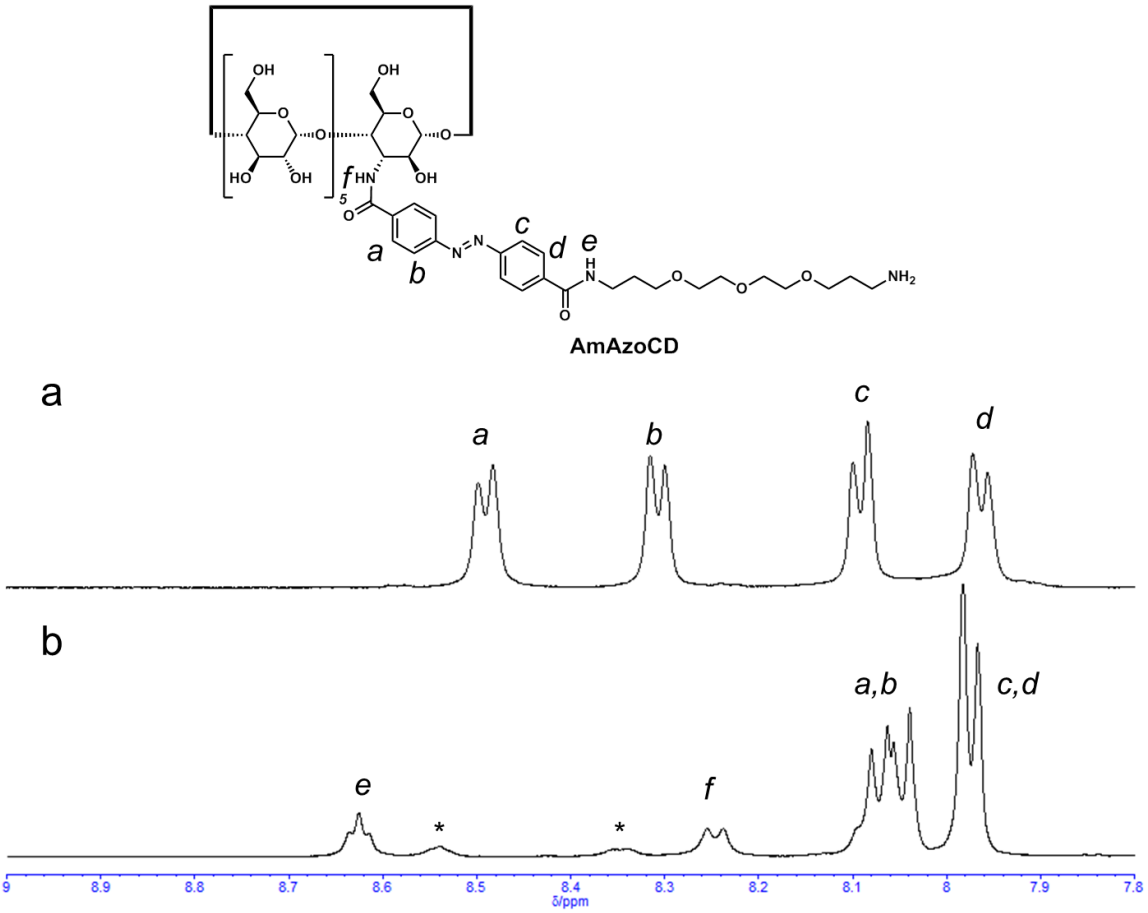

Figure 2-2. ^{1}H NMR spectra of AmAzoCD in **a)** D_2O, and **b)** DMSO-d_6. * is partial formed AmAzoCD inclusion complexes.

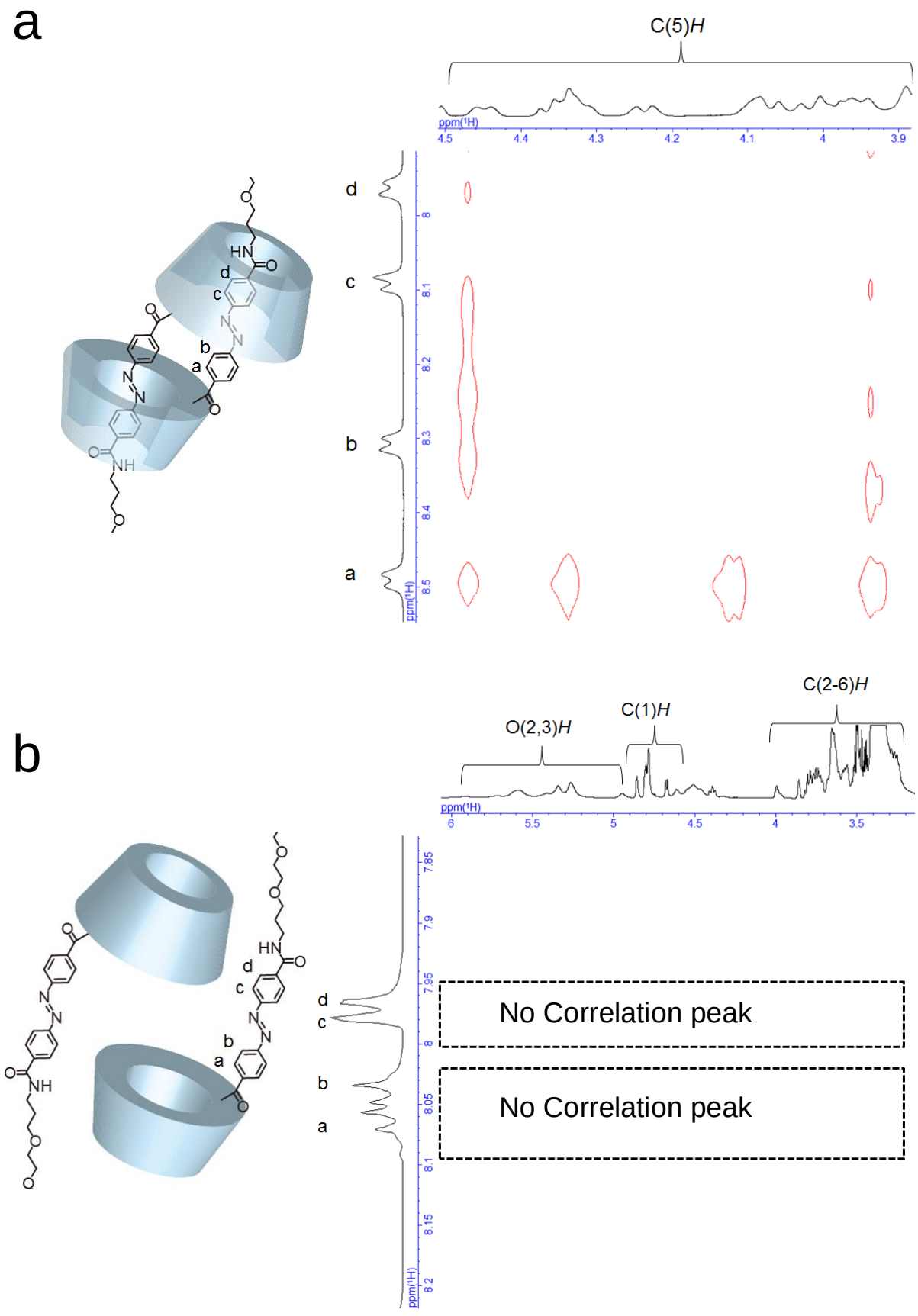

Figure 2-3. 2D ROESY NMR spectra of AmAzoCD in **a)** D_2O, and **b)** DMSO-d_6.

The introduction of bulky stopper into AmAzoCD

On the basis of the above results, AmAzoCD forms a symmetric supramolecular structure in aqueous solution. But the species of the supramolecular structure is not observed by mass spectroscopy due to dissociation of the [c2]daisy chain structure by laser impact of mass spectrometer.

To observe the species of the [c2]daisy chain structure, bulky stopper are introduced into the terminal group of the amino group of AmAzoCD, which forms a mechanically interlocked molecule ([c2]DMTAzoCD$_2$). 2-Chloro-4,6-dimethoxy-1,3,5-triazine (DMT-Cl) as a bulky stopper was introduced into AmAzoCD by nucleophilic imidoyl substitution in water. [c2]DMTAzoCD$_2$ was purified by reversed phase HPLC with an MS detector (Figure 2-4).

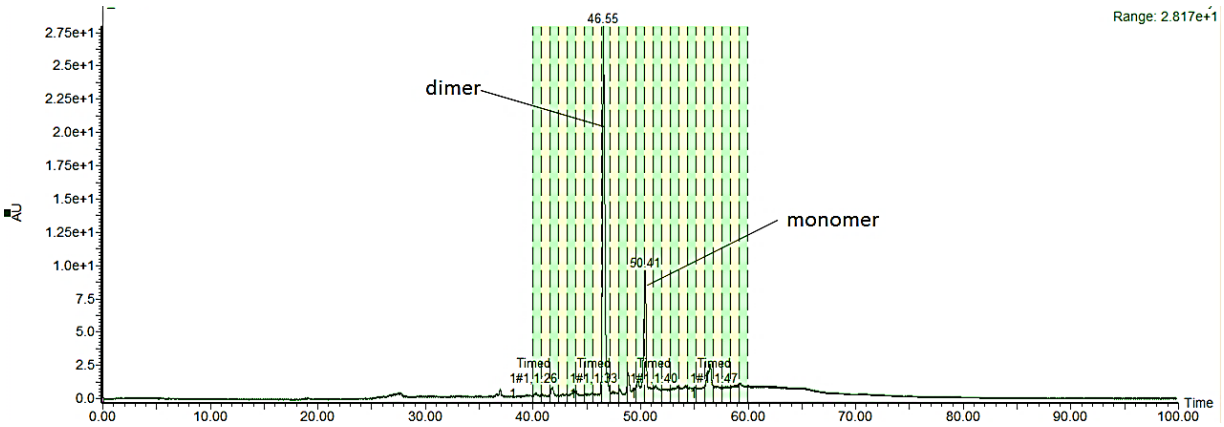

Figure 2-4. HPLC-MS chromatogram of the reaction mixture of AmAzoCD and DMT-Cl.

Figure 2-4 shows that the crude product contains two products. One is dimer of AmAzoCD ([c2]DMTAzoCD$_2$), and the other was monomeric AmAzoCD with DMT-Cl, called DMTAzoCD. [c2]DMTAzoCD$_2$ and DMTAzoCD were collected in 24 and 9% yield, respectively (Scheme 2-1). The MALDI-TOF mass spectra of these products display dimeric and monomeric peaks.

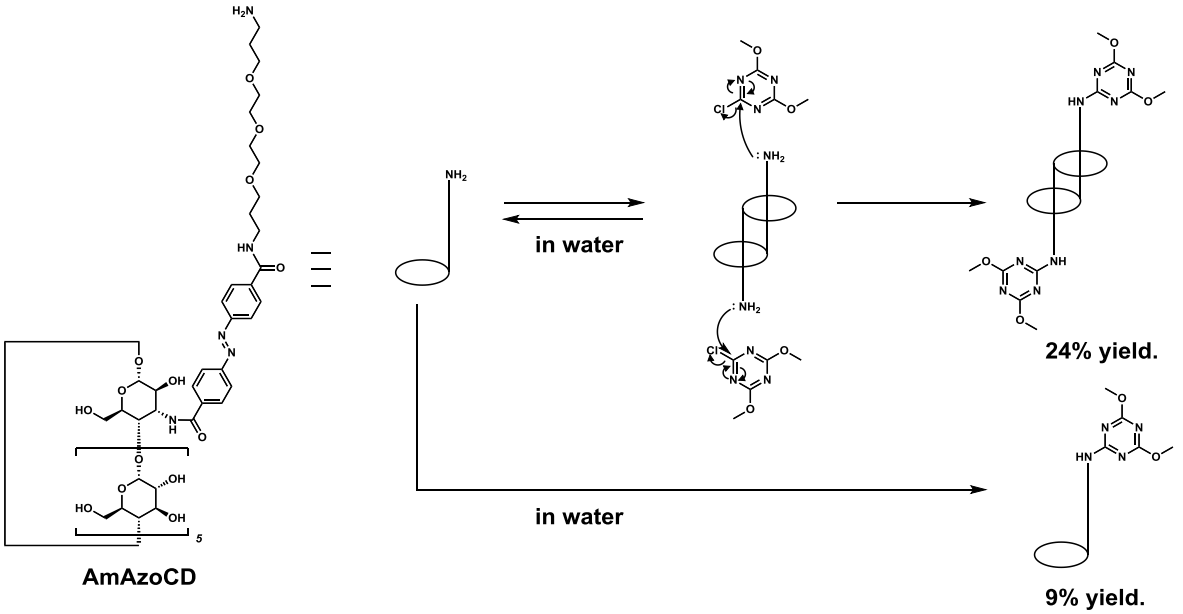

Scheme 2-1. Preparation of mechanically interlocked supramolecular structure by nucleophilic imidoyl substitution.

Structural analysis of [c2]DMTAzoCD$_2$

The author investigated the spectroscopic analysis for [c2]DMTAzoCD$_2$. The ^{1}H NMR spectrum of [c2]DMTAzoCD$_2$ in D_2O was characterized by 2D H-H TOCSY, COSY, and ROESY NMR spectra (Figure 2-5, 2-6, and 2-7). The results indicate that the structure of [c2]DMTAzoCD$_2$ a C_2 symmetric doubly-threaded dimer structure. There are two estimated structure of [c2]DMTAzoCD$_2$. One is the doubly-threaded and the other is linear dimer. 2D ROESY NMR spectrum (Figure 2-8) indicates that the correlation between all Azo protons (*a*, *b*, *c*, *d*) and inner protons of αCD (C_3, A_3, C_5, A_5). Therefore, the [c2]DMTAzoCD$_2$ has a C_2 symmetric doubly-threaded dimer structure.

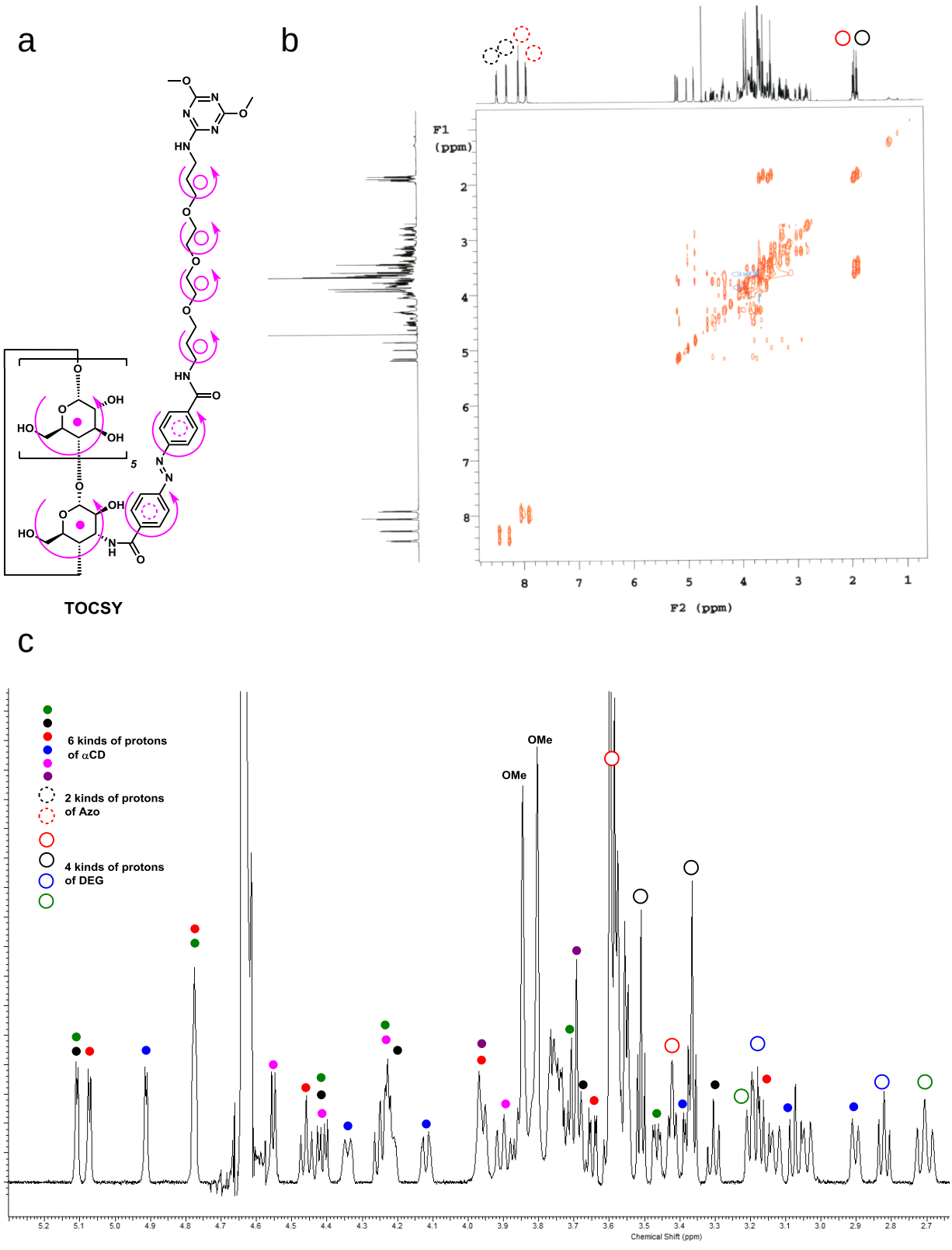

Figure 2-5. 2D TOCSY NMR spectra of [c2]DMTAzoCD$_2$. **a)** Schematic illustration of the correlation of TOCSY spectrum. Pink arrows mean the rage of indirect spin coupling. **b)** full and **c)** a partial spectrum. Dots (CD), dashed circles (Azo), and circles (DEG) mean the deference of spin coupling.

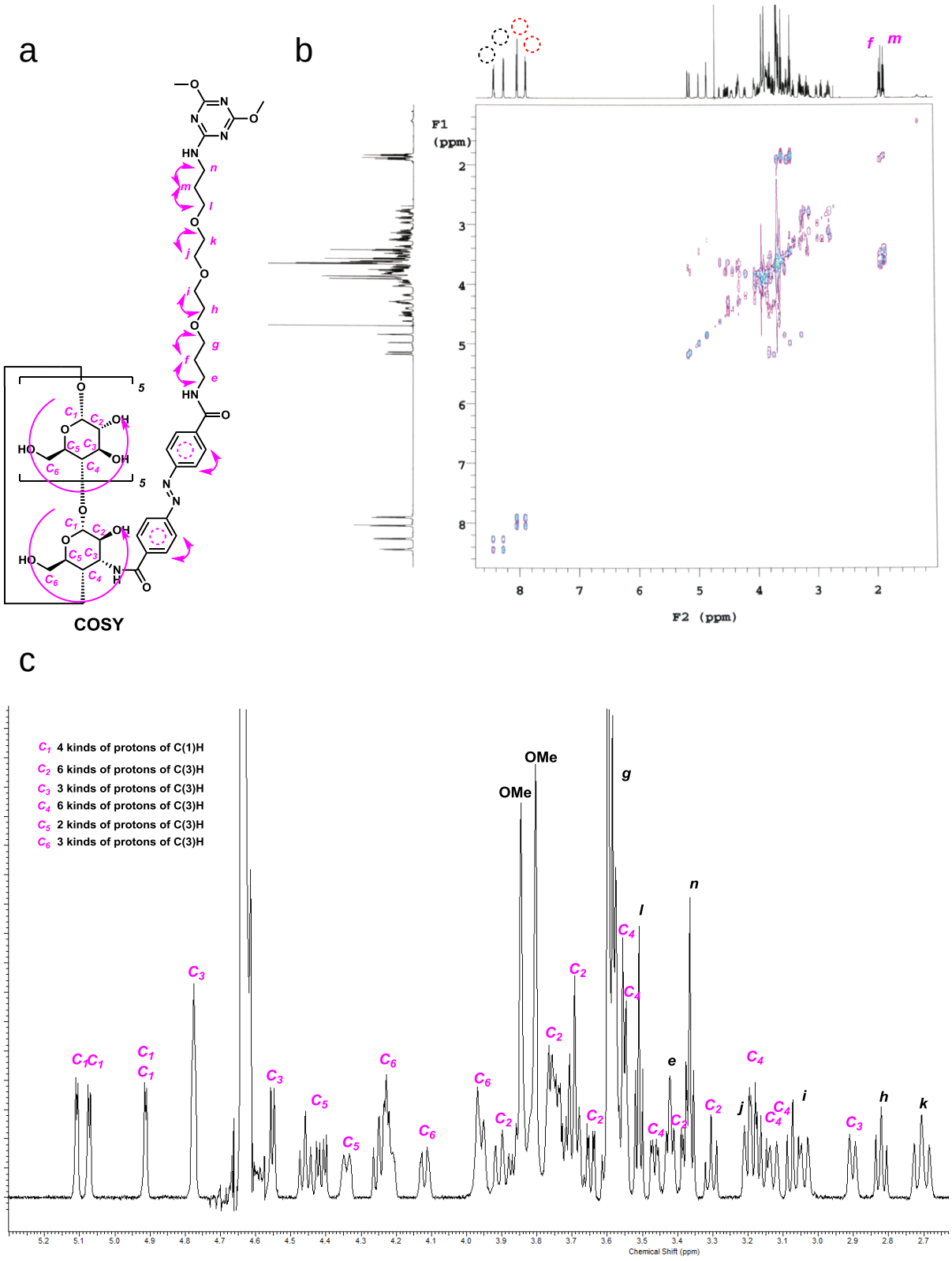

Figure 2-6. 2D COSY NMR spectra of [c2]DMTAzoCD$_2$. **a)** Schematic illustration of the correlation of COSY spectrum. Pink arrows mean the rage of direct spin coupling. **b)** full and **c)** a partial spectrum. Dashed circles mean the deference of spin coupling.

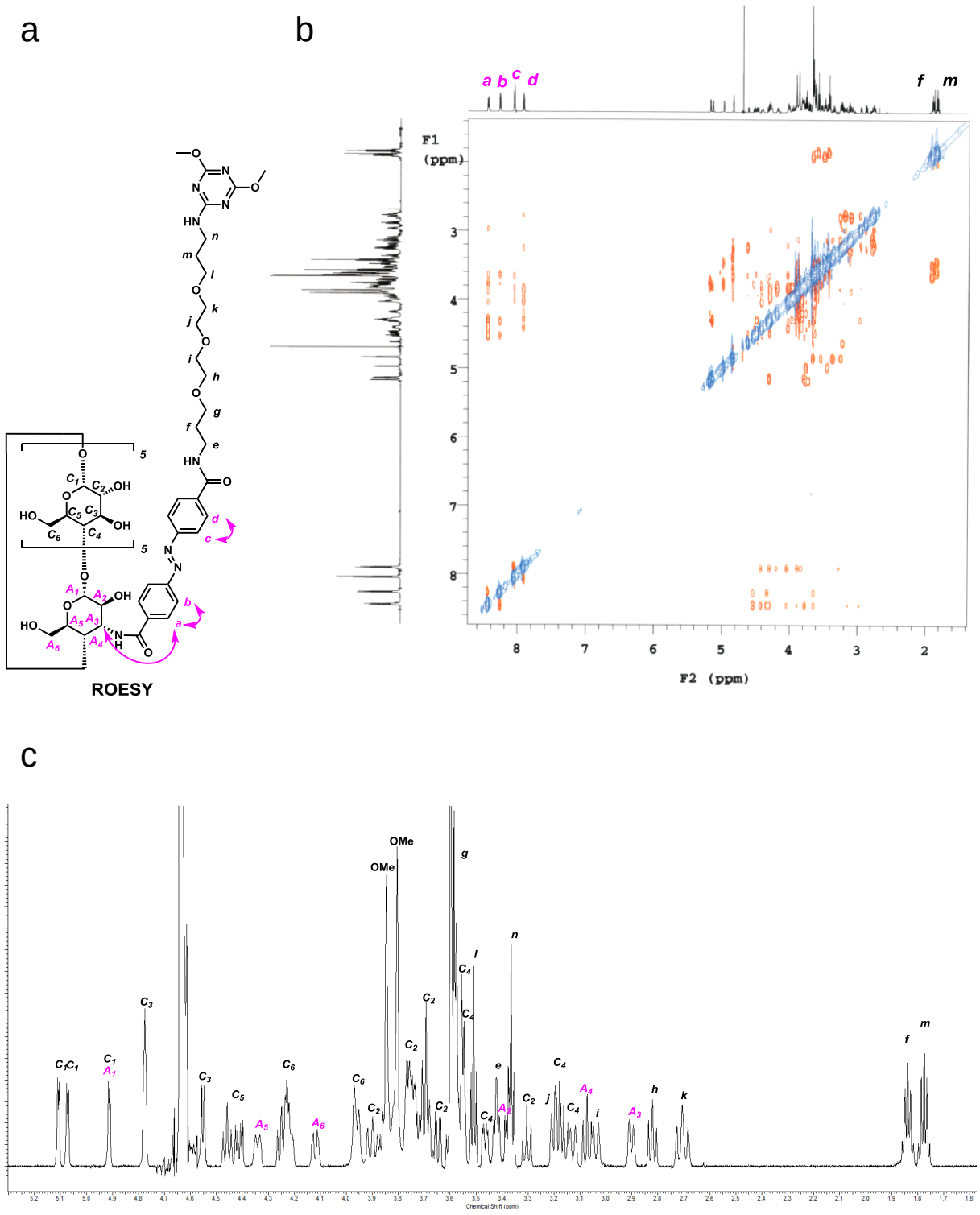

Figure 2-7. 2D ROESY NMR spectra of [c2]DMTAzoCD$_2$. **a)** Schematic illustration of the correlation of ROESY spectra. Pink arrows mean the rage of spatial spin coupling. **b)** full and **c)** a partial spectrum.

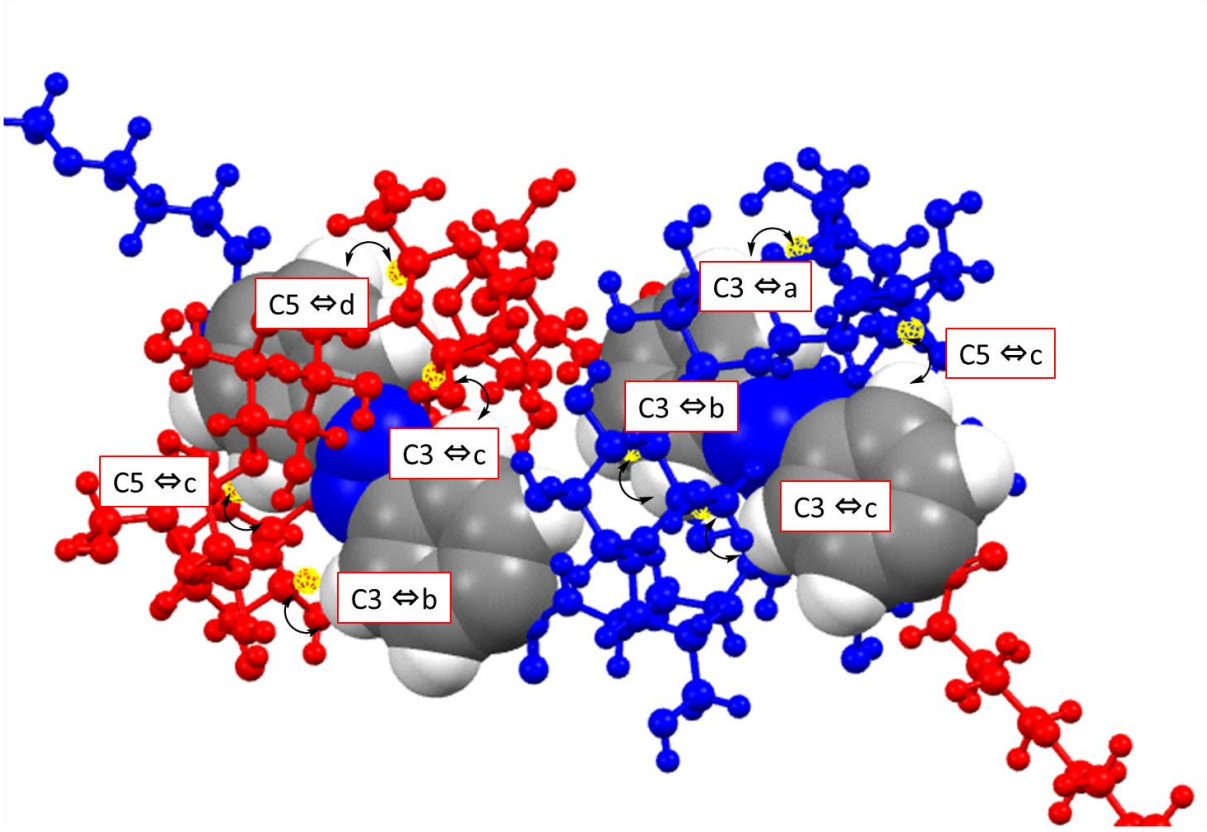

Figure 2-8. A partial structure of [c2]DMTAzoCD$_2$ to indicate the correlation between Azo protons and inner protons of αCD. The structure of [c2]DMTAzoCD$_2$ is C_2 symmetric doubly-threaded rotaxane.

^{1}H Variable Temperature NMR measurement of [c2]DMTAzoCD$_2$.

To investigate the sliding motion of [c2]DMTAzoCD$_2$, ^{1}H variable temperature (VT) NMR spectra were measured at the temperature range of 293–353 K in D$_2$O and DMSO-d_6. The molar content of [c2]DMTAzoCD$_2$ was 2 mM in 700 μL in D$_2$O or DMSO-d_6. In D$_2$O, all signals of [c2]DMTAzoCD$_2$ did not change in the range of temperature. On the other hand in DMSO-d_6, the signals of *b* protons in the methylene were broad whereas those of *a* protons were not observed (Figure 2-9). It is suggested that the αCD unit of [c2]DMTAzoCD$_2$ shows the sliding motion in DMSO-d_6, The sliding speed may be similar to the time scale of ^{1}H NMR measurements at lower temperatures, but the speed may be higher at higher temperatures. The αCD residue in [c2]DMTAzoCD$_2$ shuttles from the Azo residue to the oligomethylene residue and *vice versa*.

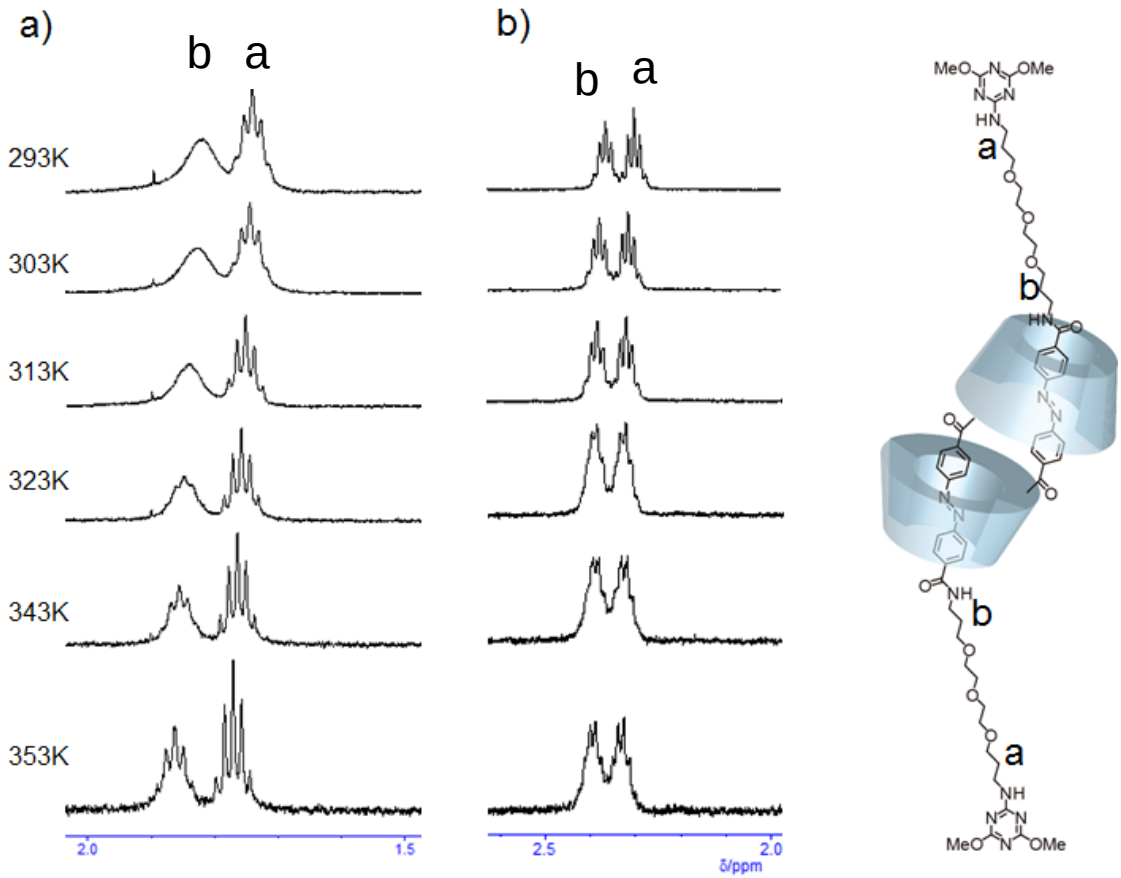

Figure 2-9. ^{1}H VT NMR spectra of [c2]DMTAzoCD$_2$ in **a)** D$_2$O and **b)** DMSO-d_6 the range of temperature was between 293–353 K.

Photo-isomerization of [c2]DMTAzoCD$_2$.

UV-Vis spectroscopy tracks the photo-isomerization of the Azo group in [c2]DMTAzoCD$_2$ (Figure 2-10). Generally, Azo derivatives show *trans*- and *cis*-photo-isomerization by UV and Vis light irradiation, respectively. The absorption band ascribable to the π–π* transition decreased upon irradiation with UV light (λ = 365 nm) and an n–π* transition band appears until 20 min. Conversely, the absorption band ascribable to the π–π* transition restored upon irradiation with Vis light (λ = 430 nm) and an n–π* transition band disappears until 80 s. These results indicate that UV irradiation causes the *trans*-Azo group of [c2]DMTAzoCD$_2$ to isomerize into the *cis*-form, whereas Vis irradiation causes the *cis*-Azo group to restore into the *trans*-form (Scheme 2-2).

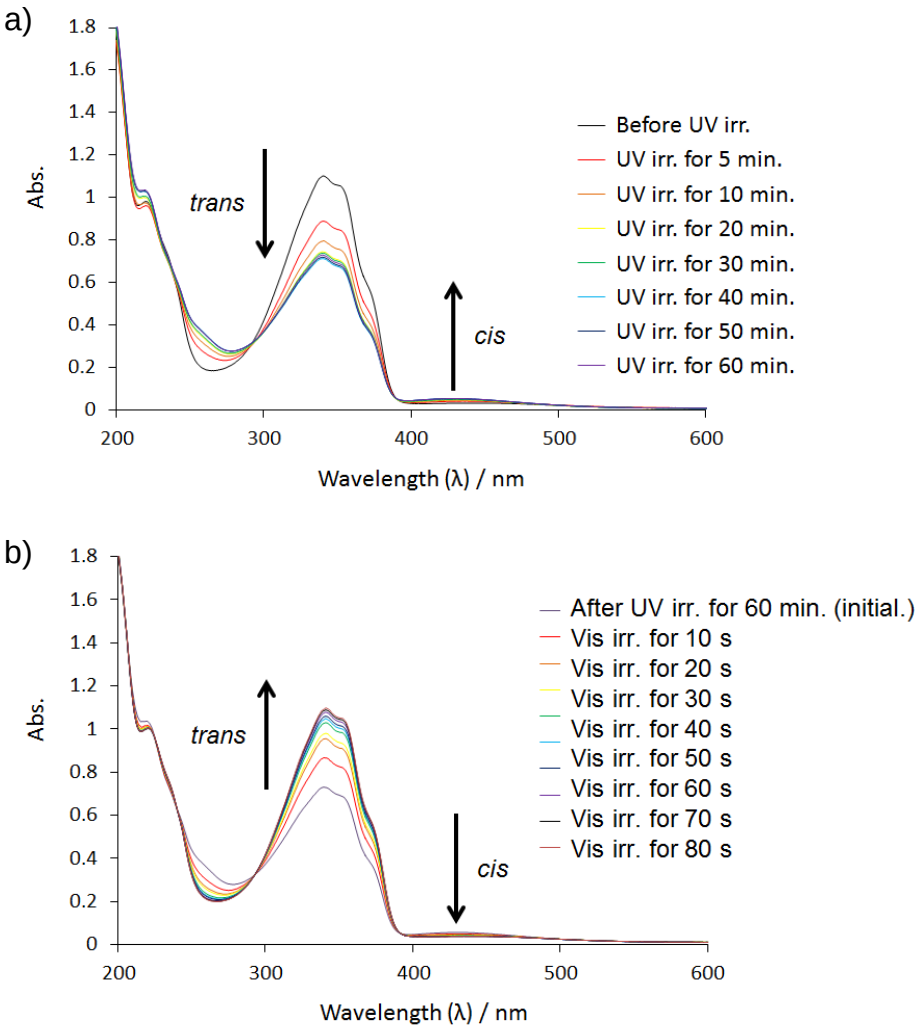

Figure 2-10. Time-resolved absorption spectra for [c2]DMTAzoCD$_2$ under photo-irradiation with **a)** UV and **b)** visible lights, respectively.

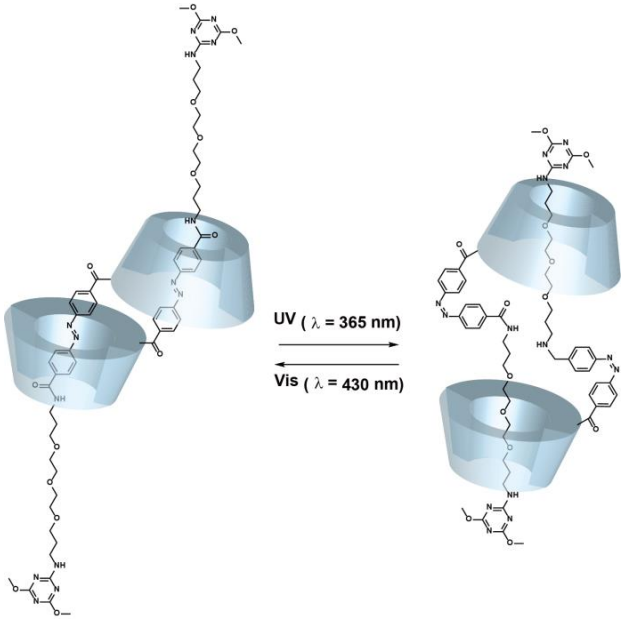

Scheme 2-2. Schematic illustration of photo-isomerization of [c2]DMTAzoCD$_2$.

Photo actuation of [c2]AzoCD$_2$

Finally, contraction and expansion crystals of [c2]AzoCD$_2$ were prepared. AmAzoCD formed needle crystals consisting of [c2]daisy chain structure by lyophilized from aqueous solution of AmAzoCD. The size of crystals nearly 100 × 50 μm^2. When the crystals irradiated by UV light following irradiating Vis light, the crystal expanded. Subsequent, the Vis light irradiation, the length of crystals restored.

Experimental

Materials. Acetone, triethylamine (Et_3N), tetrahydrofuran (THF), dimethyl sulfoxide (DMSO), *N*,*N*-dimethyl formamide (DMF), chloroform ($CHCl_3$), dichloromethane (CH_2Cl_2), methanol (MeOH), *N*,*N*´-dicyclohexylcarbodiimide (DCC), *N*-hydroxysuccinimide (HOSu), acetic acid (AcOH), 12 M hydrochloric acid (HCl aq.), ammonia water, and sodium sulfate (Na_2SO_4) were obtained from Nacalai Tesque. Di-*tert*-butyl dicarbonate was obtained from Peptide Institute Inc. 4-(4,6-Dimethoxy-1,3,5-triazine-2-yl)-4-methylmorpholinium chloride (DMT-MM) was obtained from Wako Pure Chemical Industries. (Benzotriazol-1-yloxy)-tris(dimetylamino)phosphonium hexafluorophosphate (BOP), 2-chloro-4,6-dimethoxy-1,3,5-triazine (DMT-Cl), and 3A-amino-3A-deoxy-(2AS, 3AS)-α-cyclodextrin were purchased from Tokyo Kasei. 4,7,10-Trioxa-1,13-tridecanediamine (DEG) was obtained from Sigma-Aldrich. A highly porous synthetic resin (DIAION HP-20), which was used for reverse-phase column chromatography, was purchased from Mitsubishi Chemical. SNAP Ultra 50 g was purchased from Biotage®. Water used to prepare aqueous solutions (except for NMR measurements) was purified with a Millipore Elix 5 system. Other reagents were used without further purification.

Measurements

Photo-isomerization. Azobenzene moieties were isomerized by photo-irradiation using a 300 W Xenon lamp (Asahi spectra MAX-301) equipped with suitable mirror modules (UV mirror module, λ = 250–385 nm; Vis mirror module, λ = 385–740 nm). Moreover, to extract a specific wavelength, a band-pass filter (LX0365) for UV light and a band-pass filter (LX0430) for visible light were placed on the Xenon lamp. The intensities of the transmitted UV light (λ = 365 nm) through the band-pass filters (LX0365) using a suitable mirror module were similar to those of Vis light (λ = 430 nm) using the band-pass filter (LX0430). The distance between the sample cell and the lamp was fixed at 10 cm.

NMR spectrometer. ^{1}H, ^{13}C, and 2D NMR spectra were recorded with JEOL ECA500 NMR spectrometer and VARIAN VNMRJ 600 NMR spectrometers at 30 °C. Chemical shifts were referenced to the solvents (δ = 2.49 ppm for DMSO and δ = 4.79 ppm for HOD).

UV-Vis absorption spectrometer. The UV-Vis absorption spectra were recorded with JASCO V-650 and Hitachi U-4100 spectrometers in water with a 1 mm quartz cell at room temperature.

Preparation of Am-DEG-Boc

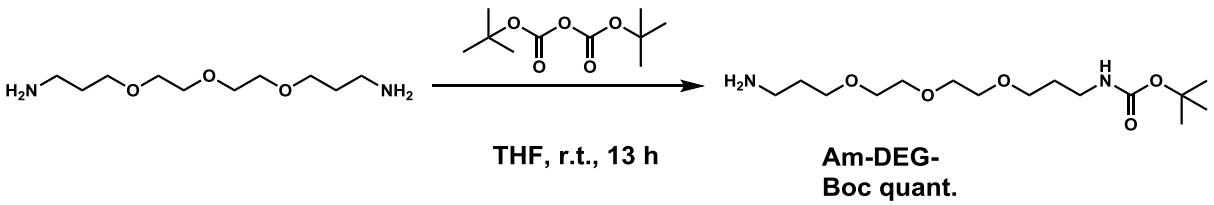

Scheme 2-3. Preparation of Am-DEG-Boc.

DEG (30 g, 140 mmol) was dissolved in THF (65 mL). Di-*tert*-butyl dicarbonate (5.3 mL, 23 mmol) dissolved in THF (65 mL) was slowly added to the THF solution of DEG over 5 min. The resulting mixture was stirred at room temperature for 16 hours. The pale-yellow solution was evaporated. The oil was poured into water (150 mL) and extracted with 50 mL CH_2Cl_2 three times. The organic layer was washed by water and dried over Na_2SO_4. After filtration, the solvent was evaporated to give Am-DEG-Boc as colorless oil (7.5 g, quant.). ^{1}H NMR (500 MHz, DMSO-d_6): δ (ppm) 6.73 (br, 1H), 3.51–3.40 (m, overlaps with H_2O), 3.37(t, J = 6.4 Hz, 2H), 2.94 (dd, J = 6.7 Hz, 6.2 Hz, 2H), 2.55 (t, J = 6.8 Hz, 2H), 1.58 (quintet, J = 6.8 Hz, 6.4 Hz, 2H), 1.54 (quintet, J = 6.6 Hz, 2H), 1.36 (s, 9H). ^{13}C NMR (125 MHz, DMSO-d_6): δ (ppm) 155.55, 77.33, 69.79, 69.77, 69.53, 69.49, 68.46, 68.08, 38.80, 37.21, 33.31, 29.69, 28.22. MALDI-TOF MS: *m/z* Calcd. for $C_{16}H_{32}O_5N_2$ ($[M + H]^+$): 321.2; Found: 321.1.

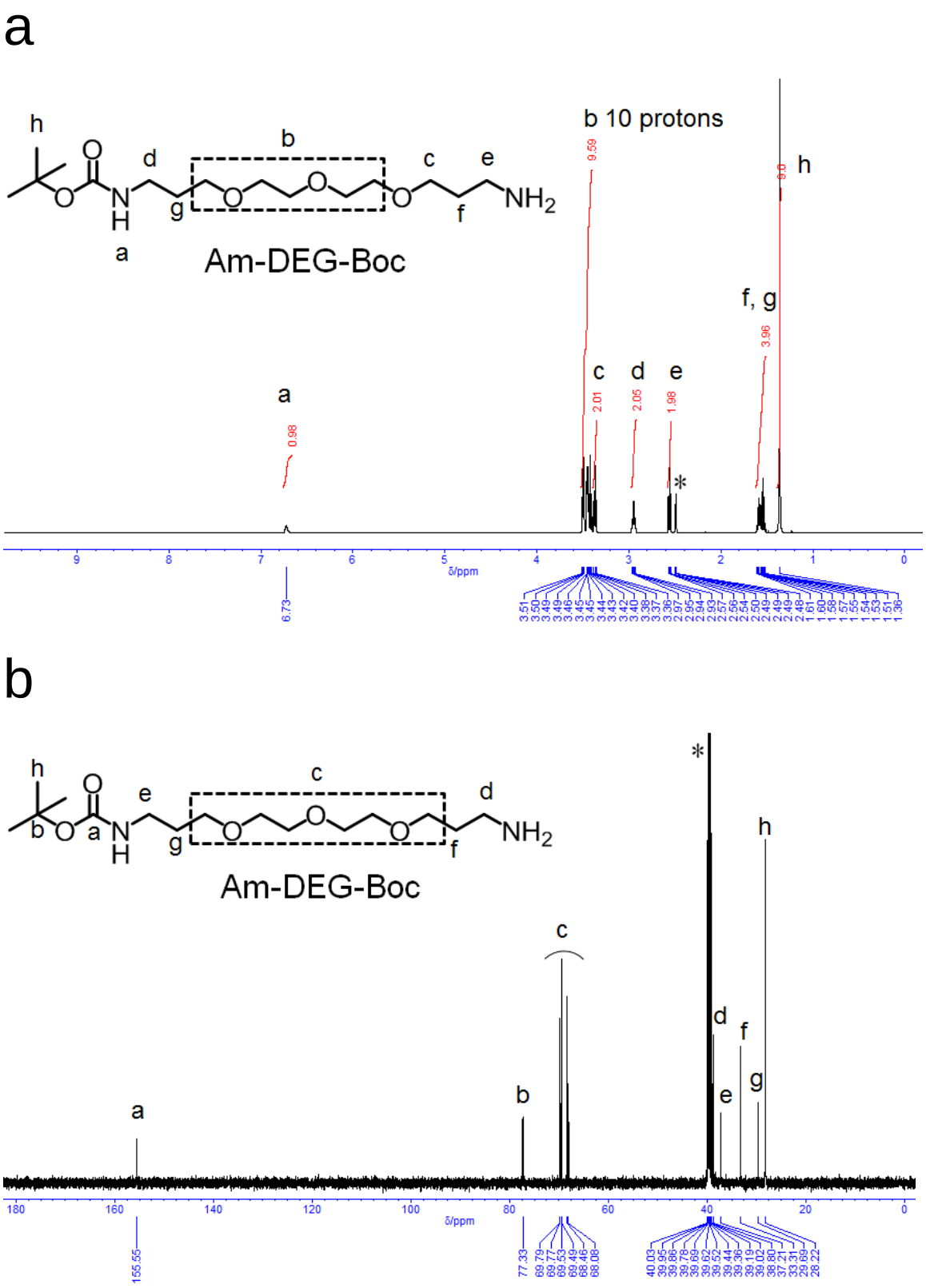

Figure 2-11. **a)** 500 MHz ^{1}H and **b)** 125 MHz ^{13}C NMR spectra of Am-DEG-Boc in DMSO-d_6. "*" denotes the signals due to the solvent used.

Preparation of compound Azo-DEG-Boc

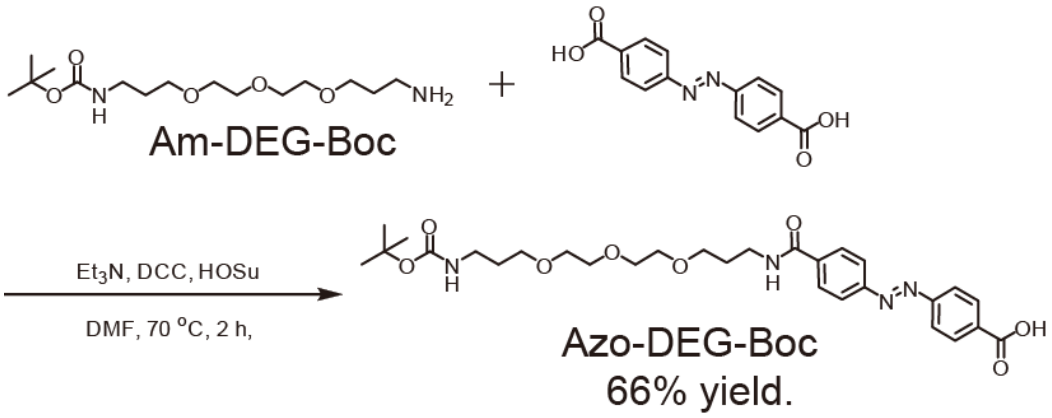

Scheme 2-4. Preparation of Azo-DEG-Boc.

4-(4-Carboxyphenyl)-azo-benzoic acid (2.4 g, 9.0 mmol), DCC (0.74 g, 3.6 mmol), HOSu (0.42 g, 3.6 mmol) and Et_3N (2.9 mL, 21 mmol) were added in DMF (40 mL). The solution was added to the DMF (20 mL) solution of Am-DEG-Boc. When stirred at 70 °C, the solution charged to the suspension to form *N*,*N*´-dicyclohexylurea. After 2 hours, AcOH (3.0 mL) was added. The solvent was evaporated from resulting mixture. The residue was dispersed in MeOH. After filtration, the filtrate was poured into water (50 mL) and crude product was extracted with $CHCl_3$ (100 mL). The organic layer was washed with water and dried over Na_2SO_4. After evaporating the organic layer, the residue was applied to a Biotage® SNAP Ultra 50 g column. The desired product was obtained in a fraction which was eluted with a mixed solvent of $CHCl_3$ and MeOH (0/100–5/95, v/v). Azo-DEG-Boc was obtained as a red solid (1.1 g, 66%). ^{1}H NMR (500 MHz, DMSO-d_6): δ (ppm) 8.61 (t, J = 5.4 Hz, 1H), 8.15 (d, J = 8.7 Hz, 2H), 8.05 (d, J = 8.7 Hz, 2H), 7.99–7.88 (m, 4H), 6.70 (br, 1H), 3.52–3.43 (m, 10H), 3.37–3.31 (m, overlaps with H_2O), 2.95 (dd, J = 6.7 Hz, 6.3 Hz, 2H), 1.78 (quintet, J = 6.7 Hz, 2H), 1.58 (quintet, J = 6.5 Hz, 2H), 1.35 (s, 9H). ^{13}C NMR (125 MHz, DMSO-d_6): δ (ppm) 166.63, 165.31, 155.55, 154.23, 153.15, 137.37, 133.21, 130.65, 128.51, 122.71, 122.60, 77.36, 69.79, 69.75, 69.57, 69.52, 68.28, 68.08, 37.22, 36.84, 29.69, 29.28, 28.23. MALDI-TOF MS: *m/z* Calcd. for $C_{29}H_{39}O_8N_4Na$ ($[M+Na]^+$): 594.3; Found: 595.2.

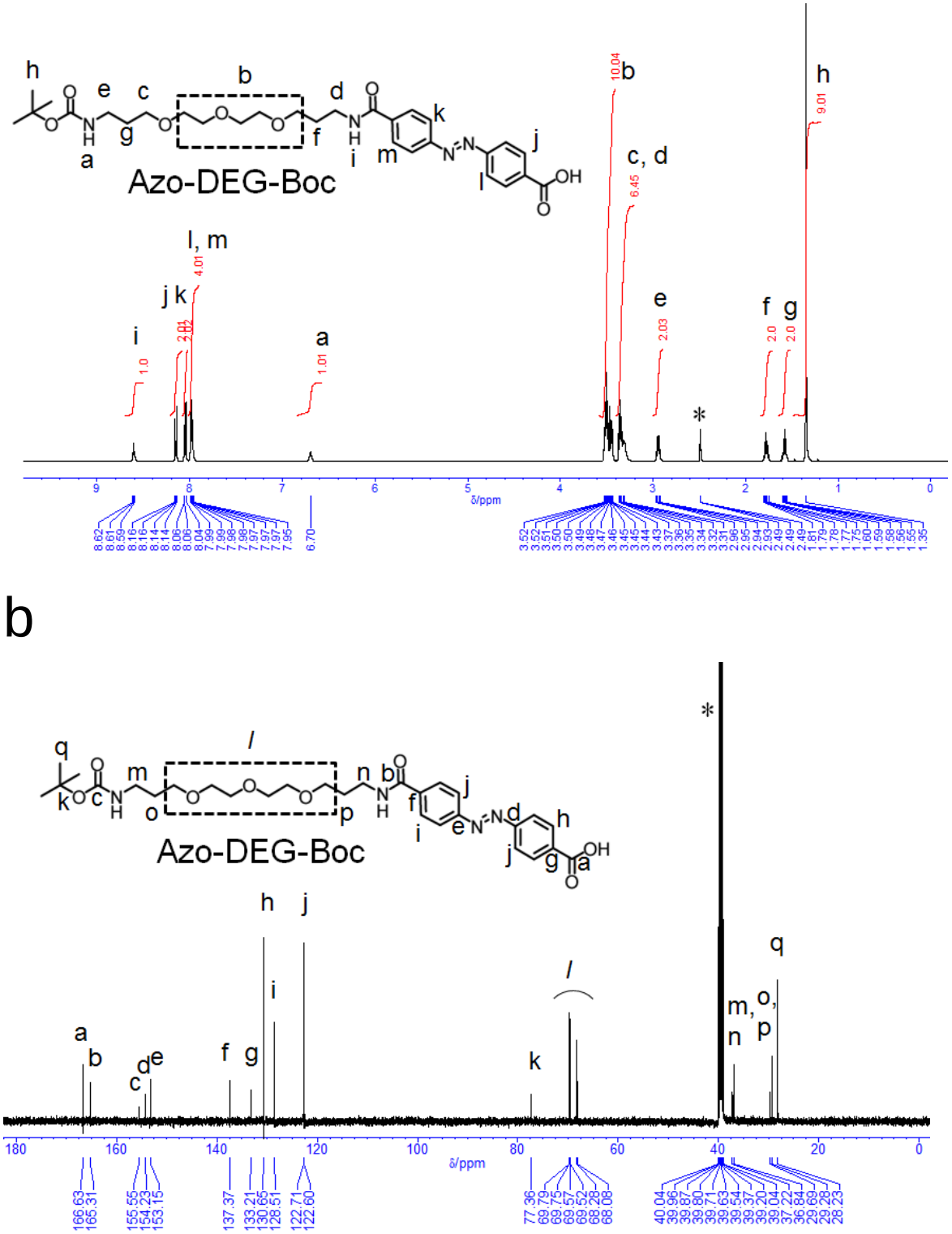

Figure 2-12. **a)** 500 MHz ^{1}H and **b)** 125 MHz ^{13}C NMR spectra of Azo-DEG-Boc in DMSO-d_6. "*" denotes the signals due to the solvent used.

Preparation of compound Boc-AmAzoCD

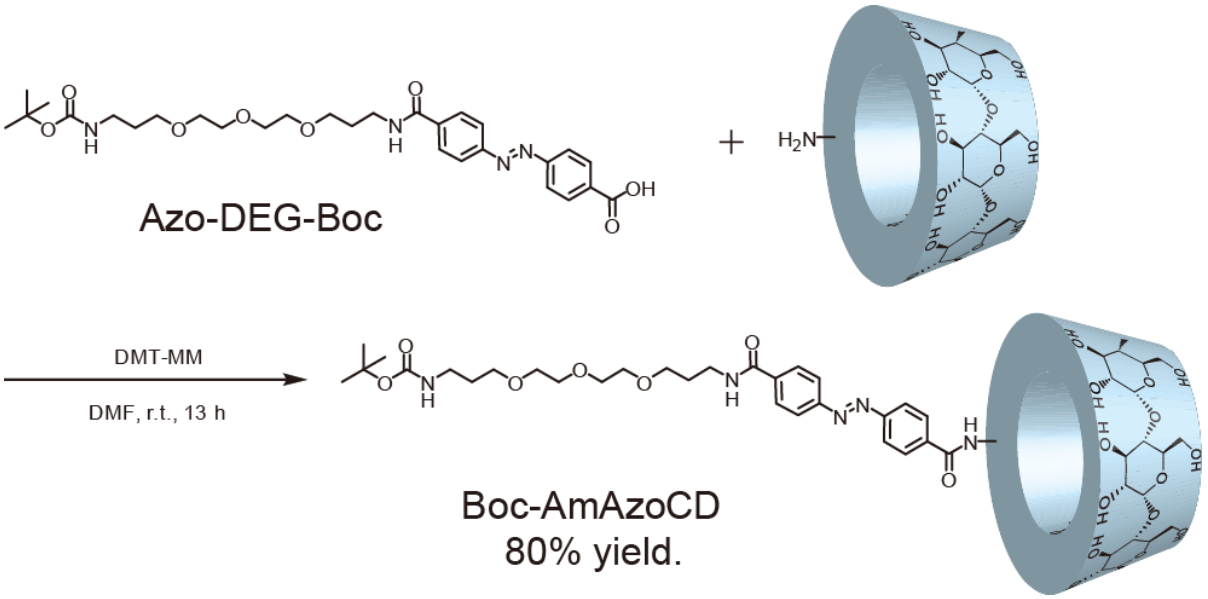

Scheme 2-5. Preparation of Boc-AmAzoCD.

Azo-DEG-Boc (0.36 g, 0.63 mmol) and 3A-amino-3A-deoxy-(2AS, 3AS)-α-CD (0.61 g 0.63 mmol) were dissolved in dry DMF (6.3 mL). DMT-MM (0.26 g, 0.95 mmol) was added to the DMF solution. After stirring for 13 hours at room temperature, the suspension changed to the homogeneous solution. The solvent was evaporated from resulting mixture and residue was dispersed in water to remove Azo-DEG-Boc. The filtrate was applied to a Diaion HP-20 resin column (15 × 13 cm^3) running using a mixed solvent of H_2O and MeOH with a gradient of the volume ratio. The desired product, Boc-AmAzoCD, was obtained in a fraction which was eluted with a mixed solvent of H_2O and MeOH (3/7–7/3, v/v). The obtained solution was lyophilised to give Boc-AmAzoCD as a pale-orange powder (0.76 g, 80%). ^{1}H NMR (500 MHz, DMSO-d_6): δ (ppm) 8.61 (br, 1H), 8.22 (d, J = 9 Hz, 1H), 8.06 (t, J = 9 Hz, 4H), 7.97 (dd, J = 9 Hz, 2 Hz, 4H), 6.70 (br, 1H), 5.90 (d, J = 6 Hz, 1H), 5.70 (d, J = 2 Hz, 1H), 5.61–5.54 (m, 3H), 5.40 (d, J = 7 Hz, 1H), 5.32–5.31 (m, 2H), 5.25–5.21 (m, 3H), 4.92 (t, J = 5 Hz, 1H), 4.86 (d, J = 4 Hz, 1H), 4.81-4.79 (m, 4H), 4.68 (d, J = 7 Hz, 1H), 4.58 (t, J = 6 Hz, 1H), 4.53-4.40 (m, 5H), 4.00 (br, 1H), 3.86-3.26 (m, overlaps with H_2O), 2.94 (q, J = 7 Hz, 2H), 1.78 (quintet, J = 7 Hz, 2H), 1.58 (quintet, J = 7 Hz, 2H), 1.35 (s, 9H).

^{13}C NMR (125 MHz, DMSO-d_6): δ (ppm) 165.38, 155.60, 153.19, 137.21, 137.19, 128.76, 128.56, 122.62, 122.57, 104.48, 102.56, 102.16, 102.03, 101.62, 101.15, 83.00, 81.88, 81.73, 81.70, 80.72, 79.78, 77.42, 77.04, 73.71, 73.69, 73.43, 73.25, 72.91, 72.89, 72.54, 72.40, 72.32, 72.22, 72.19, 72.16, 72.08, 72.02, 71.78, 71.57, 70.92, 69.81, 69.79, 69.61, 69.55, 68.28, 68.10, 60.24, 60.17, 60.13, 60.12, 60.04, 60.00, 37.24, 36.85, 29.72, 29.32, 28.27. MALDI-TOF MS: *m/z* Calcd. for $C_{65}H_{99}N_5O_{36}Na$ ($[M + Na]^+$): 1548.6; Found: 1548.2; Calcd. for $C_{65}H_{99}N_5O_{36}K$ ($[M + K]^+$): 1564.6; Found: 1564.2.

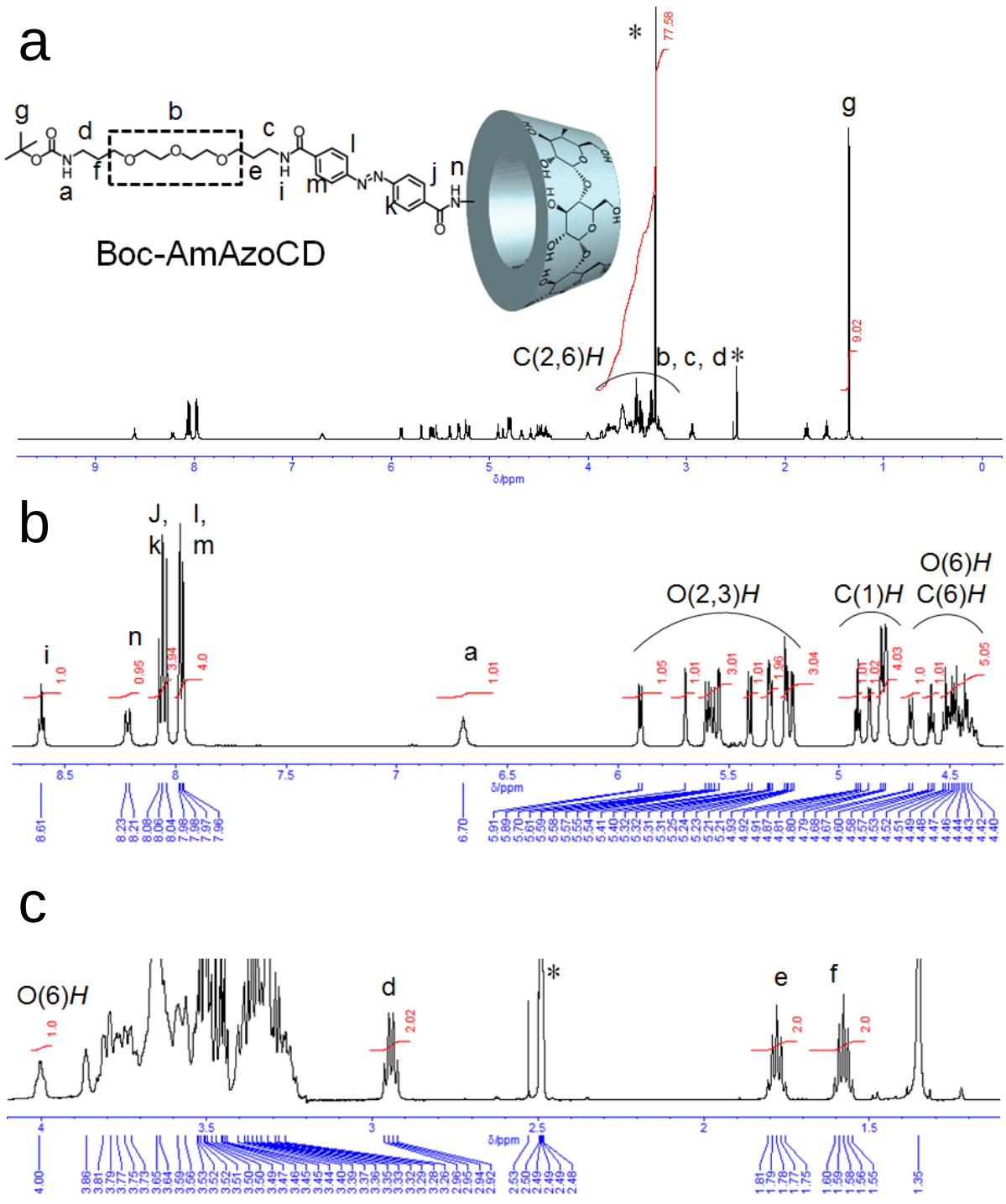

Figure 2-13. 500 MHz ^{1}H NMR spectra of Boc-AmAzoCD in DMSO-d_6. **a)** Full range spectrum. Partial spectra of **b)** 8.75–4.25 ppm and **c)** 4.10–1.10 ppm. "*" denotes the signals due to the solvent used.

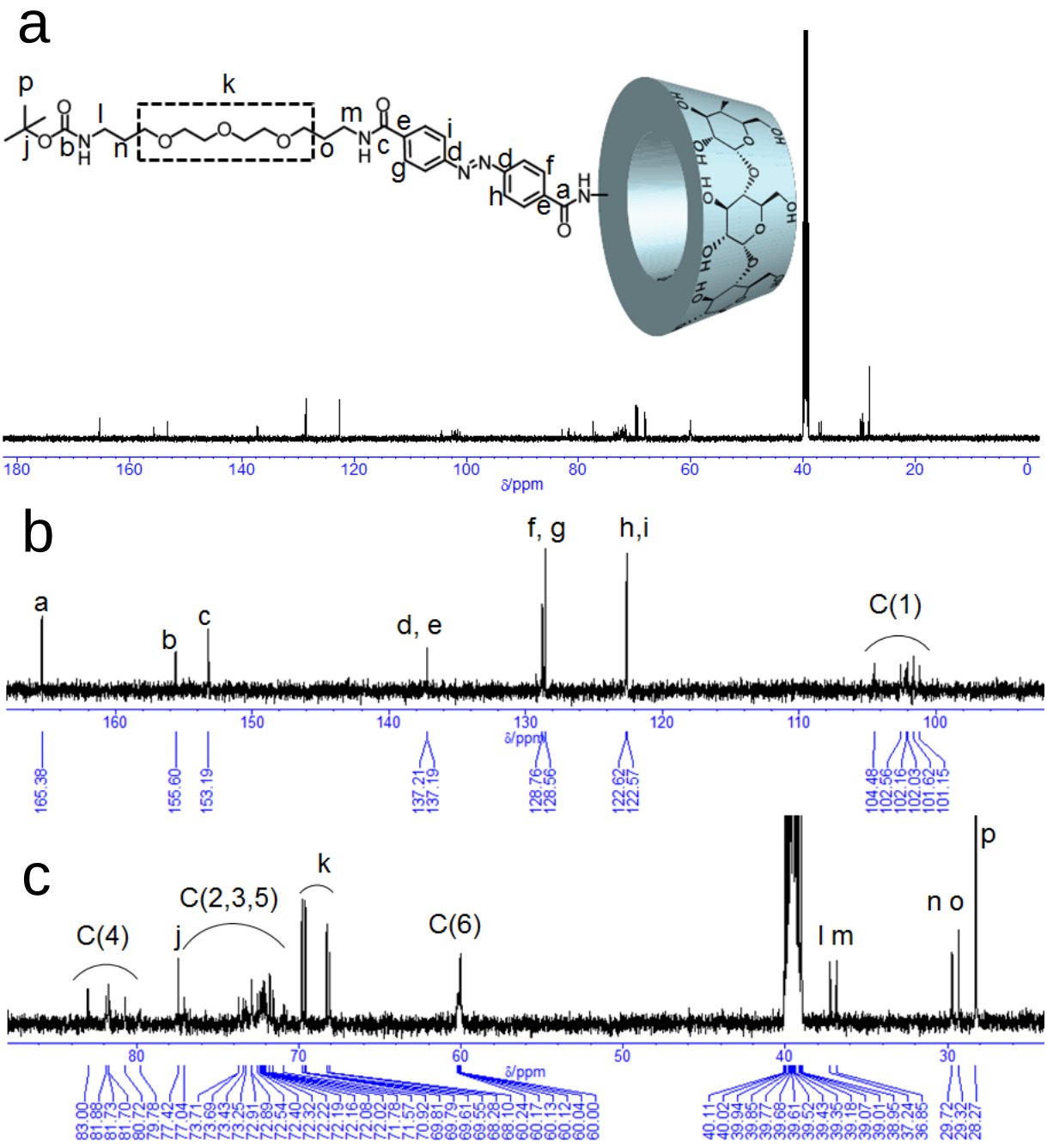

Figure 2-14. 125 MHz ^{13}C NMR spectra of Boc-AmAzoCD in DMSO-d_6. **a)** Full range spectrum. Partial spectra of **b)** 168.0–92.0 ppm and **c)** 88.0–24.0 ppm. "*" denotes the signals due to the solvent used.

Preparation of AmAzoCD

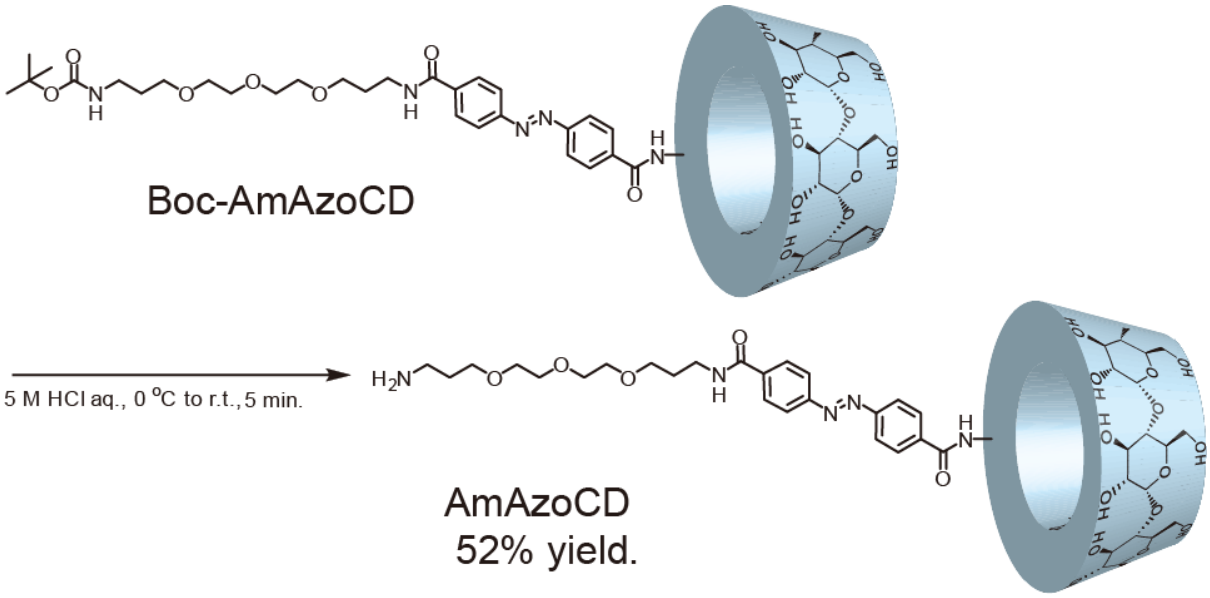

Scheme 2-6. Preparation of AmAzoCD.

Boc-AmAzoCD (0.31 g, 0.20 mmol) dissolved in 5 M HCl aq. (1.6 mL) was stirred for 5 min at room temperature. After adding Et_3N (2.0 mL, 270 mmol) to the HCl aq. solution, the solution was diluted with water (10 mL). The solution was applied to a Diaion HP-20 resin column (15 × 13 cm^3) running using a mixed solvent of H_2O and MeOH with a gradient of the volume ratio. The crude product was obtained in a fraction which was eluted with a mixed solvent of H_2O and MeOH (3/7, v/v). The solution was lyophilized to give AmAzoCD as a pale-orange powder (0.15 g, 52%). ^{1}H NMR (500 MHz, DMSO-d_6): δ (ppm) 8.63 (br, 1H), 8.25 (d, J = 8.3 Hz, 1H), 8.07 (d, J = 8.7 Hz, 2H), 8.05 (d, J = 8.7 Hz, 2H), 7.97 (d, J = 8.3 Hz, 4H), 4.86-4.79 (m, 4H), 4.68 (d, J = 6.9 Hz, 1H), 4.40 (t, J = 10.2 Hz, 1H), 4.00–2.96 (m, overlaps HOD), 2.58 (t, J = 6.4 Hz, 2H), 1.78 (quartet, J = 6.4 Hz, 2H), 1.56 (quintet, J = 6.0 Hz, 2H). ^{1}H NMR (500 MHz, D_2O): δ (ppm) 8.49 (d, J = 8.0 Hz, 2H), 8.31 (d, J = 8.0 Hz, 2H), 8.09 (d, J = 7.9 Hz, 2H), 7.96 (d, J = 8.0 Hz, 2H), 5.20 (d, J = 20.9 Hz, 2H), 5.01 (s, 1H), 4.88 (br, 2H), 4.67 (d, J = 5.7 Hz, 1H), 4.59–4.44 (m, 3H), 4.38–4.23 (m, 4H), 4.08–3.39 (m, 37H), 3.30–3.14 (m, 5H), 3.01–2.78 (m, 6H), 1.98 (quintet, J = 6.2 Hz, 2H), 1.83 (quintet, J =

6.1 Hz, 2H). ^{13}C NMR (150 MHz, DMSO-d_6): δ (ppm) 165.86, 153.61, 137.61, 129.16, 128.94, 122.96, 104.95, 102.97, 102.57, 102.43, 102.02, 101.54, 83.37, 82.15, 82.09, 81.14, 77.42, 74.09, 73.88, 73.67, 73.49, 73.34, 73.30, 72.96, 72.83, 72.74, 72.62, 72.60, 72.48, 72.42, 72.19, 72.12, 72.00, 71.28, 70.24, 70.21, 70.01, 69.91, 68.79, 68.74, 60.68, 60.49, 51.27, 38.99, 37.32, 32.96, 29.71. MALDI-TOF MS: *m/z* Calcd. for $C_{60}H_{92}N_5O_{34}$ ([M + H]$^+$): 1426.56; Found: 1426.62. Calcd. for $C_{60}H_{91}N_5O_{34}Na$ ([M + Na]$^+$): 1448.54; Found: 1448.56. HR MS (ESI+): *m/z* Calcd. for $C_{60}H_{92}O_{34}N_5$ ([M+H]$^+$): 1426.5621; Found: 1426.5622 (Δppm 0.189).

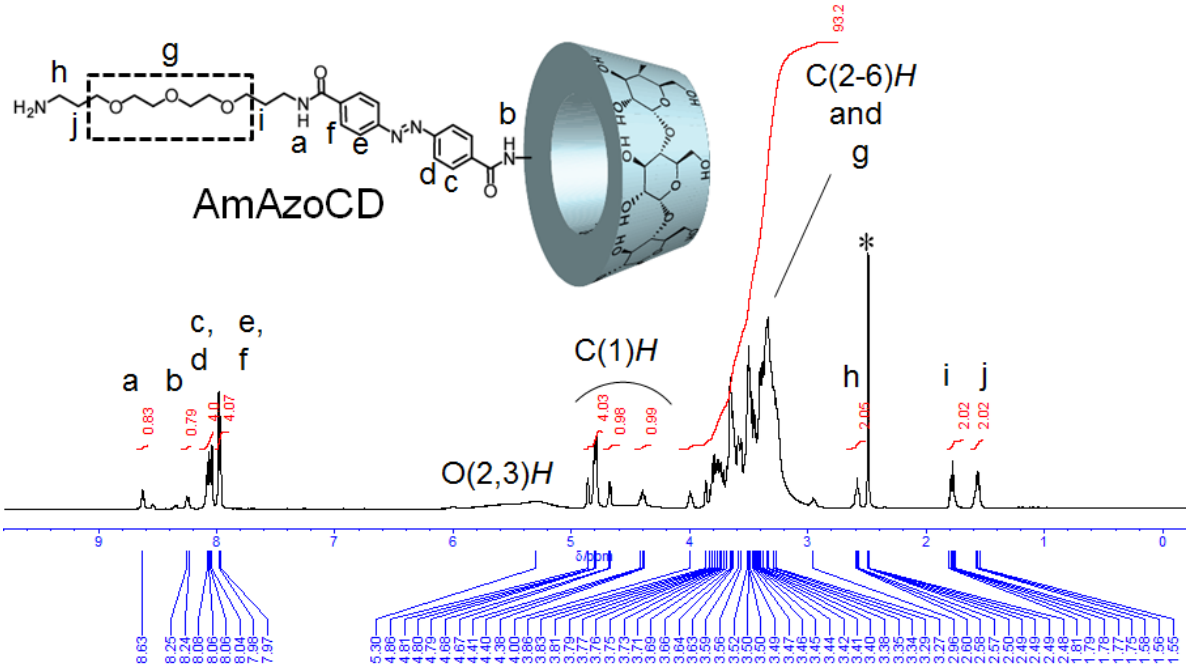

Figure 2-15. 500 MHz ^{1}H NMR spectrum of AmAzoCD in DMSO-d_6. "*" denotes the signals due to the solvent used.

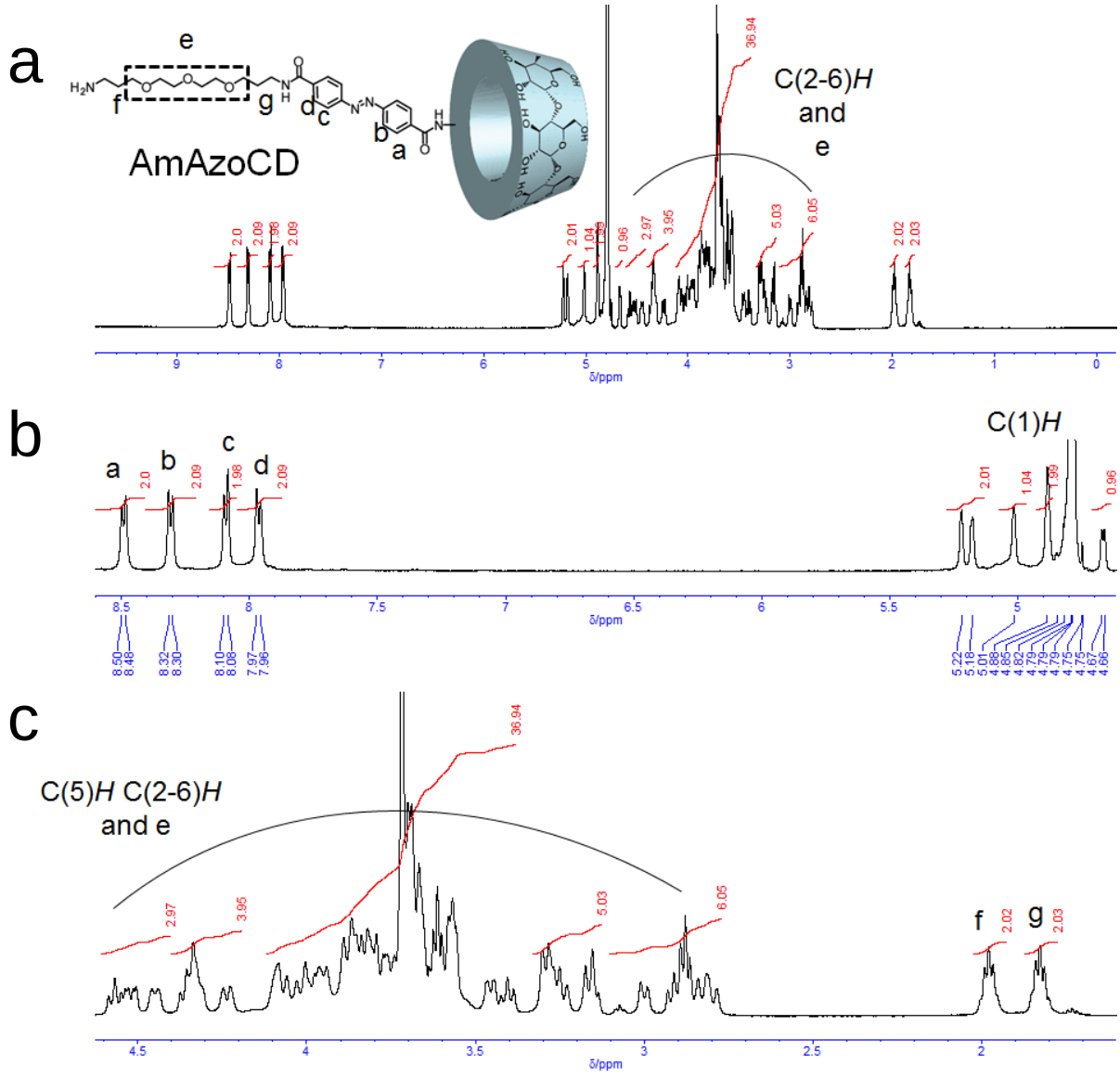

Figure 2-16. 500 MHz ^{1}H NMR spectra of AmAzoCD in D_2O. **a)** Full range spectrum. Partial spectra of **b)** 8.60–4.66 ppm and **c)** 4.65–1.60 ppm. "*" denotes the signals due to the solvent used.

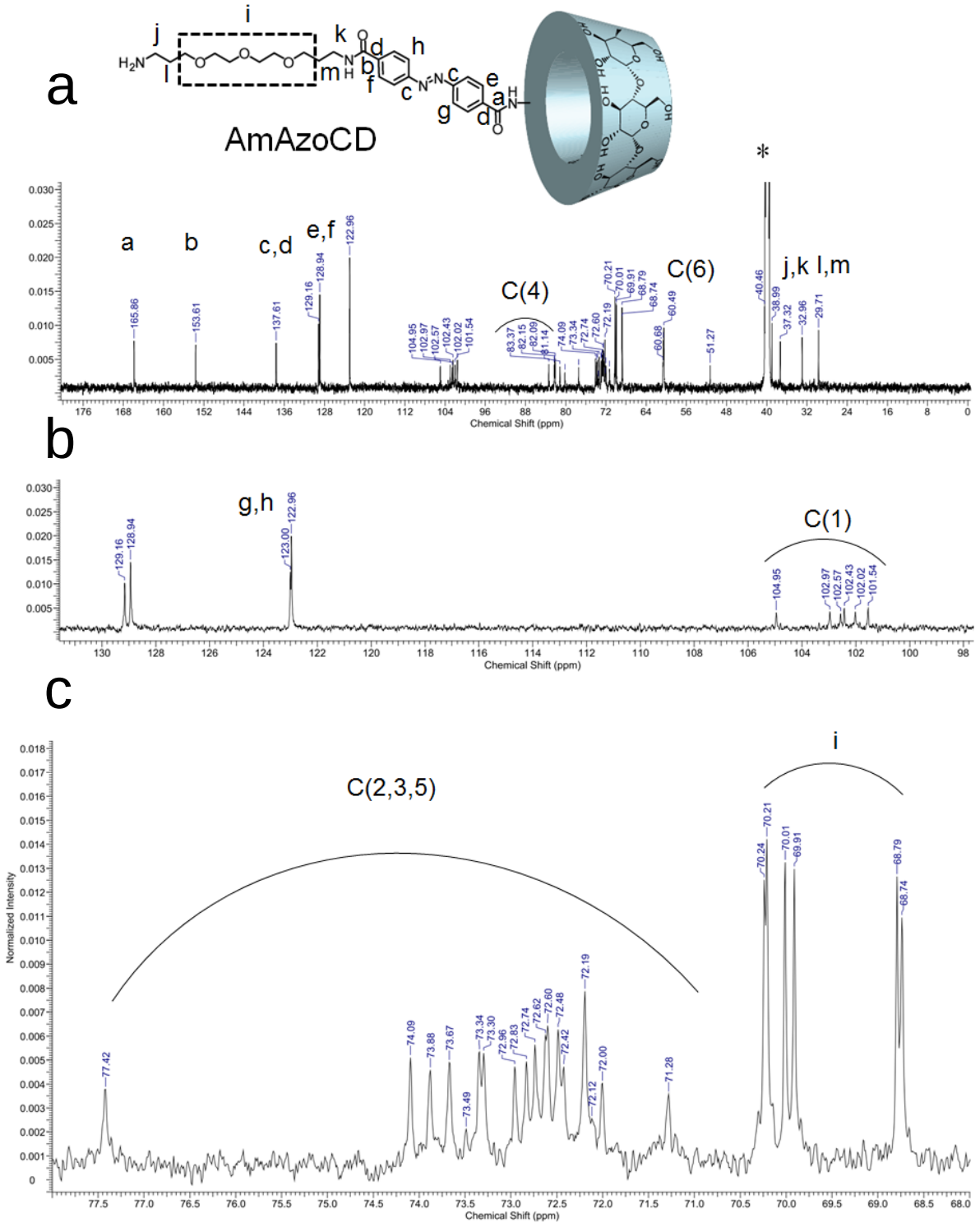

Figure 2-17. 150 MHz ^{13}C NMR spectra of AmAzoCD in DMSO-d_6. **a)** Full range spectrum. Partial spectra of **b)** 131.6–97.6 ppm and **c)** 78.5–68.0 ppm. "*" denotes the signals due to the solvent used.

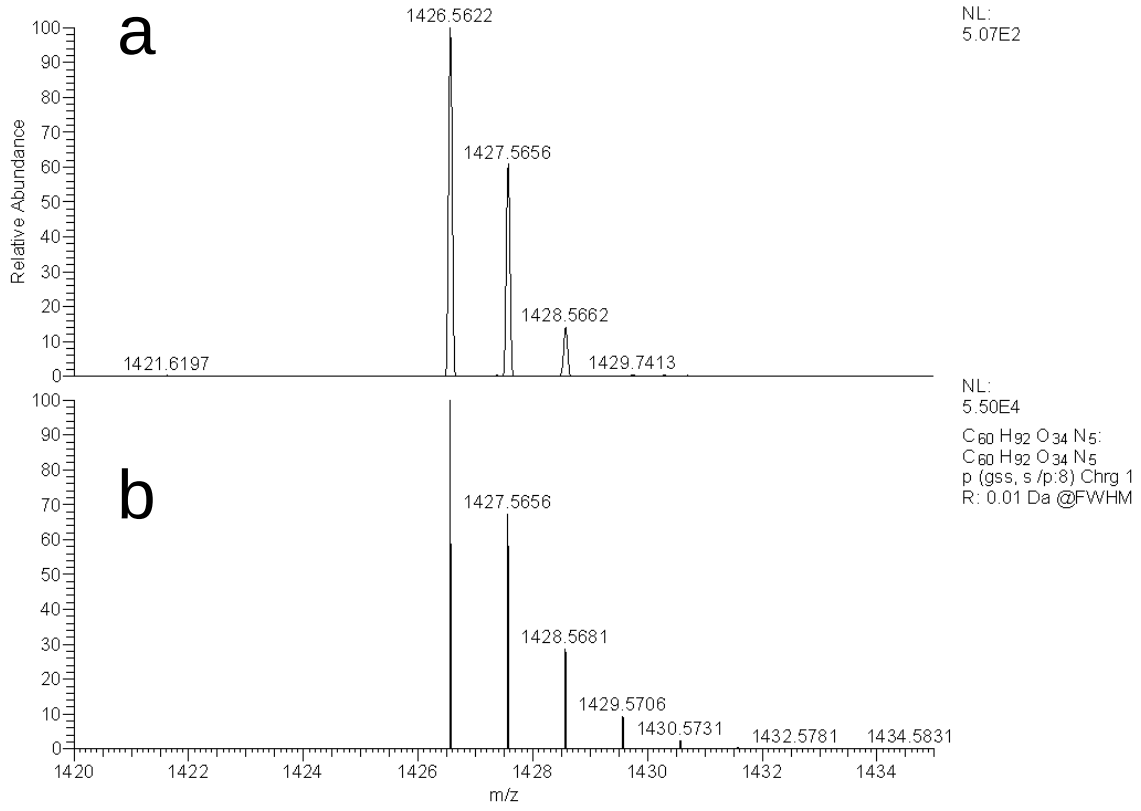

Figure 2-18. High resolution mass spectrum of AmAzoCD. **a)** Observed mass 1426.5622 Da (Δppm 0.189). **b)** *m/z* Calcd. for $C_{60}H_{92}O_{34}N_5$ ($[M+H]^+$): 1426.5621 Da.

Preparation of [c2]DMTAzoCD$_2$.

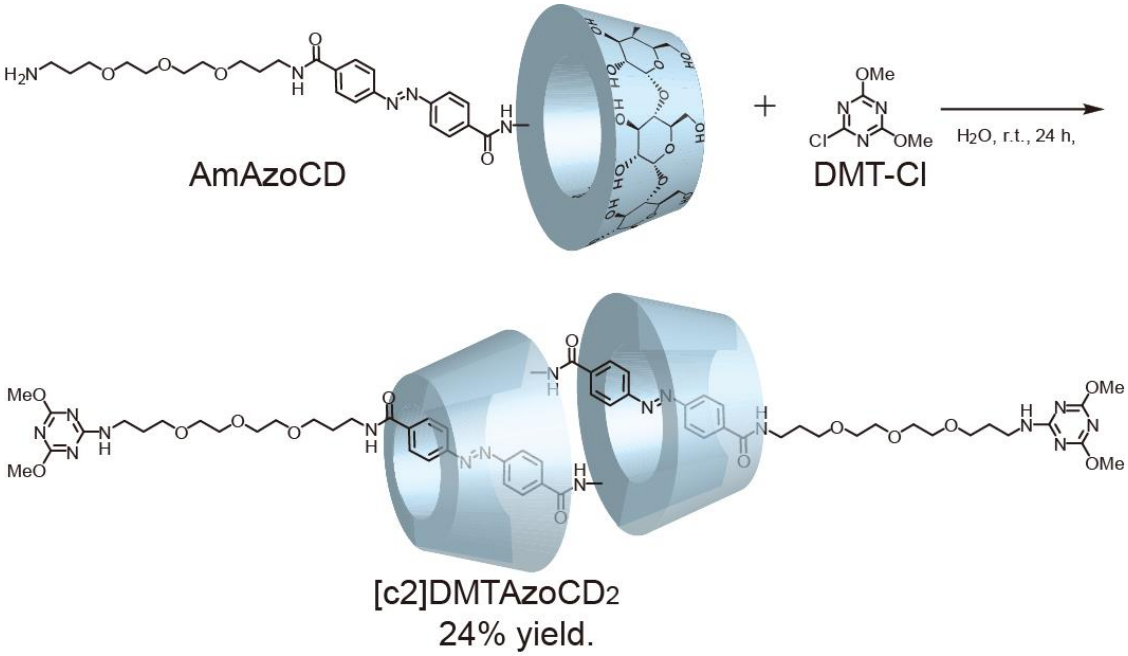

Scheme 2-7. Preparation of [c2]DMTAzoCD$_2$.

Et_3N was added to aqueous solution (5.0 mL) of AmAzoCD (0.11 g, 73 μmol) until reaching to pH = 9. DMT-Cl (0.014 g, 79 μmol) was then added to the aqueous solution. The resulting suspension was stirred for 24 hours. After the prescribed time the reaction mixture was filtered and dispersed in water. Resulting mixture was subjected to preparative reverse-phase HPLC running with an H_2O/MeCN gradient. The desired fractions were lyophilised to give [c2]DMTAzoCD$_2$ as a pale-orange powder (27 mg, 24%). ^{1}H NMR (500 MHz, DMSO-d_6): δ (ppm) 8.74–7.79 (br, 11H), 6.78–2.73 (br, overlaps with HOD) 1.83 (br, 2H), 1.75 (quintet, J = 5.8 Hz, 2H). ^{1}H NMR (500 MHz, D_2O): δ (ppm) 8.49 (d, J = 8.5 Hz, 4H), 8.31 (d, J = 8.5 Hz, 4H), 8.09 (d, J = 8.5 Hz, 4H), 7.95 (d, J = 8.5 Hz, 4H), 5.21 (dd, J = 19 Hz, 3.7Hz, 4H), 5.02 (d, J = 3.7 Hz, 2H), 4.88 (br, 4H), 4.66 (d, J = 5.7 Hz, 2H), 4.59–4.44 (m, 6H), 4.38–4.22 (m, 8H), 4.08–3.40 (m, 84H), 3.32–3.13 (m, 10H), 3.01 (d, J = 10.5 Hz, 2H), 2.93 (t, J = 9.3 Hz, 2H), 2.81 (t, J = 11.3 Hz, 4H), 1.95 (quintet, J = 6.0 Hz, 4H), 1.88 (quintet, J = 6.4 Hz, 4H). ^{13}C NMR (150 MHz, DMSO-d_6): δ (ppm) 172.42, 171.97, 168.06, 165.90, 153.23, 137.02, 128.91, 128.53, 124.63, 122.89, 106.89, 102.67, 102.41, 102.02, 101.84, 101.81, 82.06, 82.01, 81.98, 81.83, 79.76, 79.72, 74.22, 74.14, 73.27, 72.65, 72.48, 72.44, 72.33, 71.99, 71.71, 70.24, 70.19, 70.02, 69.94, 68.82, 68.56, 61.06, 60.49, 60.42, 60.31, 60.29, 60.25, 54.42, 51.32, 38.15, 38.03, 29.89, 29.48. MALDI-TOF MS: *m/z* Calcd. for $C_{130}H_{192}N_{16}O_{72}Na$ ($[M + Na]^+$): 3152.18; Found: 3152.88. Calcd. for $C_{130}H_{192}N_{16}O_{72}K$ ($[M + K]^+$): 3168.15; Found: 3168.82. HR MS (ESI+): *m/z* Calcd. for $C_{125}H_{192}O_{72}N_{16}Na_3$ ($[M+3Na]^{3+}$): 1066.0510; Found: 1066.0518 (Δppm 0.755).

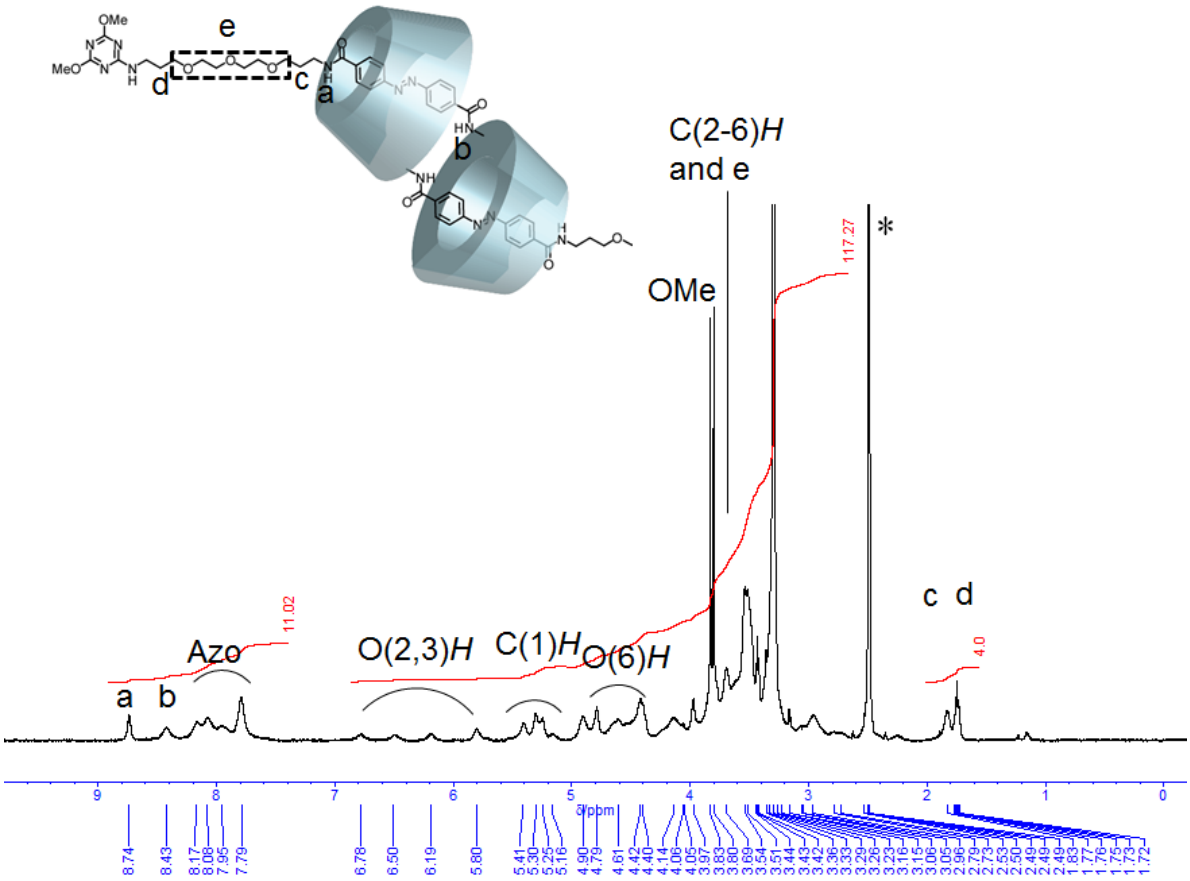

Figure 2-19. 500 MHz ^{1}H NMR spectrum of [c2]DMTAzoCD$_2$ in DMSO-d_6. "*" denotes the signals due to the solvent used.

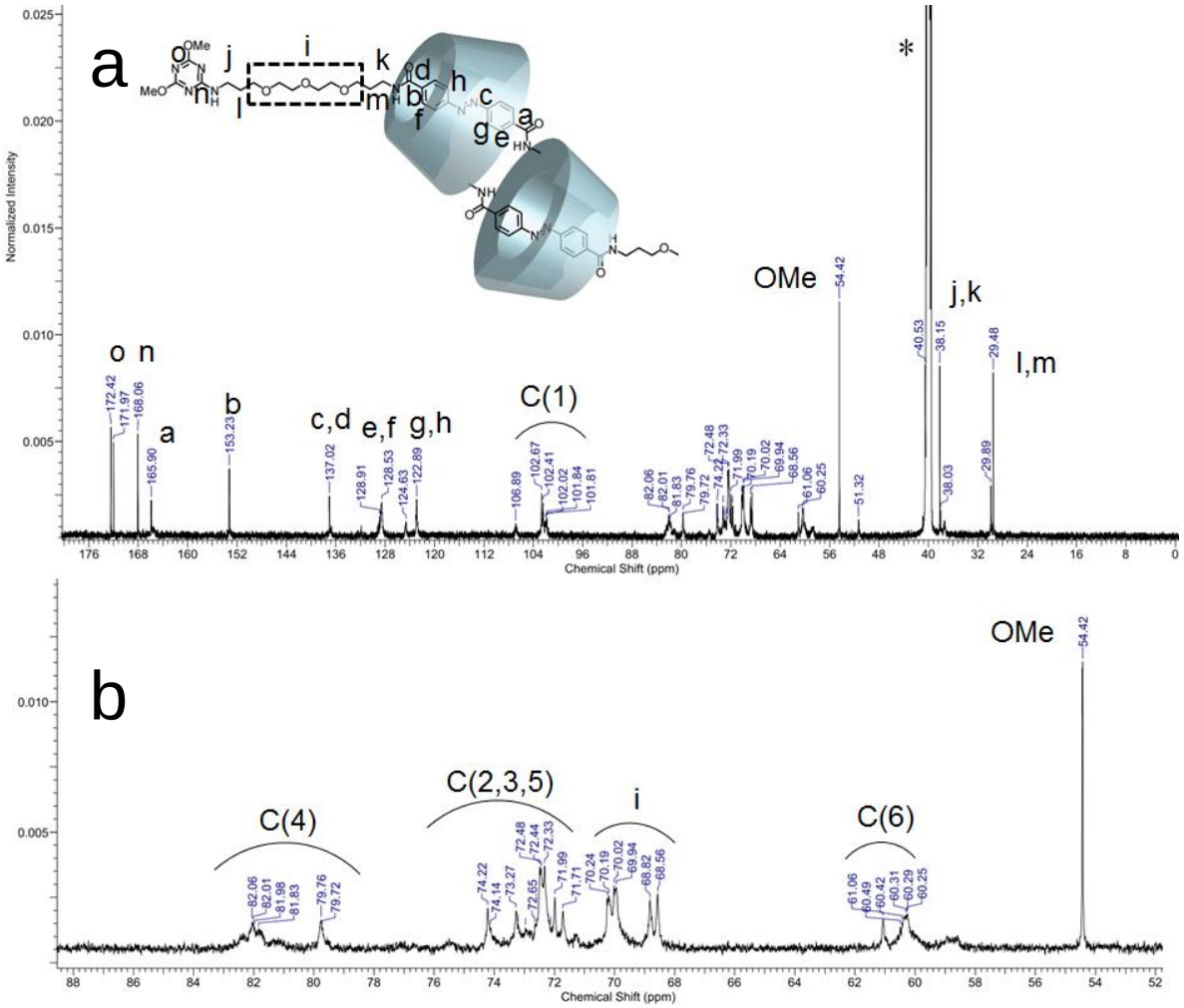

Figure 2-20. 150 MHz ^{13}C NMR spectra of [c2]DMTAzoCD$_2$ in DMSO-d_6. **a)** Full range spectrum. **b)** Partial spectrum of 51.8–88.4 ppm. "*" denotes the signals due to the solvent used.

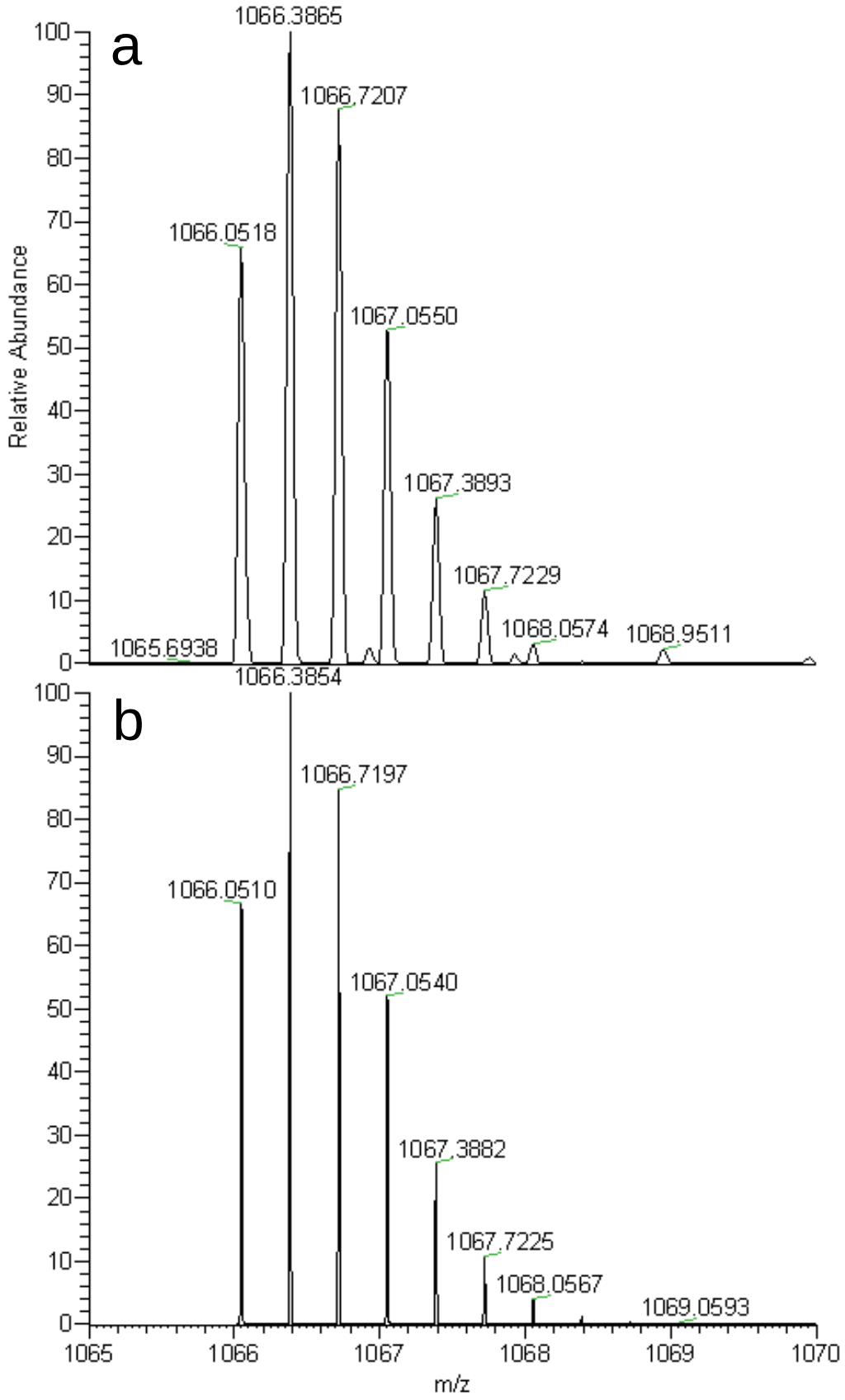

Figure 2-21. High resolution mass spectrum of [c2]DMTAzoCD$_2$. **a)** Observed mass 1066.0518 Da (Δppm 0.755). **b)** *m/z* Calcd. for $C_{125}H_{192}O_{72}N_{16}Na_3$ ($[M+3Na]^{3+}$): 1066.0510 Da.

References

1 Dietrich-Buchecker, C. O., Sauvage, J. P. Interlocking of molecular threads: from the statistical approach to the templated synthesis of catenands. *Chem. Rev.* **87,** 795–810 (1987).

2 Amabilino, D. B., Stoddart, J. F. Interlocked and intertwined structures and superstructures. *Chem. Rev.* **95,** 2725–2828 (1995).

3 Collin, J. P., Dietrich-Buchecker, C., Gaviña, P., Jimenez-Molero, M. C., Sauvage, J. P. Shuttles and muscles: linear molecular machines based on transition metals. *Acc. Chem. Res.* **34,** 477–487 (2001).

4 Jimenez-Molero, M. C., Dietrich-Buchecker, C., Sauvage, J. P. Chemically induced contraction and stretching of a linear rotaxane dimer. *Chem. Eur. J.* **8,** 1456–1466 (2002).

5 Schill, G. *Catenanes, Rotaxanes, and Knots*; Academic Press: New York, (1971).

6 Kay, E. R., Leigh, D. A., Zerbetto, F. Synthetic molecular motors and mechanical machines. *Angew. Chem. Int. Ed.* **46,** 72–191 (2007).

7 Coskun, A., Banaszak, M., Astumian, R. D., Stoddart, J. F., Grzybowski, B. A. Great expectations: can artificial molecular machines deliver on their promise? *Chem. Soc. Rev.* **41,** 19–30 (2012).

8 Bruns, C. J., Stoddart, J. F. Rotaxane-based molecular muscles. *Acc. Chem. Res.* **47,** 2186–2199 (2014).

9 Zhang, Z., Han, C., Yu, G., Huang, F. A solvent-driven molecular spring. *Chem. Sci.* **3,** 3026–3031 (2012).

10 Rotzler, J., Mayor, M. Molecular daisy chains. *Chem. Soc. Rev.* **42,** 44–62 (2013).

11 Ashton, P. R., Baxter, I., Cantrill, S. J., Fyfe, M. C., Glink, P. T., Stoddart, J. F., White, A. J. P., Williams, D. J. Supramolecular daisy chains. *Angew. Chem. Int. Ed.* **37,** 1294–1297 (1998).

12 Jimenez-Molero, M. C., Dietrich-Buchecker, C., Sauvage, J. P. Towards artificial muscles at the nanometric level. *Chem. Commun.* 1613–1616 (2003).

13 Wu, J., Leung, K. C. F., Benítez, D., Han, J. Y., Cantrill, S. J., Fang, L., Stoddart, J. F. An Acid–Base-Controllable [c2] Daisy Chain. *Angew. Chem. Int. Ed.* **47,** 7470–7474(2008).

14 Coutrot, F., Romuald, C., Busseron, E. A new pH-switchable dimannosyl [c2] daisy chain molecular machine. *Org. Lett.* **10,** 3741–3744 (2008).

15 Du, G., Moulin, E., Jouault, N., Buhler, E., Giuseppone, N. Muscle-like Supramolecular Polymers: Integrated Motion from Thousands of Molecular Machines. *Angew. Chem. Int. Ed.* **51,** 12504–12508 (2012).

16 Bruns, C. J., Li, J., Frasconi, M., Schneebeli, S. T., Iehl, J., Jacquot de Rouville, H. P., Stupp, S. I., Voth, G. A., Stoddart, J. F. An Electrochemically and Thermally

Switchable Donor–Acceptor [c2] Daisy Chain Rotaxane. *Angew. Chem. Int. Ed.* **53,** 1953–1958 (2014).

17 Fujimoto, T., Nakamura, A., Inoue, Y., Sakata, Y., Kaneda, T. Photoswitching of the association of a permethylated α-cyclodextrin-azobenzene dyad forming a Janus [2] pseudorotaxane. *Tetrahedron Lett.* **42,** 7987–7989 (2001).

18 Tsuda, S., Aso, Y., Kaneda, T. Linear oligomers composed of a photochromically contractible and extendable Janus [2] rotaxane. *Chem. Commun.* 3072–3074 (2006).

19 Li, S., Taura, D., Hashidzume, A., Harada, A. Light-switchable Janus [2] rotaxanes based on α-cyclodextrin derivatives bearing two recognition sites linked with oligo-(ethylene glycol). *Chem. Asian J.* **5,** 2281–2289 (2010).

Chapter 3

Photo-generated actuation of supramolecular artificial muscle materials with [c2]daisy chains.

Introduction

Myosin and actin filaments in muscle cells insert into each other to form alternating layered structures and slide to demonstrate contraction and expansion behaviour in the power stroke process.[1–4] The sliding motion, which is reminiscent of the muscle fibril, has inspired researchers in supramolecular chemistry to realize artificial linear motors using supramolecular complexes. Polyrotaxanes and [c2]daisy chains (doubly-threaded dimers) are important components to create supramolecular artificial muscles.[5–12] Stimuli-responsive [c2]daisy chains based on host–guest conjugates can display specific sliding actuation controlled by external stimuli, e.g., chemicals,[13–17] pH,[18, 19] redox[20] and light.[21–23]

Sauvage[13] *et al.* found nanoscale conformational change. Stoddart[24–28] *et al.* have prepared poly-[c2]daisy chains using crown ethers and found that the poly-[c2]daisy chains show contraction and expansion behaviour by addition of an acid. Grubbs *et al.* also reported poly-[c2]daisy chains containing crown ether-based [c2]daisy chains, which expand and contract in response to pH change.[29] Some cyclodextrin (CD)-based [c2]daisy chains show expansion and contraction motions due to the solvent polarity change[17] or photo-stimuli[21–23] in aqueous solutions. However, macroscopic supramolecular actuators remain a challenge not only in supramolecular chemistry but also in materials science, and such actuators consisting of [c2]daisy chains should be reported.

Two structural approaches may realize supramolecular actuators through host–guest interactions: a method with a linear main chain and one with a side chain in the polymer structure. Previously, poly-[c2]daisy chains have been reported by several groups as

linear-type supramolecular actuators that show a contraction–expansion behaviour responsive to external stimuli.[24–29] Harada's research employs the polymer side chain method because various functions (e.g., selective adhesion,[30] self-healing,[31, 32] and atuation[33, 34]) are relatively easy to be introduced into materials (Figure 3-1). Harada *et al.* have previously reported photo or redox responsive supramolecular actuators by integrating host–guest interactions on the polymer side chains.[33, 34] The association and dissociation of inclusion complexes as cross-linking units on the polymer side chains demonstrate contraction and expansion motions due to changes in the cross-linking density. A plate-shaped actuator bent against the incident ultraviolet (UV) light.[33]

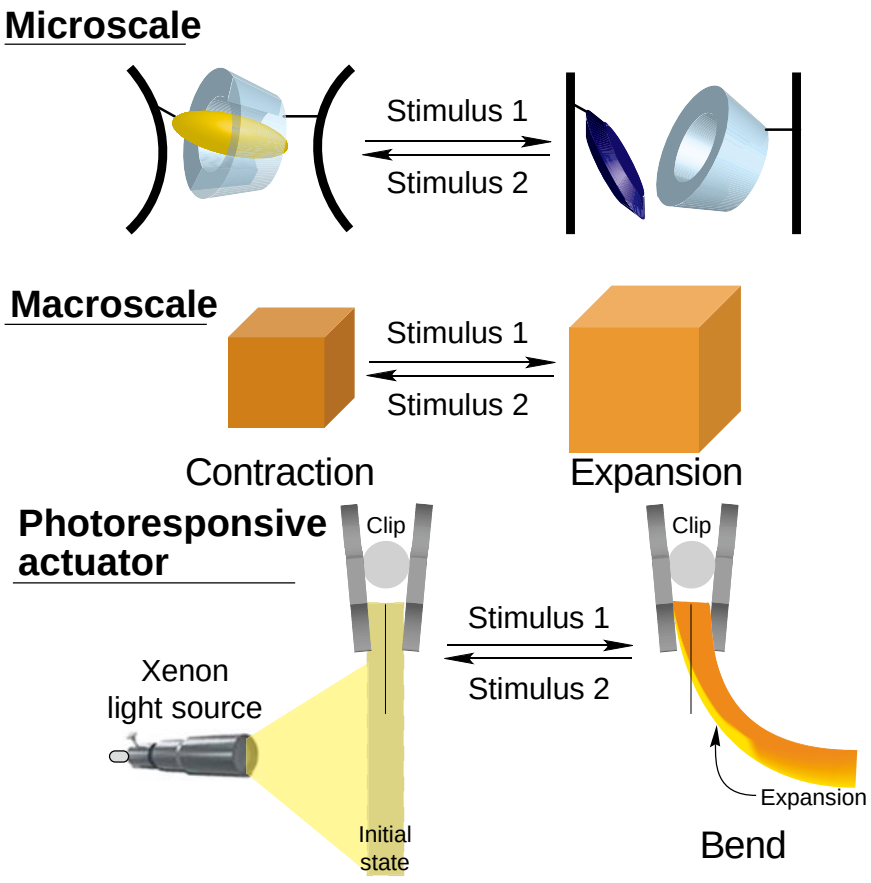

Figure 3-1. Supramolecular actuator using host–guest interactions on the polymer side chain. On the macroscale, the volume of the supramolecular actuator expands by external stimuli. In the case of photo-responsive actuator, exposing the left side to UV light causes the plate-shaped actuator to bend to the right side.[33]

However, the author hypothesized that polymer chains cross-linked with [c2]daisy chains would realize a novel supramolecular actuator whose volume contracts upon UV light irradiation but expands upon visible (Vis) light irradiation. This contraction would bend the flat plate actuator toward the incident UV light because UV irradiation causes the shrinkage of the end-to-end distance of the [c2]daisy chain to shrink polymeric materials due to desorption of the solvent on the exposed surface (Figure 3-2).

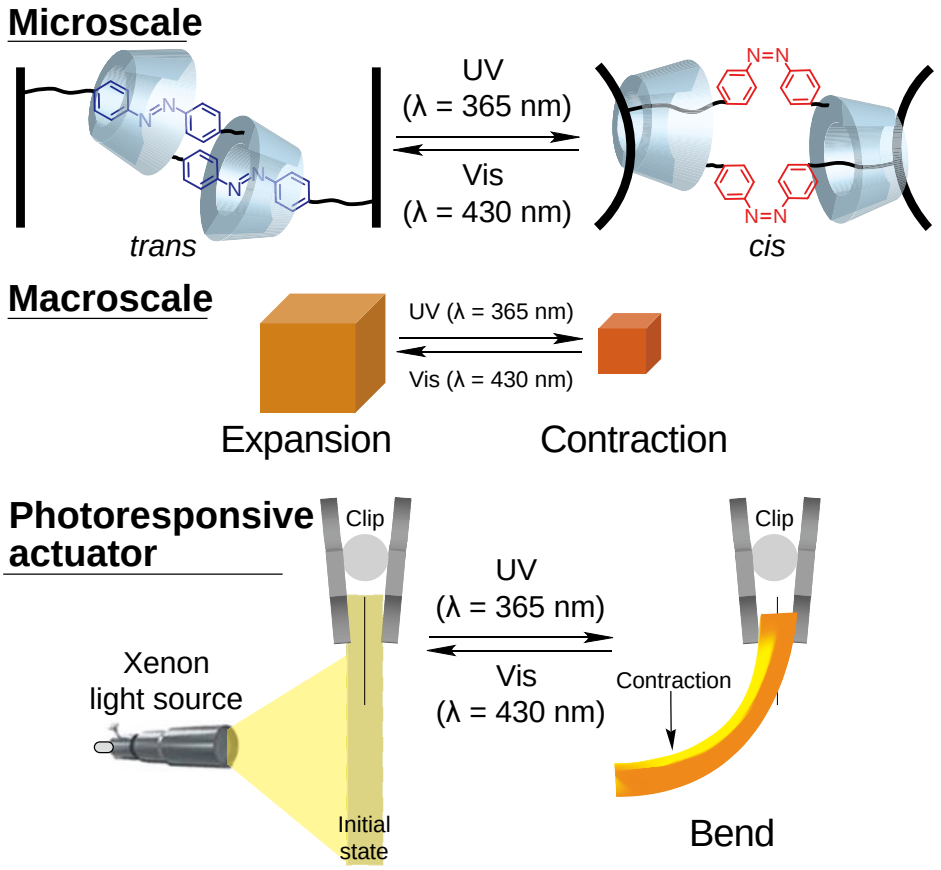

Figure 3-2. Supramolecular actuator using a polymer cross-linked with [c2]daisy chain at the polymer side chains. On the macroscale, the volume of the supramolecular actuator contracts by UV light irradiation; exposing the left side to UV light, the plate-shaped actuator bends to the left side.

In this Chapter, the author report that supramolecular hydrogels containing CD-based [c2]daisy chains as cross-linkers contract and expand through photo-responsive sliding of the [c2]daisy chain to the incident light (Figure 3-3) and successfully prepare a photo-responsive

supramolecular actuator.

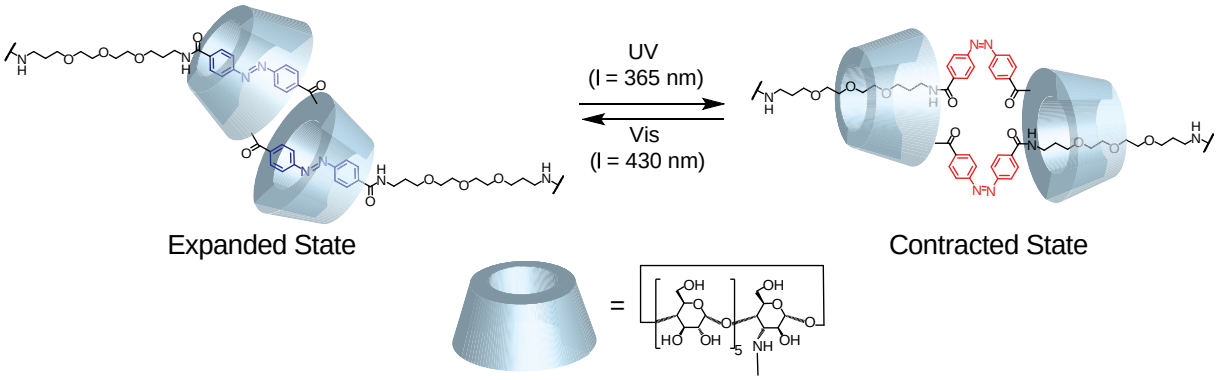

Figure 3-3. Chemical structure and scheme of photo-isomerization of αCD-based [c2]daisy chain with an azobenzene derivative as the axis.

Preparation of hydrogels in this study

Based on the formation of [c2]AzoCD$_2$, the author prepared a supramolecular hydrogel ([c2]AzoCD$_2$ hydrogel) cross-linked with four-armed poly(ethylene glycol) with succinimidyl ester groups at the end (TetraPEG, M_w = 10,000). To prepare a photo-responsive supramolecular actuator, TetraPEG was selected as polymer backbone because it is highly water soluble, lacks absorption bands at λ = 365 and 430 nm, which are correlated to the photo-isomerization of Azo, and the interaction of its PEG unit with CDs or Azo units is weak. Additionally, we are fascinated by the highly symmetric structure of TetraPEG. The [c2]AzoCD$_2$ hydrogel was prepared by polycondensation of the amino group in [c2]AzoCD$_2$ and succinimidyl ester groups at the end of TetraPEG in an aqueous solution (Scheme 3-2). On the other hand, hydrogel was not formed from AmAzoCD with the TetraPEG in DMSO, in which AmAzoCD existed as monomer. To characterize the topological effect of the [c2]AzoCD$_2$ gel, we prepared two types of covalently cross-linked TetraPEG gel as references: an Azo gel covalently cross-linked with 4,4´-bis(diamino-diethylene glycol)-azobenzene (Am-DEG-Azo-DEG-Am) and the succinimidyl ester groups of TetraPEG (Scheme 3-3) and a PEG gel covalently-cross-linked with poly(ethylene glycol)-bis-(3-aminopropyl)ether (DE-10PA) (Scheme 3-4).

Characterization of [c2]AzoCD$_2$, Azo- and PEG- hydrogels

Hydrogels were characterized by ^{1}H field gradient magic angle spining (FGMAS) NMR spectroscopy (Figure 3-4, 3-5 and 3-6) and IR spectroscopy (Figure 3-7). The molar ratios of functional cross-linkers ([c2]daisy chain, Azo, and PEG) in hydrogels were determined. The conversion of *N*-hydroxysuccinimidyl group (NHS) to amide bond (C_{amide}) and ratio of hydrolyzed NHS group (C_{COOH}) were calculated by following equation.

$$C_{amide} = \frac{Pa}{\text{Ideal } Pa\ (4.0)} \quad \cdots (1)$$

$$C_{COOH} = 100 - C_{amide} \quad \cdots (2)$$

Where *Pa* is the area intensity of signals due to the propylene protons in cross-linker.

The formation ratio of [c2]daisy chain (F_{c2}) cross-linker was calculated by the following equations.

$$Pm = Pb - Pc \quad \cdots (3)$$

$$F_{c2} = \frac{Pm}{Pc} \times 100 \quad \cdots (4)$$

Where *Pm* and *Pb* are the area intensities of the monomeric AmAzoCD residue, the total Azo residue, respectively, and *Pc* is the calculated area intensity of total Azo residues.

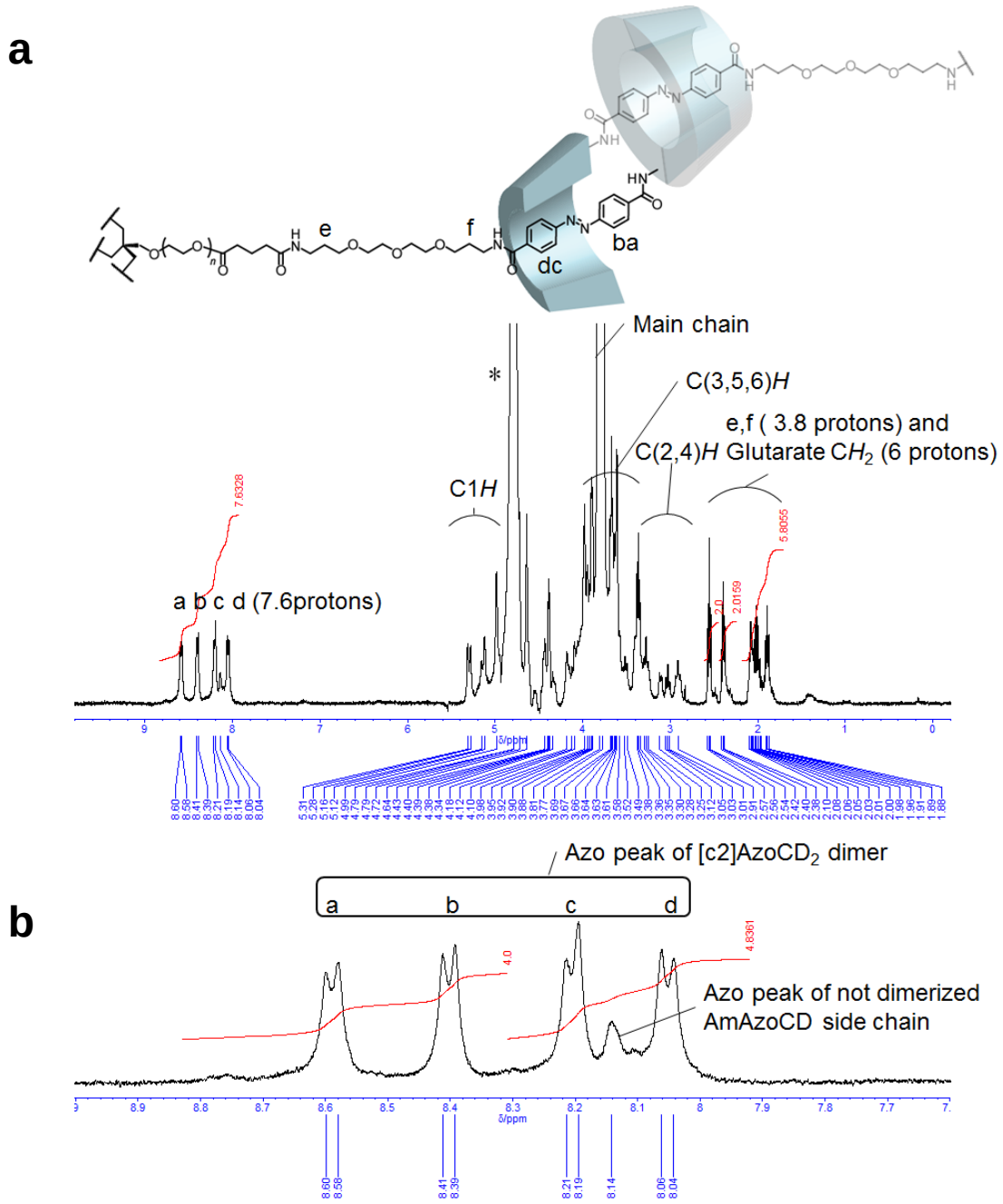

Figure 3-4. 400 MHz ^{1}H FGMAS NMR spectra of the [c2]AzoCD$_2$ hydrogel in D_2O. **a)** Full range spectrum to quantify the conversion of NHS group on PTE-100GS. The conversion of NHS to amide was 95%. **b)** Partial spectrum of 7.60–9.00 ppm to quantify the ratio between [c2]AzoCD$_2$ dimer unit and monomeric AmAzoCD unit. The ratio of [c2]AzoCD$_2$ dimer was 90%. The ratio of [c2]AzoCD$_2$ did not dimerized AmAzoCD : partly-hydrolyzed NHS = 85.5 : 9.5 : 5. A sample spinning rate was 10 kHz by using a nano probe. "*" denotes the signals due to the solvent used.

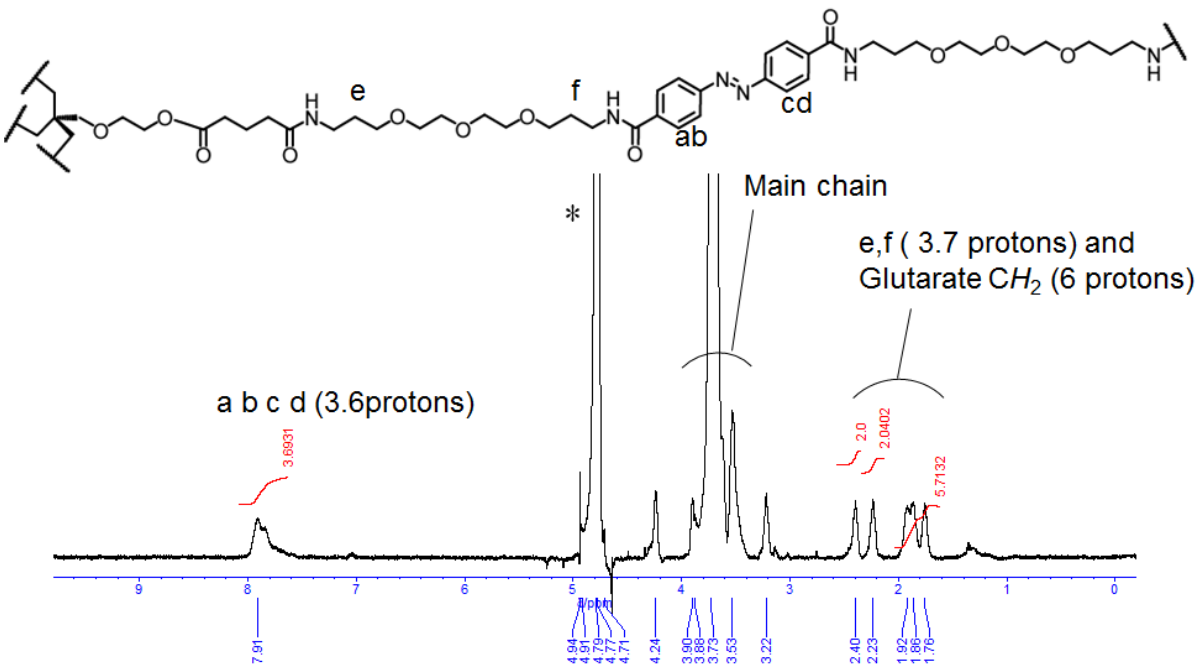

Figure 3-5. 400 MHz ^{1}H FGMAS NMR spectrum of the Azo hydrogel to quantify the conversion of NHS group on PTE-100GS in D_2O. The conversion of NHS to amide was 93%. The ratio of Azo : partly-hydrolyzed NHS = 93 : 7. A sample spinning rate was 10 kHz by using a nano probe. "*" denotes the signals due to the solvent used.

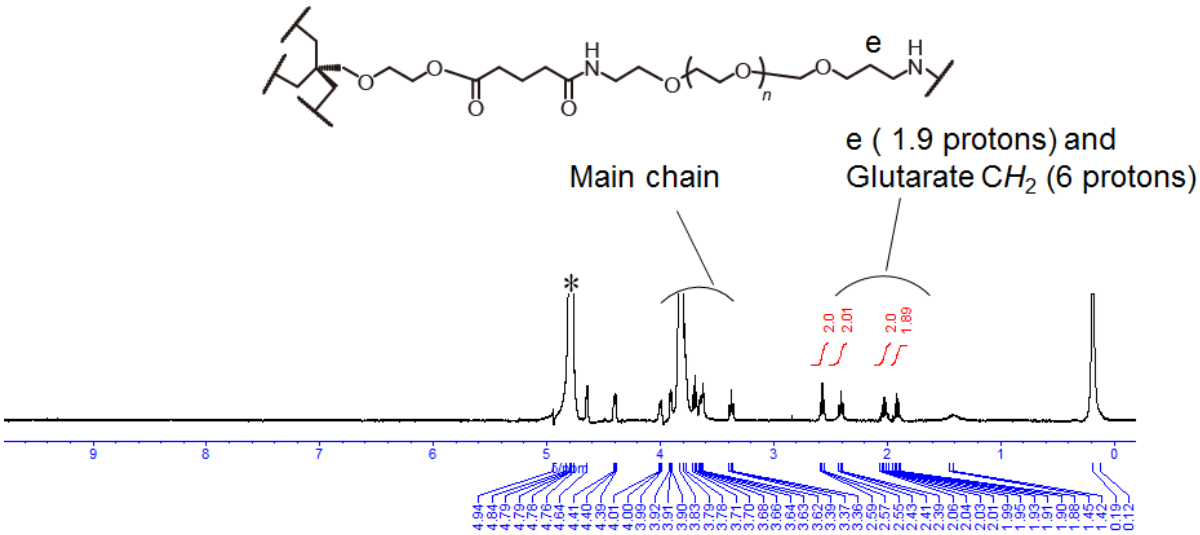

Figure 3-6. 400 MHz ^{1}H FGMAS NMR spectrum of the PEG hydrogel to quantify the conversion of NHS group on PTE-100GS in D_2O. The conversion of NHS to amide was 94%. The ratio of PEG : partly-hydrolyzed NHS = 94 : 6. A sample spinning rate was 10 kHz by using a nano probe. "*" denotes the signals due to the solvent used.

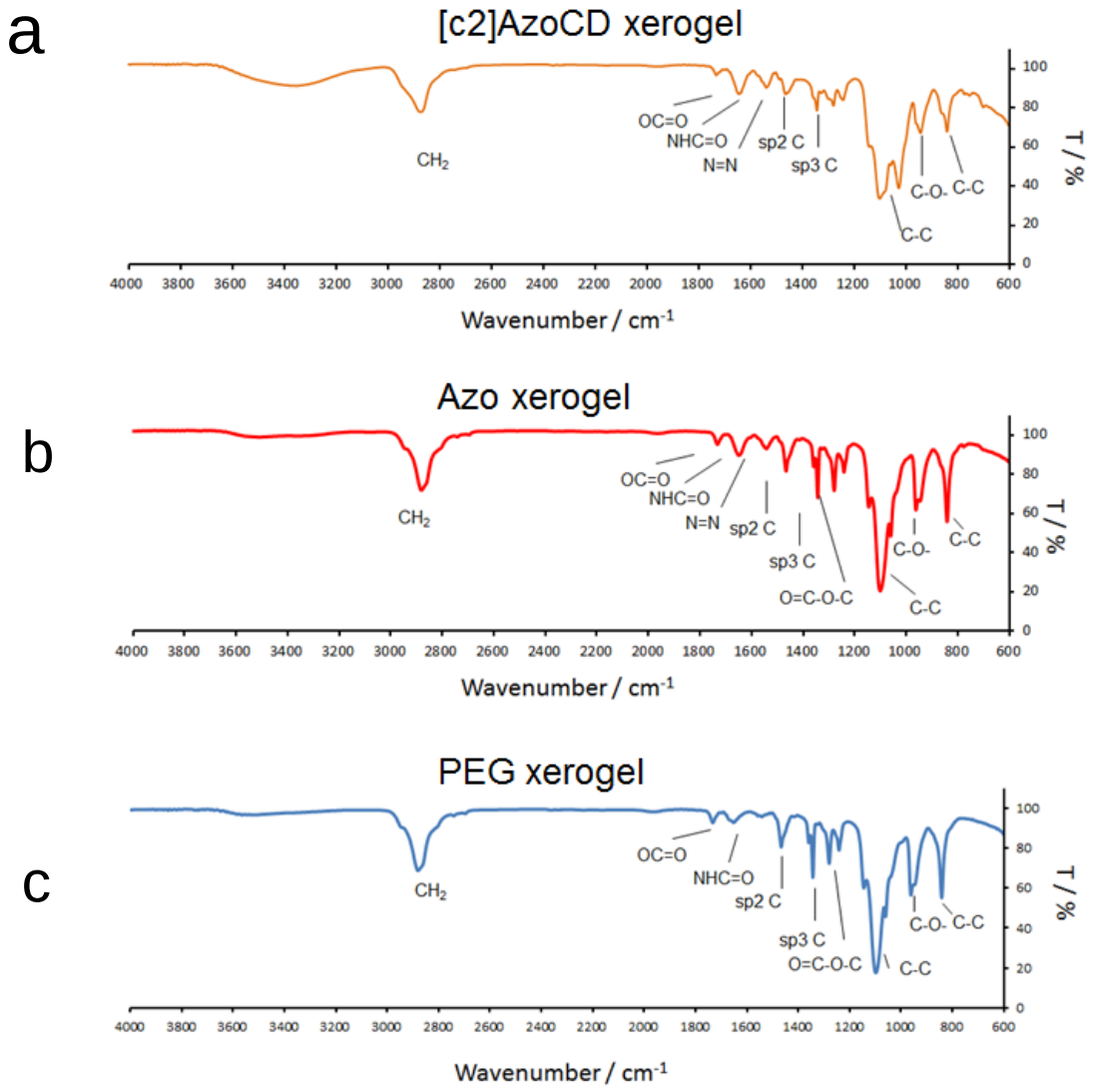

Figure 3-7. FT-IR spectra (ATR method) of **a)** the [c2]AzoCD$_2$ xerogel, **b)** the Azo xerogel, and **c)** the PEG xerogel.

These spectroscopic data indicate that the [c2]AzoCD$_2$, Azo, and PEG moiety are incorporated in hydrogels.

Results and discussions

Effect of the solvent polarity in the polycondensation

The author investigated the effect of the solvent polarity (water or DMSO) on the polycondensation of TetraPEG and [c2]AzoCD$_2$. The physical properties of the hydrogels were characterized by storage elastic modulus (G') and loss elastic modulus (G''). Figures 3-8–3-11 show G' and G'' for the [c2]AzoCD$_2$ hydrogel prepared in **a)** water and **b)** DMSO for an angular frequency range of 0.1–10 rad s^{-1}.

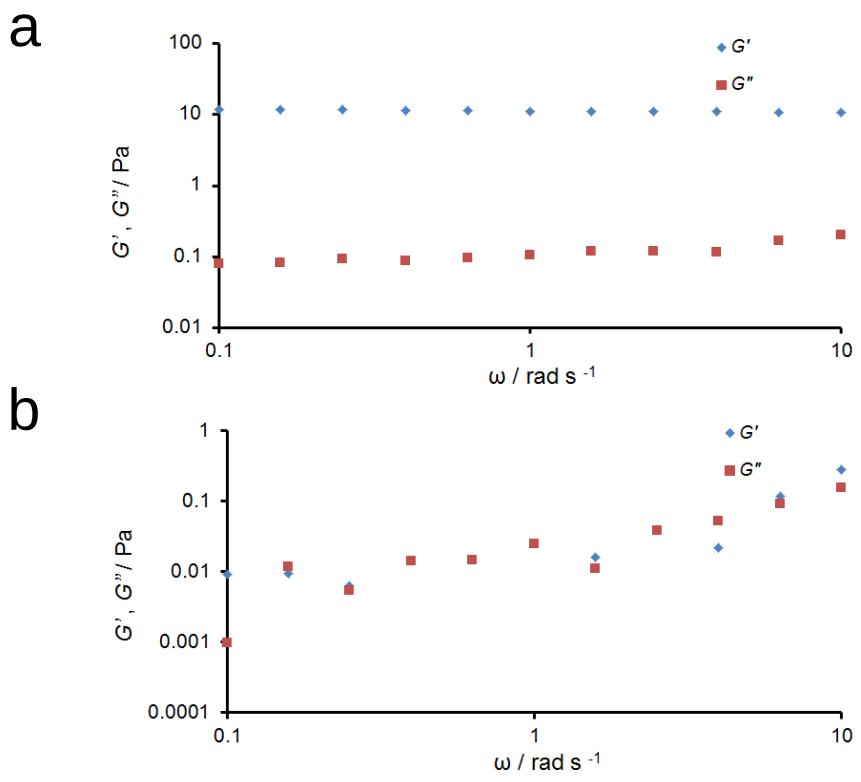

Figure 3-8. Data of dynamic viscoelastic measurements. Dependency of the storage and loss moduli, G' and G'' on angular frequency (ω) for an aqueous solution of the mixture of the **a)** [c2]AzoCD$_2$ hydrogel and **b)** a DMSO solution of the mixture of [c2]AzoCD$_2$ and PTE-100GS on polycondensation.

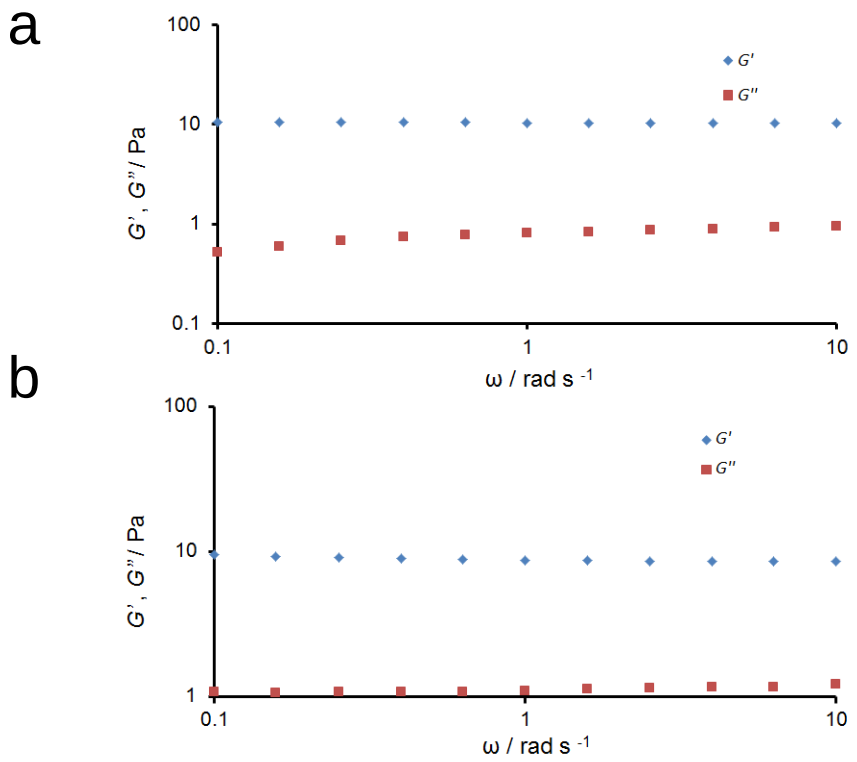

Figure 3-9. Data of dependency of the storage and loss moduli, G' and G'' on angular frequency (ω) for the Azo hydrogel prepared in **a)** water and in **b)** DMSO.

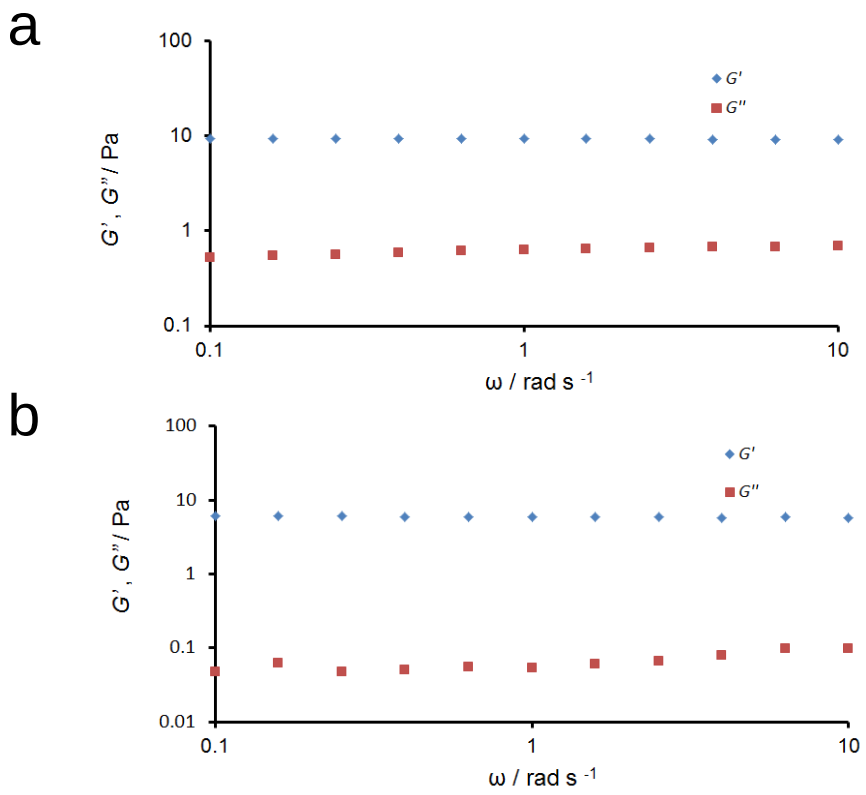

Figure 3-10. Data of dependency of the storage and loss moduli, G' and G'' on angular frequency (ω) for the PEG hydrogel prepared in **a)** water and in **b)** DMSO.

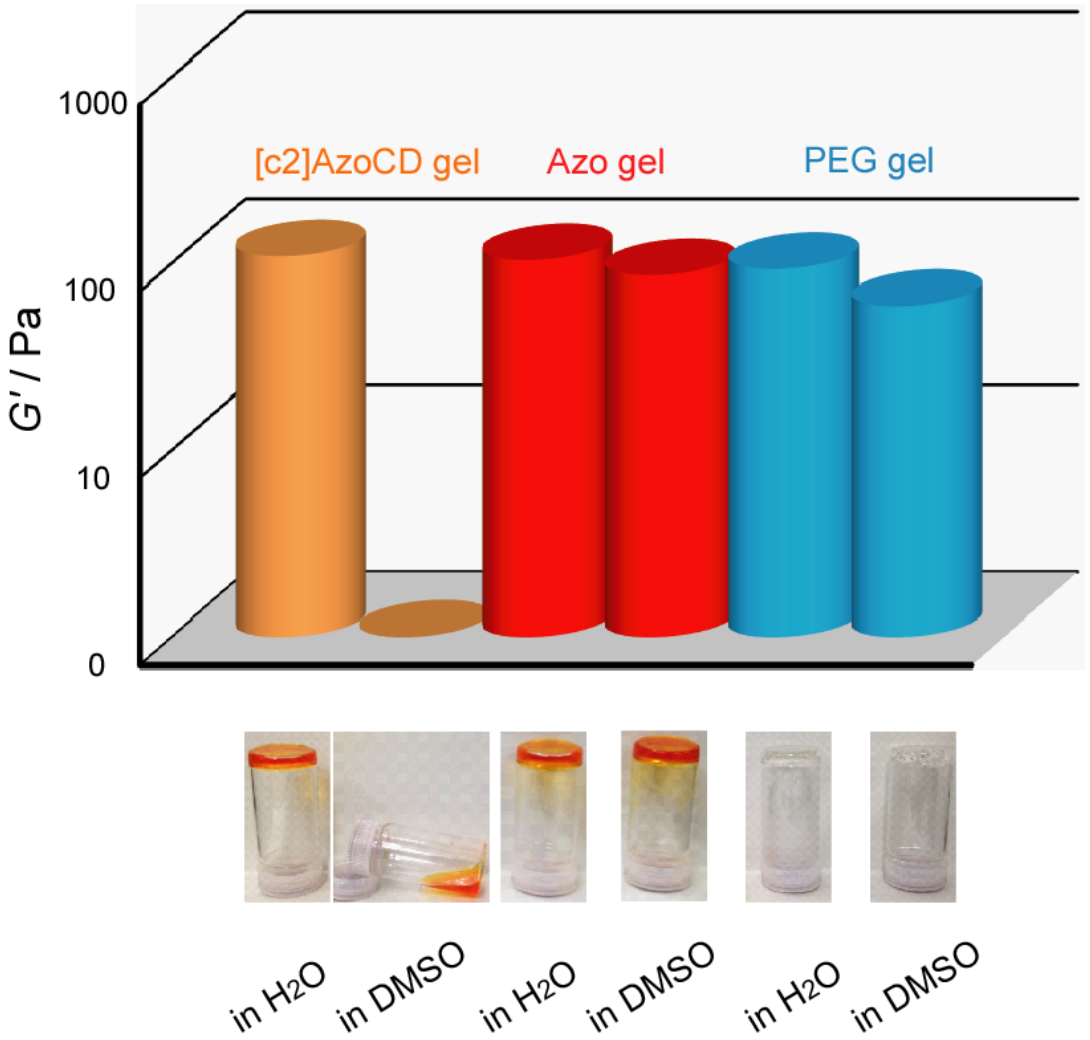

Figure 3-11. Storage elastic modulus of [c2]AzoCD$_2$ hydrogel in H_2O, a DMSO solution of the mixture of [c2]AzoCD$_2$ and PTE-100GS, Azo hydrogel in H_2O, Azo organogel in DMSO, PEG hydrogel in H_2O, and PEG organogel in DMSO. Insets are photographs of reaction mixtures.

The values of *G′* for the [c2]AzoCD$_2$ hydrogel prepared in water do not relax (*G′* > *G″*), suggesting that the obtained hydrogel is similar to a chemically cross-linked gel. In contrast, the values of *G″* for the product with [c2]AzoCD$_2$ reacted in DMSO are larger than those of *G′*, which suggests the formation of an unstable state with relaxation. However, the polycondensation solvent does not affect the storage elastic modulus of the Azo hydrogel and the PEG hydrogel due to the formation of covalent cross-linked structures (Figure 3-11). The elastic viscosity of the product with [c2]AzoCD$_2$ prepared in DMSO was significantly lower than that prepared in water because [c2]AzoCD$_2$ dissociates in DMSO prior to

polycondensation reaction. In other words, [c2]AzoCD$_2$ functions as an interpenetrated cross-linker, resulting in the formation of supramolecular hydrogel.

Photo-responsive volume change of the [c2]AzoCD$_2$ hydrogel

Then, the author investigated the volume change of the [c2]AzoCD$_2$ hydrogel and the Azo hydrogel by UV light (λ = 365 nm) and Vis light (λ = 430 nm) irradiation. Figure 3-12a shows the experimental conditions for photo-irradiation of a cuboid gel. The rod lens with the a Xenon lamp was located above the hydrogels.

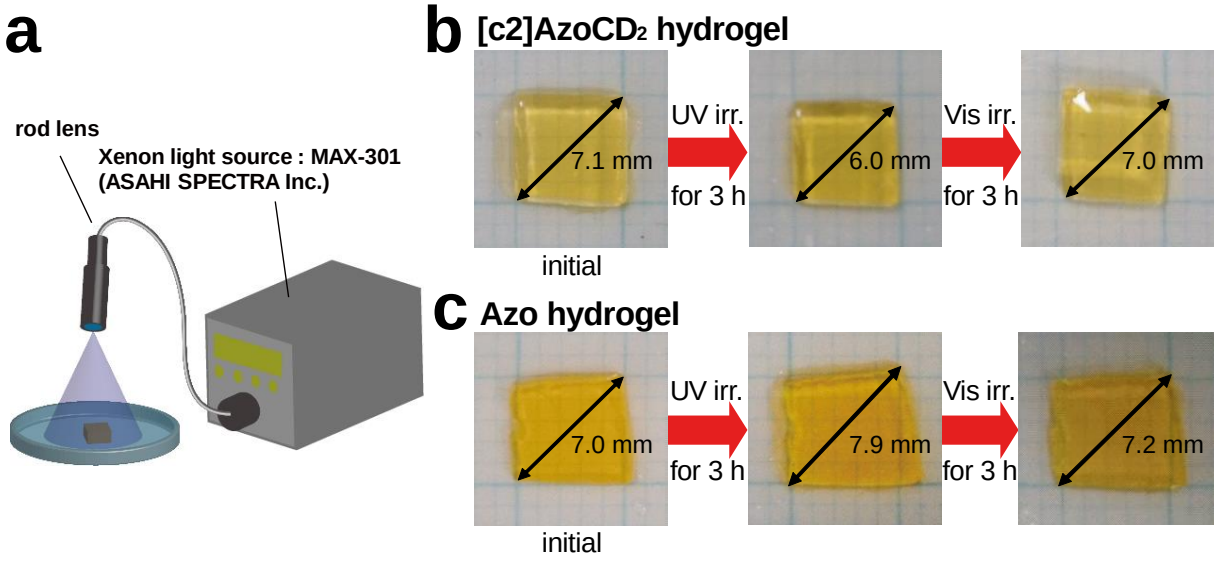

Figure 3-12. Photo-responsive properties of the [c2]AzoCD$_2$ hydrogel and the Azo hydrogel. **a)** Irradiation experimental setup of the cuboid gels (5 × 5 × 1 mm^3) in water. **b)** and **c)** Photographs of the volume changes of the [c2]AzoCD$_2$ hydrogel and the Azo hydrogel upon irradiation with UV (λ = 365 nm) and Vis light (λ = 430 nm) for three hours, respectively.

Figures 3-12b and 3-12c show photographs of volume changes of the [c2]AzoCD$_2$ hydrogel and the Azo gel upon UV and Vis light irradiation, respectively. Irradiating the cuboid [c2]AzoCD$_2$ hydrogel with UV light for 3 hours decreases the volume, whereas continuously irradiating the shrunken gel with Vis light for 3 hours recovers the initial volume (Figure 3-12b). On the contrary, irradiating the Azo hydrogel with UV light increases the

volume, and continuously irradiating with Vis light restores the initial volume (Figure 3-12c). Figure 3-13 shows the correlation between the weight ratio and irradiation wavelength. As seen above, the [c2]AzoCD$_2$ hydrogel and the Azo hydrogel show opposite contraction and expansion behaviour. Of course, irradiation does not change the volume of the PEG hydrogel at all. The contraction–expansion motion of [c2]AzoCD$_2$ induces a volume change in the [c2]AzoCD$_2$ hydrogel.

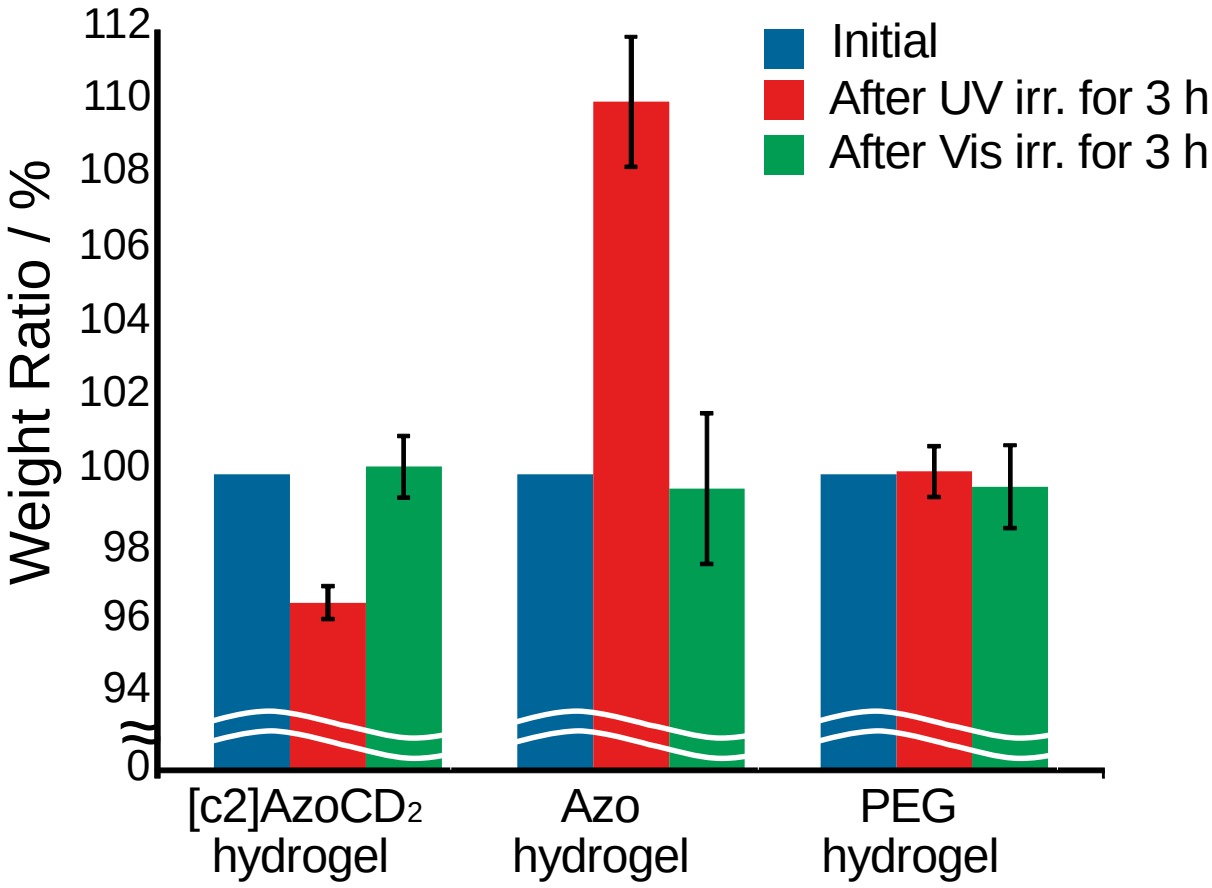

Figure 3-13. Weight change of the [c2]AzoCD$_2$ hydrogel, Azo hydrogel, and PEG hydrogel before and after photo-irradiation with UV and Vis light. The weight ratio (%) is measured with a scale.

The conformational change induced by UV light irradiation discharges the adsorbed water of the [c2]AzoCD$_2$ hydrogel, shrinking the gel pore (Figure 3-14a). The contracted state of [c2]AzoCD$_2$ is restored to the initial expanded state. The recovering the

conformation causes the absorption of water upon Vis irradiation due to the swelling of the gel pore. On the other hand, the Azo hydrogel prior to UV irradiation forms the contracted state because the hydrophobic *trans*-Azo groups assembles to function as noncovalent cross-linkers (Figure 3-14b). After UV irradiation, the assembly decomposes to decrease the cross-link density with photo-isomerization from *trans*- to *cis*-Azo.

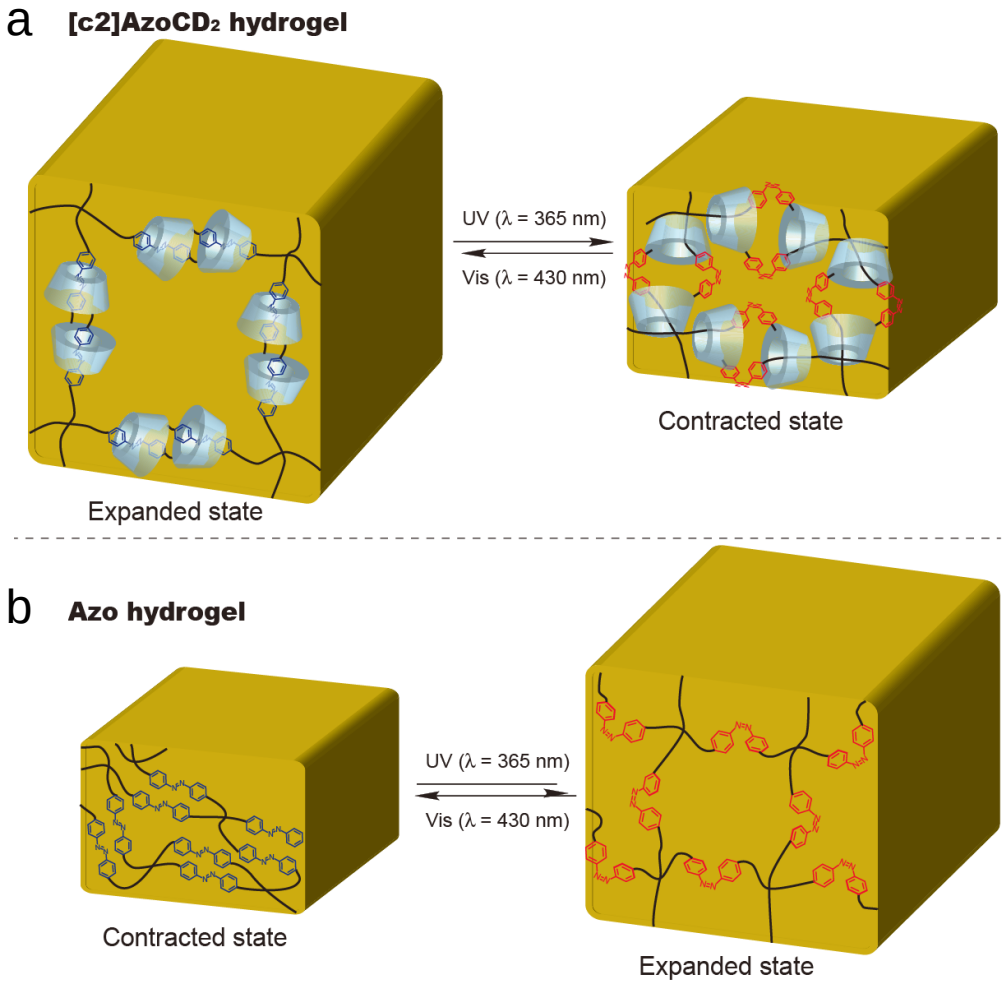

Figure 3-14. **a)** Schematic illustration of the expansion–contraction of the [c2]AzoCD$_2$ hydrogel upon photo-irradiation. UV irradiation induces isomerization of the Azo unit from the *trans*- to *cis*-form. The structure of [c2]AzoCD$_2$ changes from the expanded state to the contracted state upon UV irradiation. Vis irradiation causes isomerization from the *cis*- to *trans*-form, and the contracted state of [c2]AzoCD$_2$ recovers to the initial expanded state due to Vis light irradiation. **b)** Schematic illustration of the expansion–contraction of the Azo hydrogel upon photo-irradiation. The *trans*-Azo units associate hydrophobically to act as cross-linkers. After UV irradiation, the assembly dissociates to increase the volume of the Azo hydrogel.

Photo-isomerization of azobenzene moieties in the gel

Azo derivatives are known to show the *trans*-to-*cis* and *cis*-to-*trans* photo-isomerization under irradiation with UV and Vis light, respectively. UV-Vis spectroscopy and ^{1}H FGMAS NMR spectrometry were carried out by the photo-isomerization of the azobenzene group in the gels (Figure 3-15, 3-16 and 3-17). As similar to the photo-isomerization of [c2]DMTAzoCD$_2$, the intensity of π-π* transition band of the *trans*-Azo group decreases and an *n*-π* transition band appears upon UV light irradiation.

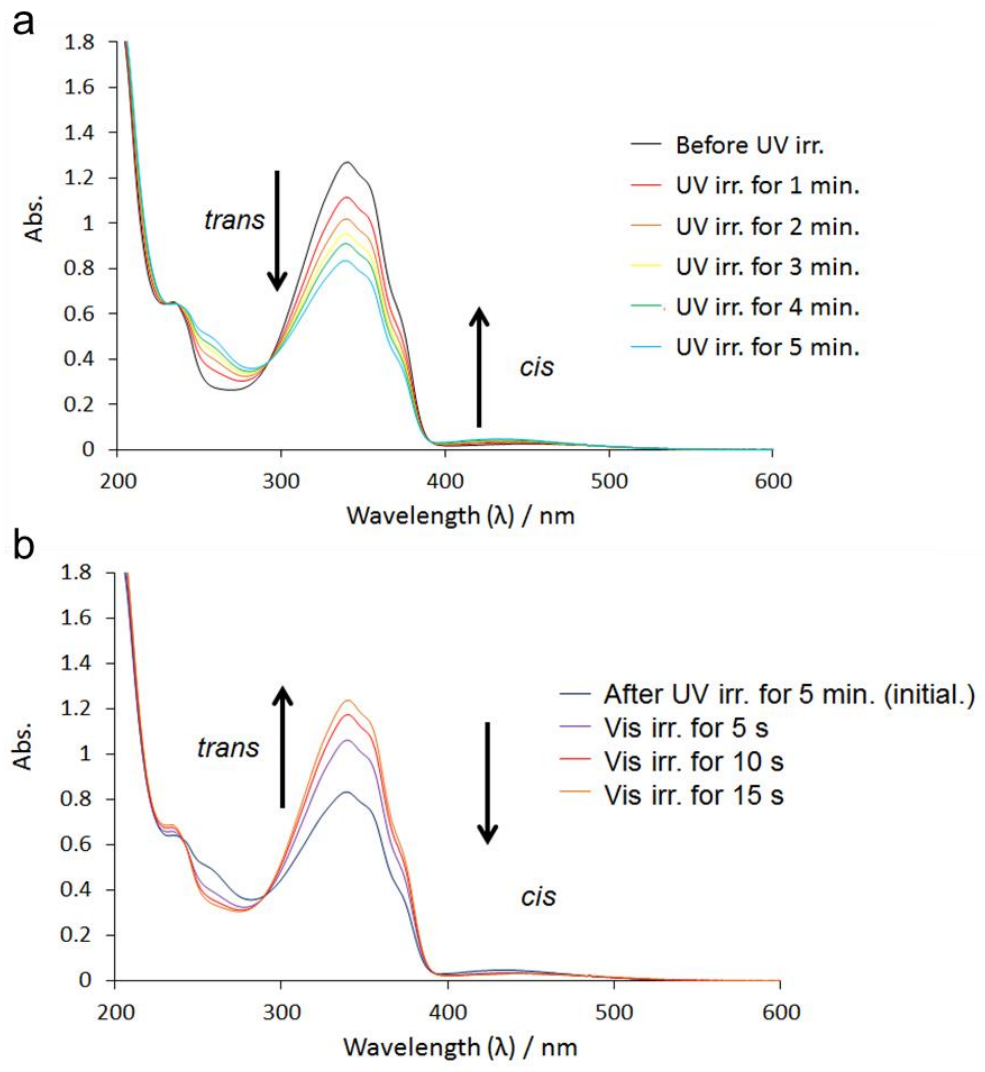

Figure 3-15. Time-resolved absorption spectra for the [c2]AzoCD$_2$ hydrogel under photo-irradiation with **a)** UV (λ = 365 nm) and **b)** visible (λ = 430 nm) lights respectively.

Conversely, Vis light irradiation recovers the intensity of π-π* transition band and the n-π* transition band disappears. These results indicate that the Azo units in the [c2]AzoCD$_2$ gel and the Azo gel have the reversible photo-isomerization ability inside the gels.

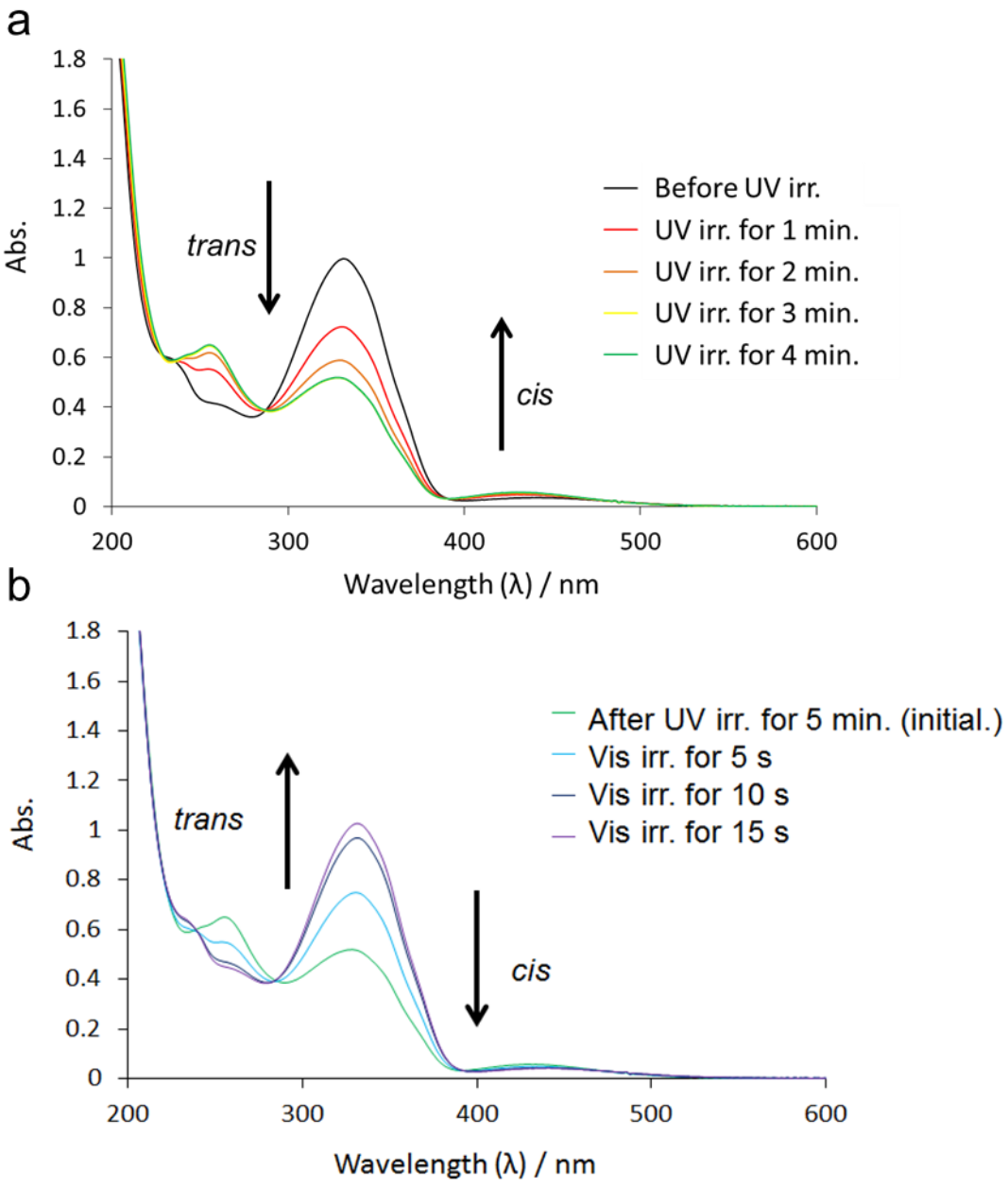

Figure 3-16. Time-resolved absorption spectra for the Azo hydrogel under photo-irradiation with **a)** UV (λ = 365 nm) and **b)** visible (λ = 430 nm) light respectively.

The degree of photo-isomerization ratio of Azo moiety in the [c2]AzoCD$_2$ hydrogel was evaluated by ^{1}H FGMAS NMR spectrometry. Figure 3-17 shows the ^{1}H NMR spectra of [c2]AzoCD$_2$ hydrogel. Before UV irradiation, the ratio of *trans*- and *cis*-Azo was 99.9 : 0.1. After UV irradiation, the ratio of *trans*- and *cis*-isomers was changed to 98.4 : 1.6. Subsequent Vis light irradiation, the ratio was restored to the initial one.

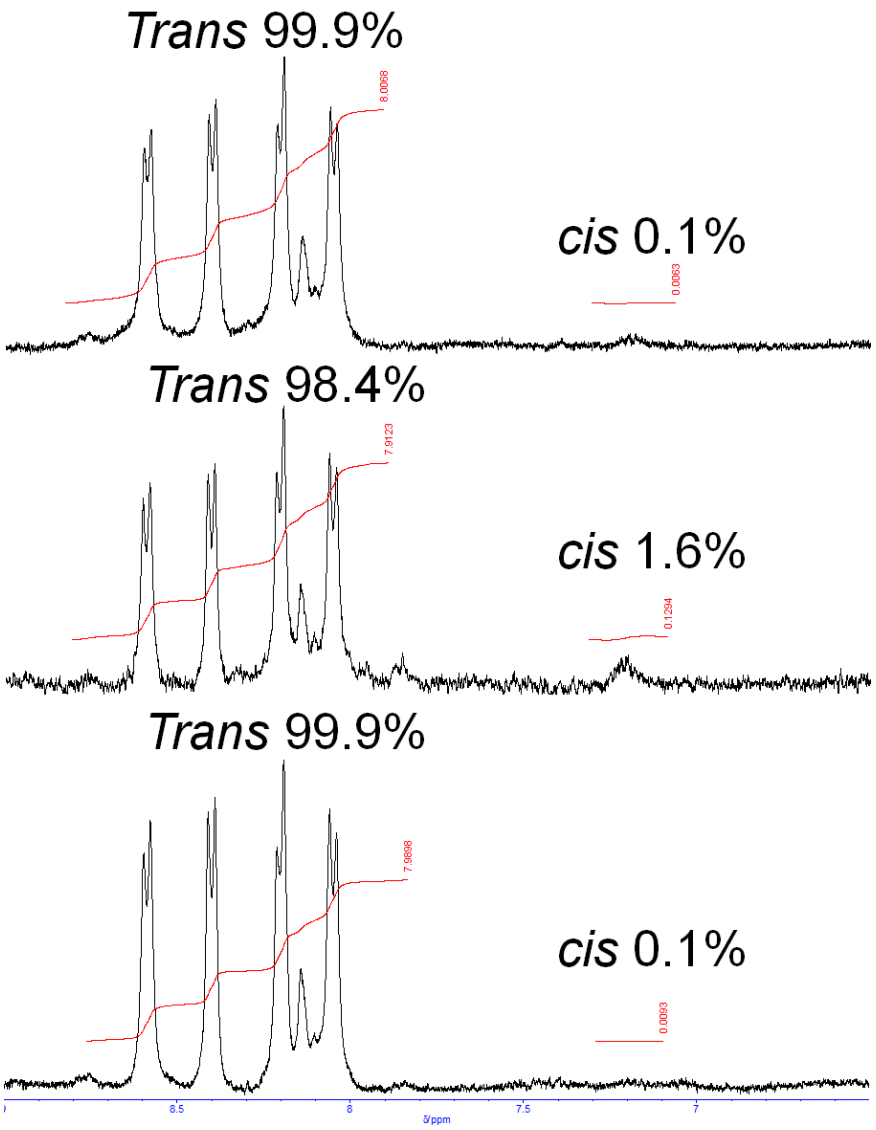

Figure 3-17. ^{1}H FGMAS NMR spectra of the [c2]AzoCD$_2$ hydrogel **a)** before UV irradiation, **b)** after UV (λ = 365 nm) irradiation, and **c)** after Vis (λ = 430 nm) irradiation. The degree of photo-isomerization ratios of Azo groups were evaluated by the integral value before and after light irradiations.

Photo-responsive actuation of the [c2]AzoCD$_2$ hydrogel

The correlation between the direction of the incident light and the deformation directions with UV light (λ = 365 nm) and Vis light (λ = 430 nm) was investigated. The [c2]AzoCD$_2$ hydrogel or the Azo gel actuator composed of the plate gels (20 × 10 × 1–2 mm^3) were immersed in water. A rod lens with a xenon lamp was placed on the right side of the gel. When the [c2]AzoCD$_2$ hydrogel was bent to the right side upon UV light irradiation, subsequent under irradiation with Vis light from the right side, the hydrogel restored to the initial condition (Figure 3-18a). Similarly, irradiation of the [c2]AzoCD$_2$ hydrogel from the left side with UV light causes the hydrogel to bend to the left, and the initial state is restored upon irradiation of the bent hydrogel with Vis light. By contrast, irradiation of the Azo hydrogel with UV light from the right side bends the hydrogel to the left, and irradiation of the bent Azo hydrogel with Vis light restores the initial condition (Figure 3-18e). These results demonstrate that the flexion behaviour of the [c2]AzoCD$_2$ hydrogel and Azo hydrogel have opposite motions dependence on the light direction. Figures 3-18b and 3-18f show the flexion angle (θ) of hydrogels irradiated with UV and Vis light, respectively, for 3 hours. The (θ) value becomes saturated after ca. 3 hours of UV irradiation and does not significantly decrease upon standing under its own weight for 1 hour in the dark. By contrast, irradiation with Vis light immediately restores the bent gel to the initial state. It takes shorter time than that bending of [c2]AzoCD$_2$ gel by UV light irradiation. Because the photo-isomerization speed of Azo units which are outside of CD cavity is faster than its inside one. Figure 3-16c shows the repetition experiment for the [c2]AzoCD$_2$ hydrogel upon alternating irradiation with UV and Vis light for 1 hour. The plate hydrogel exhibits a back-and-forth motion that depends on the wavelength regardless of the irradiation history. The bending behaviour of the [c2]AzoCD$_2$ gel can be repeated for at least ten cycles with various strains.

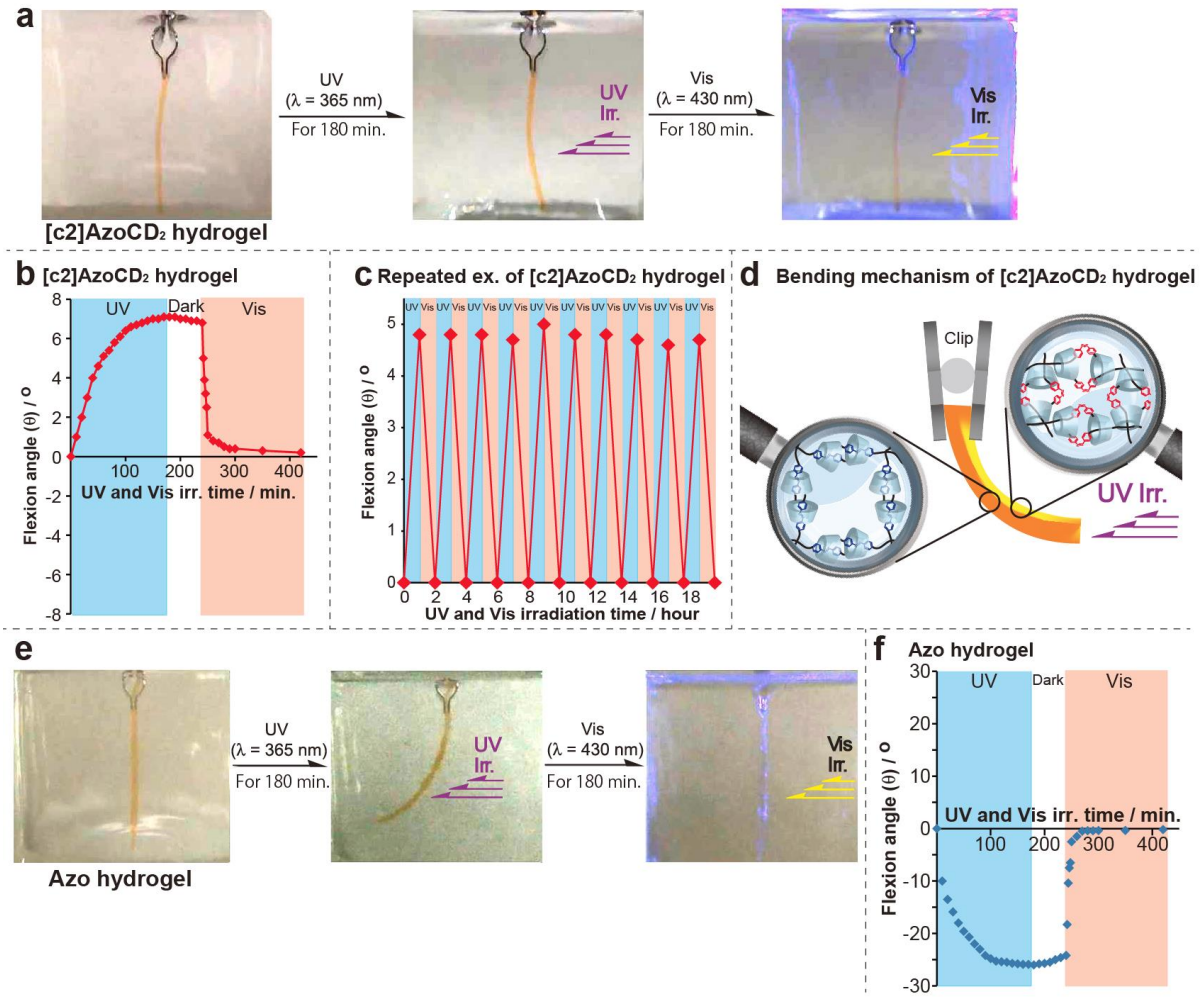

Figure 3-18. **a)** Photographs of the [c2]AzoCD$_2$ hydrogel irradiated with UV and Vis light. Upon UV irradiation, the [c2]AzoCD$_2$ hydrogel bends to the right but continuous Vis light irradiation results in recovery of the initial form. **b)** Plot of the flexion angle (θ) as a function of irradiation time of the [c2]AzoCD$_2$ hydrogel. The blue, red, and white areas denote UV irradiation, Vis irradiation, and dark storage without light exposure, respectively. The flexion angle (θ) was measured using snapshots. **c)** Repetition experiment of the [c2]AzoCD$_2$ hydrogel irradiated with UV and Vis light for 1 hour. The plot shows the correlation between the irradiation time and flexion angle (θ). **d)** Schematic illustration of the bending mechanism of the [c2]AzoCD$_2$ hydrogel upon photo-irradiation. UV light decreases the volume of the exposed surface of the [c2]AzoCD$_2$ hydrogel, and the volume of the non-exposed side remains constant. The strain between the exposed and unexposed areas results in flexion. **e)** Photographs of the Azo hydrogel irradiated by UV and Vis light. UV light irradiation bends the Azo hydrogel but continuous Vis light irradiation results in recovery of the initial form. **f)** Plot of the flexion angle (θ) as a function of irradiation time for the Azo hydrogel.

These results indicate that the flex behaviour of the [c2]AzoCD$_2$ hydrogel is the opposite that of the Azo hydrogel. θ of the [c2]AzoCD$_2$ hydrogel is positive (Figure 3-18b) but θ of the Azo hydrogel is negative (Figure 3-18f). Because, the flexion mechanism of the [c2]AzoCD$_2$ hydrogel and Azo hydrogel were different. The [c2]AzoCD$_2$ hydrogel bends towards the light source because the exposed surface of the hydrogel preferentially absorbs UV light energy. The conformation change of the [c2]AzoCD$_2$ unit induced by UV light irradiation and the gel was shrunk by discharge of water from the [c2]AzoCD$_2$ gel. UV light irradiation decreased the volume of the exposed surface, and the non-exposed side remained constant (Fig. 3-18d). In contrast, the Azo hydrogel bends away from the light source because prior to UV irradiation, the *trans*-Azo units associate hydrophobically to act as cross-linkers. After UV irradiation, the assembly dissociates, and the cross-linking density was decreased. Then, the volume of the exposed surface increased upon photo-isomerization from *trans*- to *cis*-Azo.

Response rate of the [c2]AzoCD$_2$ hydrogel

As can be seen in Figures 3-18b and 3-18f, the initial bending rate (V_0) of the [c2]AzoCD$_2$ and the Azo hydrogel are clearly different. To determine the initial bending rate (V_0) of the [c2]AzoCD$_2$ and Azo hydrogel, the author compared the bending efficiency of the [c2]AzoCD$_2$ and the Azo hydrogel. V_0 of the Azo hydrogel ($V_0 = 1.7\times10^{-2}$ deg s^{-1}) is faster than that of the [c2]AzoCD$_2$ hydrogel ($V_0 = 1.7\times10^{-3}$ deg s^{-1}). The [c2]AzoCD$_2$ hydrogel and the Azo hydrogel have different contraction–expansion mechanisms. The contraction–expansion mechanism of the [c2]AzoCD$_2$ hydrogel is based on the change in the end-to-end distance of the [c2]daisy chain and desorption of water upon irradiation with UV light. On the other hand, contraction–expansion mechanism of Azo hydrogel is based on the change in the cross-linking density. These are related to the swelling pressure (absorption and

desorption of water) and isomerization of the Azo unit. As shown in Figure 3-15, the isomerization rate of the Azo unit in the [c2]AzoCD$_2$ hydrogel is slower than that in the Azo hydrogel because the formation of the inclusion complex suppresses the isomerization of the Azo unit. In regards to the thickness of the [c2]AzoCD$_2$ hydrogel, V_0 of the [c2]AzoCD$_2$ hydrogel decreased with the thickness (Figure 3-19). If the hydrogel is more than 4 mm thick, the [c2]AzoCD$_2$ hydrogel does not exhibit any bending behaviour upon irradiation with UV light. In addition, the strain between the exposed and unexposed areas creates the flexion behaviour of the [c2]AzoCD$_2$ hydrogel and Azo hydrogel.

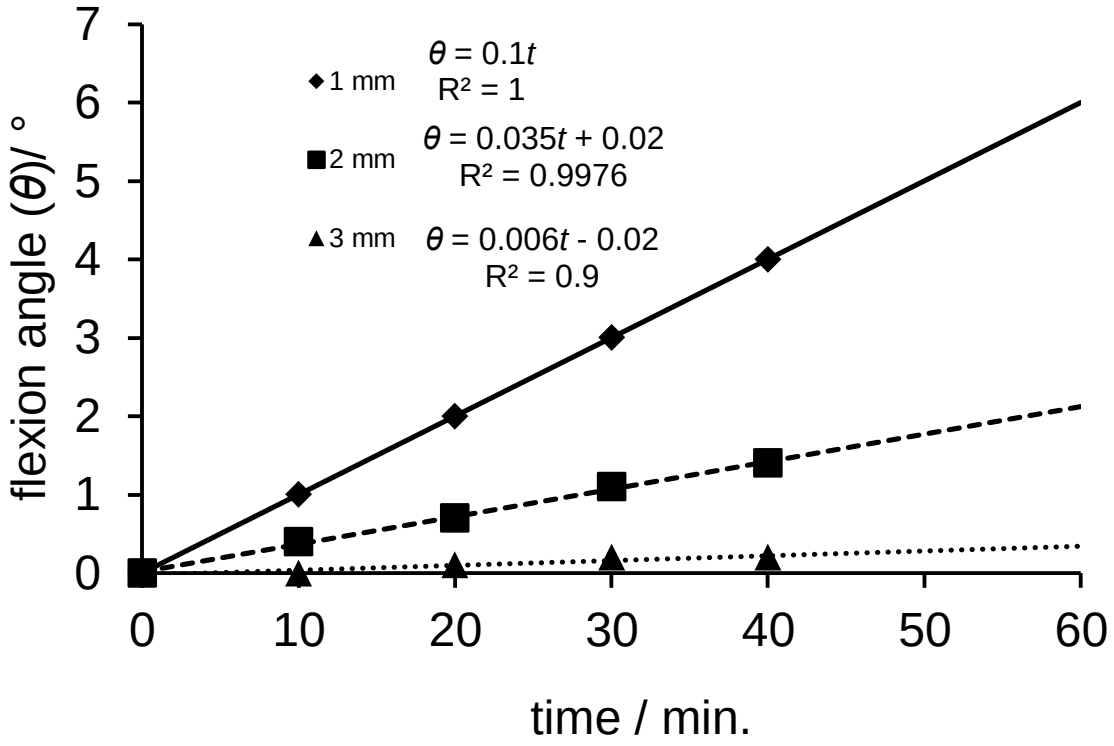

Figure 3-19. Plot of the flexion angle versus irradiation time in the case of the [c2]AzoCD$_2$ hydrogel with different thicknesses. Thickness; 1 mm (◆), 2 mm (■) and 3 mm (▲). The initial rate (V_0) was calculated from the slopes. Each initial velocities were 1.7×10^{-3} deg s^{-1} (1 mm), 5.8×10^{-4} deg s^{-1}) (2 mm) and 1.0×10^{-4} deg s^{-1}.

Mechanical property of [c2]AzoCD$_2$ hydrogel

The author evaluated the change in the cross-link density in response to photo-stimuli by using stress–strain measurements. In general, the Young's modulus is related to the cross-link density of materials. Figure 3-20 shows stress-strain curves with the UV light irradiation. The rupture stress of the [c2]AzoCD$_2$ hydrogel does not change because a number of the covalent cross-link points are not fundamentally influenced by photo-irradiation. However, the rupture strain value of the [c2]AzoCD$_2$ hydrogel increased with UV light irradiation. Continuous irradiation with Vis light recovered the initial rupture strain. The Young's modulus of the [c2]AzoCD$_2$ hydrogel decreased slightly after UV irradiation for 3 hours.

Upon comprehensive consideration of the rupture stress, strain, and Young's modulus, the expanded state of the [c2]AzoCD$_2$ unit with the *trans*-Azo forms a relatively stable inclusion complex that functions as a non-covalent cross-linker because the association constant of αCD with *trans*-Azo is higher than that of *cis*-Azo. After UV light irradiation, the *cis*-Azo unit leaves the cavity of αCD, which increases the sliding mobility of the AmAzoCD unit and leads to an increased rupture strain (stretching property) and decreased Young's modulus (decreasing cross-link density). By contrast, the Azo hydrogel exhibits different material properties in response to photo-irradiation. The Young's modulus and rupture stress of the Azo hydrogel (20 kPa and 20 kPa) decreased to 5.0 kPa and 14 kPa, respectively, after UV light irradiation for 3 hours, indicating that UV light irradiation decreased the cross-linking density. The change in the cross-linking density in response to the photo-stimuli leads to uptake and release of water in the Azo hydrogel. The decreasing cross-link density results in a decrease in the rupture stress and an increase in the rupture strain. These results demonstrate that the [c2]AzoCD$_2$ hydrogel has an entirely different contraction–expansion mechanism from that of the Azo hydrogel.

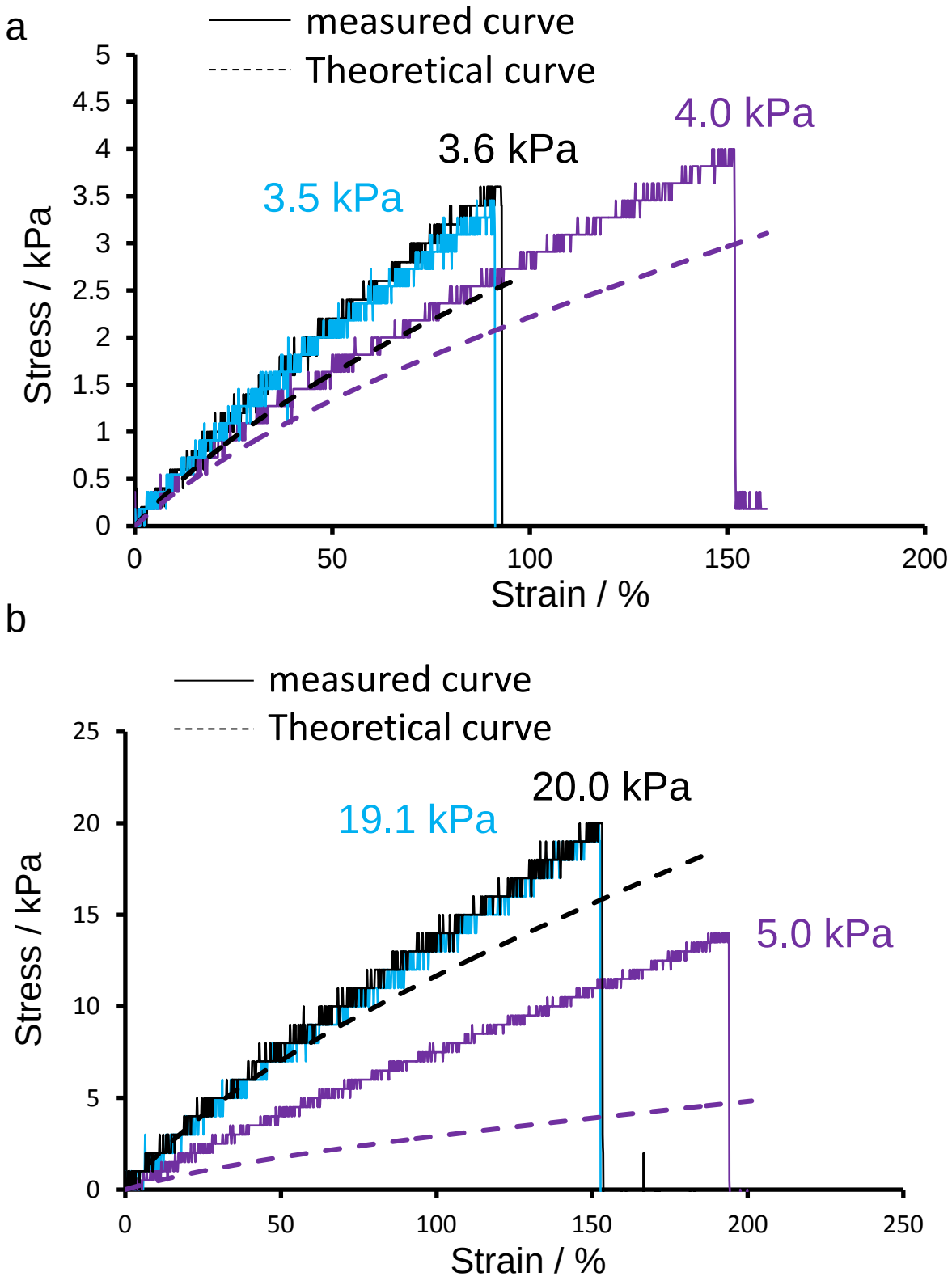

Figure 3-20. Stress–strain curves of **a)** the [c2]AzoCD$_2$ and **b)** Azo hydrogel. Before UV irradiation (—), after UV (λ = 365 nm) irradiation (—) and after Vis (λ = 430 nm) irradiation (—). (---) indicates theoretical curve following affine network model.

Mechanical works of [c2]AzoCD$_2$ hydrogel

The conversion of the photo-irradiation energy to mechanical work is important for estimating the mechanical work conversion efficiency of the [c2]AzoCD$_2$ hydrogel (Figure 3-21) upon UV irradiation. A weight (34.4 mg) was attached to the bottom of a rectangular gel (size: 10×5×1 mm^3). UV light irradiation results in the contraction of the gel, lifting the weight. Figure 3-22 shows the position of the weight as a function of irradiation time. During UV light irradiation, the weight undergoes a mechanical work (W), which is determined by $W = (m\text{-}\rho V)\,gx$ (m: the mass of weight; ρ: the density of buffer; V: the volume of weight; g: the gravitational acceleration; x: the difference in height of the weight). The mechanical work of the [c2]AzoCD$_2$ hydrogel and xerogel was estimated to be ca. 0.12 μJ.

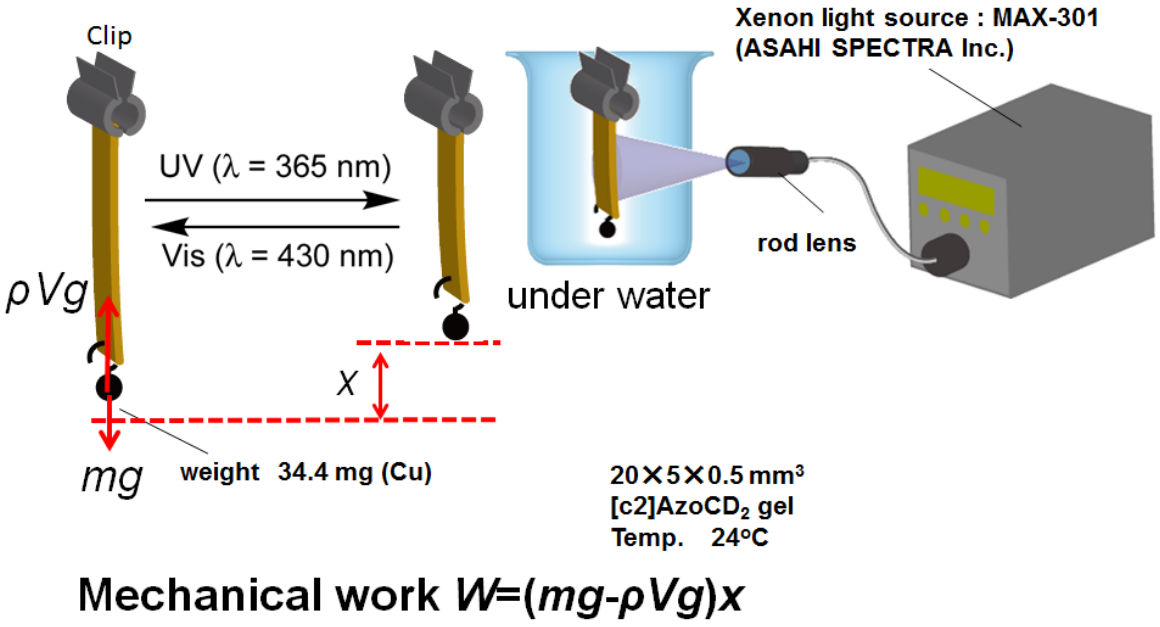

Figure 3-21. Experimental setup of the [c2]AzoCD$_2$ hydrogel actuator in response to photo-stimuli. After UV light irradiation, the length of the hydrogel shorten and the weight became up. Subsequent Vis light irradiation restored the weight to the original position. Here m, ρ, V, g and x denotes the mass of weight, the density of buffer, the volume of weight, the gravitational acceleration and the difference in height of the weight, respectively.

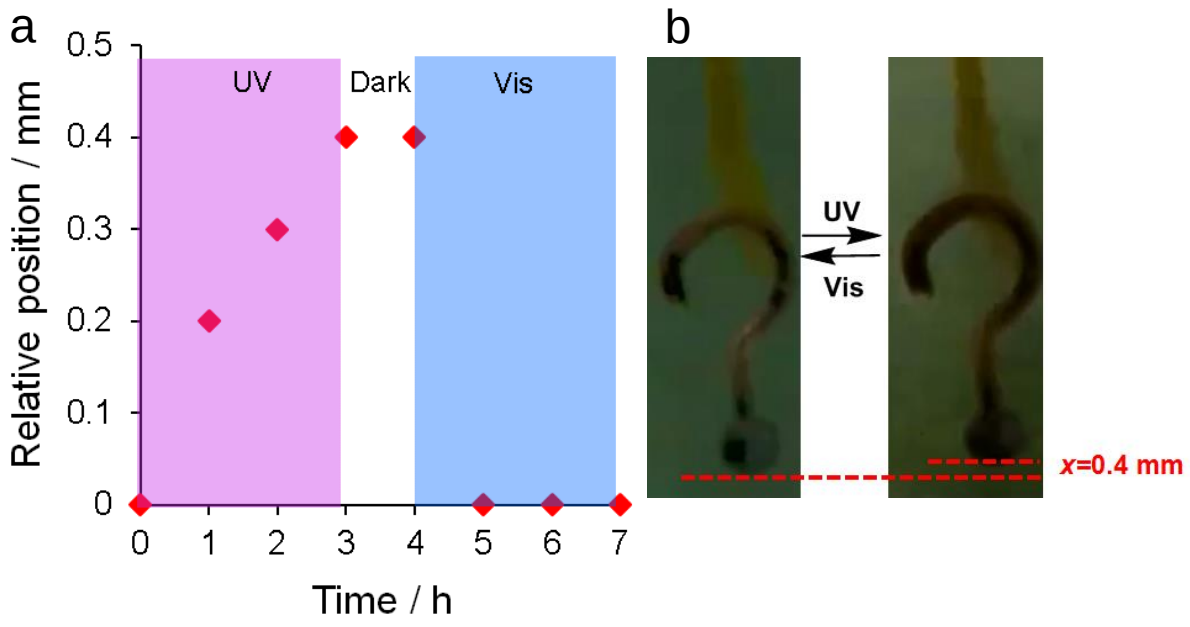

Figure 3-22. **a)** Plot of the relative position of the weight versus irradiation time in the case of the [c2]AzoCD$_2$ hydrogel with a weight (34.4 mg). The mechanical work of the [c2]AzoCD$_2$ hydrogel was estimated to be ca. 0.12 µJ. The energy density was 12 µW/ cm^2. **b)** Photographs of before UV and after UV irradiated [c2]AzoCD$_2$ gel attached copper weight.

Experimental

Materials. Four-armed poly(ethylene glycol) (PTE-100GS) and poly(ethylene glycol)-bis-(3-aminopropyl)ether DE-10PA were obtained from NOF American Corporation.

Measurements

Photo-isomerization. The azobenzene moieties in hydrogel were isomerized by the same Xenon lamp (Asahi spectra MAX-301) in Chapter 2. The distance between the sample cell and the lamp was fixed at 10 cm. The bending experiments of [c2]AzoCD$_2$ xerogel irradiated with UV light (λ = 365 nm) were carried out by a 1 W LED lamp (Asahi spectra POT365).

NMR spectrometer. The solid-state ^{1}H FGMAS NMR spectra were recorded at 400 MHz with a JEOL JNM-ECA 400WB NMR spectrometer. The sample spinning rate was 10 kHz with a relaxation delay of 10 s at 30 °C. Chemical shifts were referenced to adamantane as an external standard (δ = 1.91 ppm).

IR spectrometer. The IR spectra were measured using a JASCO FT/IR-410 spectrometer.

UV-Vis absorption spectrometer. The UV-Vis absorption spectra were recorded with a JASCO V-650 and a Hitachi U-4100 spectrometer in water with a 1-mm quartz cell at room temperature.

Dynamic viscoelasticity measurements.

Dynamic viscoelasticity of hydrogels were measured by an Anton Paar MCR301 rheometer at strain of 0.1%.

Mechanical properties measurements.

Mechanical properties of hydro- and xerogels were measured by a rupture tensing system (Creep meter, RE-33005B, Yamaden Ltd. and Autograph AG-X plus, Shimadzu).

Preparation ofAm-DEG-Azo-DEG-Am

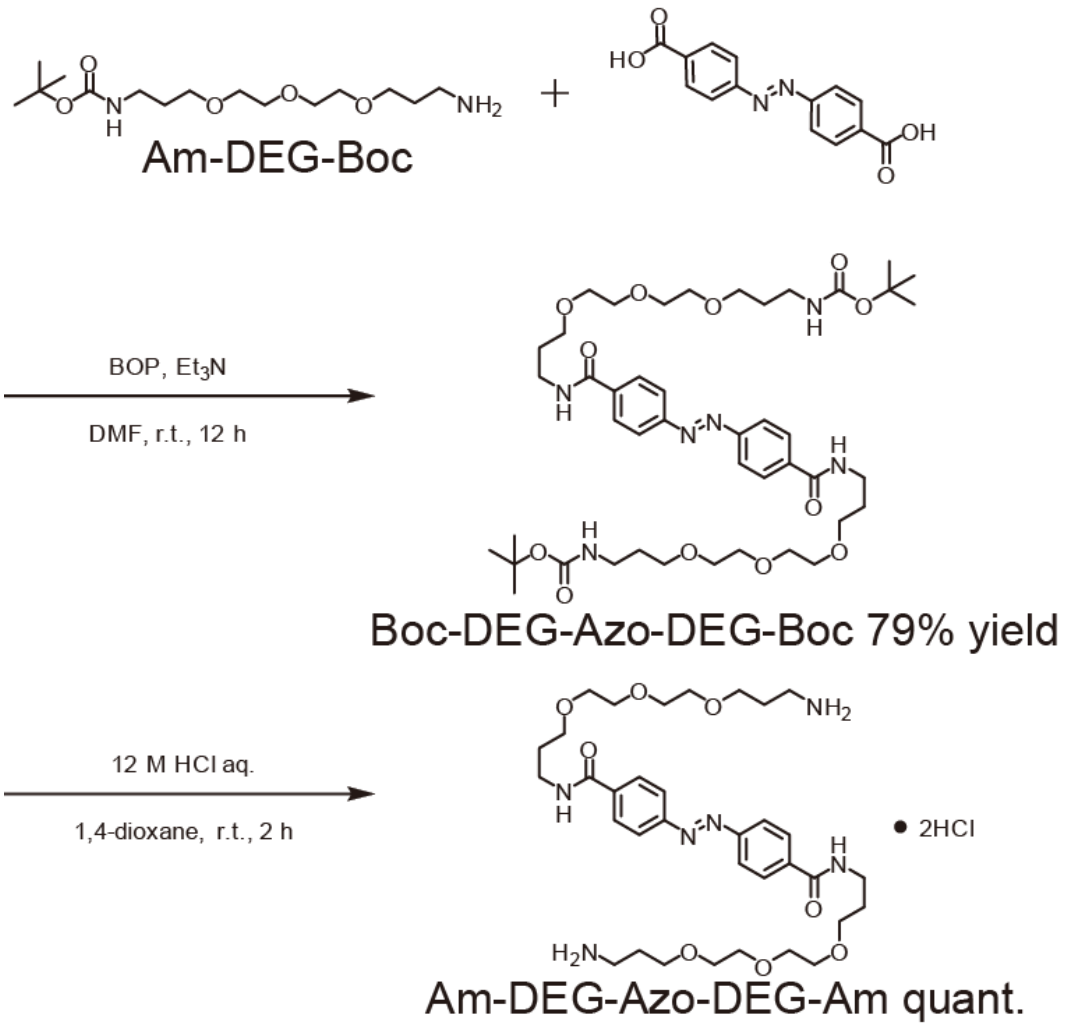

Scheme 3-1. Preparation of Boc-DEG-Azo-DEG-Boc and Am-DEG-Azo-DEG-Am.

Boc-DEG-Azo-DEG-Boc. Am-DEG-Boc (1.5 g, 4.8 mmol), 4-(4-carboxyphenyl)-azo-benzoic acid (0.54 g, 2.0 mmol) and triethylamine (1.4 mL 10 mmol) were dissolved in DMF (10 mL). BOP (3.0 g, 4.8 mmol) was added to the DMF solution at room temperature. After stirred for 12 hours, the reaction mixture was poured into water (100 mL) to remove the reacted BOP reagent. The desired compound was extracted with $CHCl_3$ (60 mL). The $CHCl_3$ layer was washed with 0.1 M $NaHCO_3$ aq., 0.1 M HCl aq., and water several times. The solution was dried over Na_2SO_4. After evaporation, the residue was dispersed into *n*-hexane. The precipitate was separated from organic layer by centrifugalization. After drying the precipitate, the resulting mixture was applied to a Biotage SNAP Ultra 50 g column running a

$CHCl_3$ / MeOH gradient. The crude product eluted in the range of 0–10% $CHCl_3$ / MeOH. The solvents in desired fractions were evaporated to give Boc-DEG-Azo-DEG-Boc as a pale-orange solid (1.4 g, 79%). ^{1}H NMR (500 MHz, DMSO-d_6): δ (ppm) 8.60 (t, J = 5.4 Hz, 2H), 8.04 (d, J = 8.6 Hz, 4H), 7.97 (d, J = 8.4 Hz, 4H), 6.70 (br, 2H), 3.53-3.44 (m, overlaps with H_2O), 2.95 (q, J = 6.7 Hz, 6.3 Hz, 4H), 1.78 (quintet, J = 6.7Hz, 6.5 Hz, Hz, 4H), 1.58 (quintet, J = 6.7 Hz, 6.6 Hz, 4H), 1.35 (s, 9H). ^{13}C NMR (125 MHz, DMSO-d_6): δ (ppm) 165.31, 155.55, 153.15, 137.14, 128.50, 122.51, 77.35, 69.75, 69.57, 69.52, 68.25, 68.07, 37.20, 36.81, 29.69, 29.28, 28.22. MALDI-TOF MS: *m/z* Calcd. for $C_{44}H_{70}N_6O_{12}Na$ ([M + Na]$^+$): 897.5; Found: 897.5; $C_{44}H_{70}N_6O_{12}K$ ([M + K]$^+$): 913.5; Found: 913.5.

Am-DEG-Azo-DEG-Am. Boc-DEG-Azo-DEG-Boc (1.2 g, 1.4 mmol) was dissolved in 1,4-dioxane (9.0 mL). HCl aq. (12 M) (6.0 mL, 68 mmol) was added to the 1,4-dioxane solution. After stirred at r.t. for 2 hours, the solvent in the mixture was evaporated to give Am-DEG-Azo-DEG-Am as a pale-orange powder (1.0 g, quant.). ^{1}H NMR (500 MHz, DMSO-d_6): δ (ppm) 8.72 (br, 2H), 8.08 (d, J = 8 Hz, 4H), 7.99 (br, 3H), 7.96 (d, J = 8 Hz, 4H), 3.53–3.31 (m, overlaps with H_2O), 2.82 (t, J = 7 Hz, 4H), 1.79 (m, 8H). ^{13}C NMR (125 MHz, DMSO-d_6): δ (ppm) 165.31, 153.15, 137.10, 128.56, 122.50, 69.76, 69.65, 69.54, 69.44, 68.26, 67.31, 36.80, 36.58, 29.30, 27.11. MALDI-TOF MS: *m/z* Calcd. for $C_{34}H_{55}N_6O_8$ ([M + H]$^+$): 675.4; Found: 675.2; $C_{34}H_{54}N_6O_8Na$ ([M + Na]$^+$): 697.4; Found: 697.2; $C_{34}H_{54}N_6O_8K$ ([M + K]$^+$): 713.4; Found: 713.2.

a

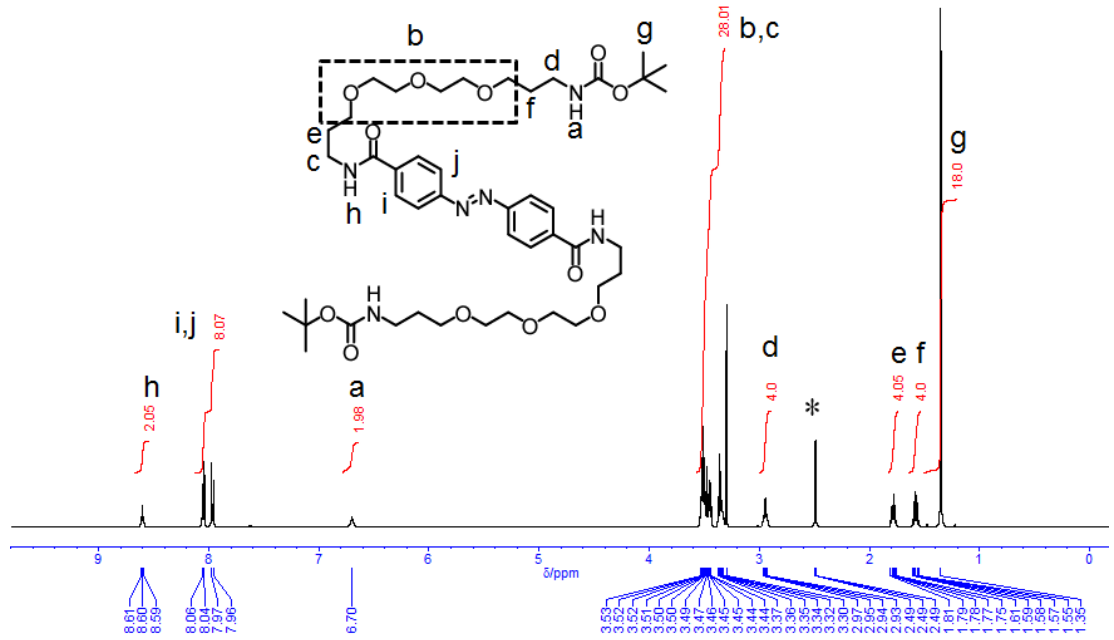

b

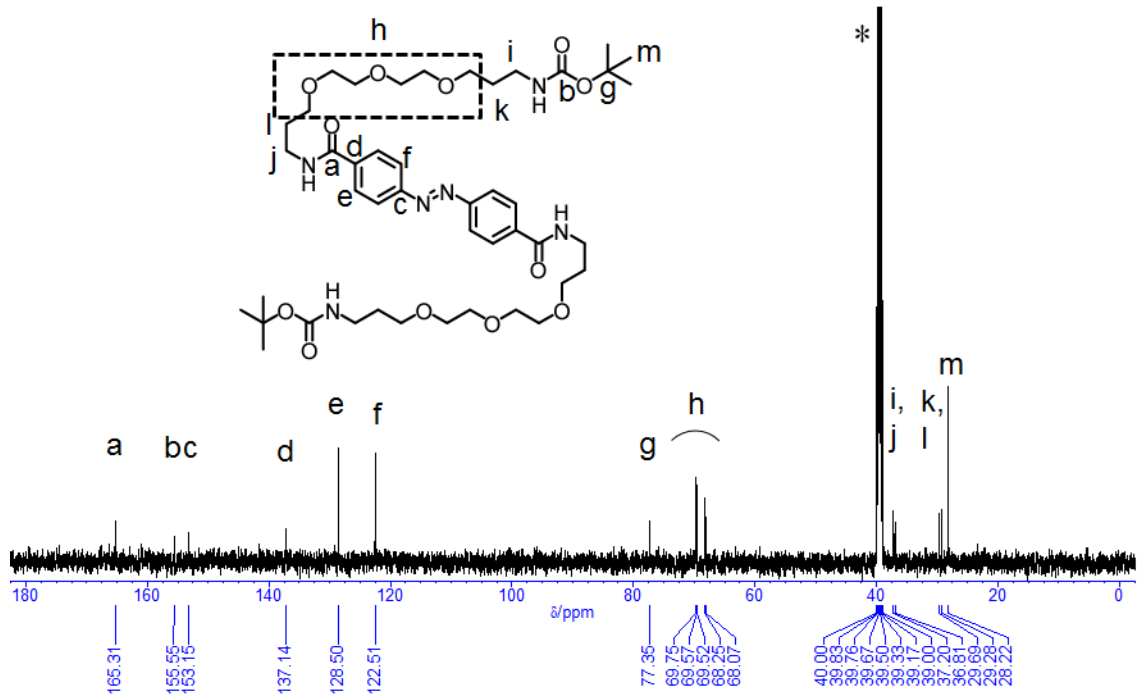

Figure 3-23. **a)** 500 MHz ^{1}H and **b)** 125 MHz ^{13}C NMR spectra of Boc-DEG-Azo-DEG-Boc in DMSO-d_6. "*" denotes the signals due to the solvent used.

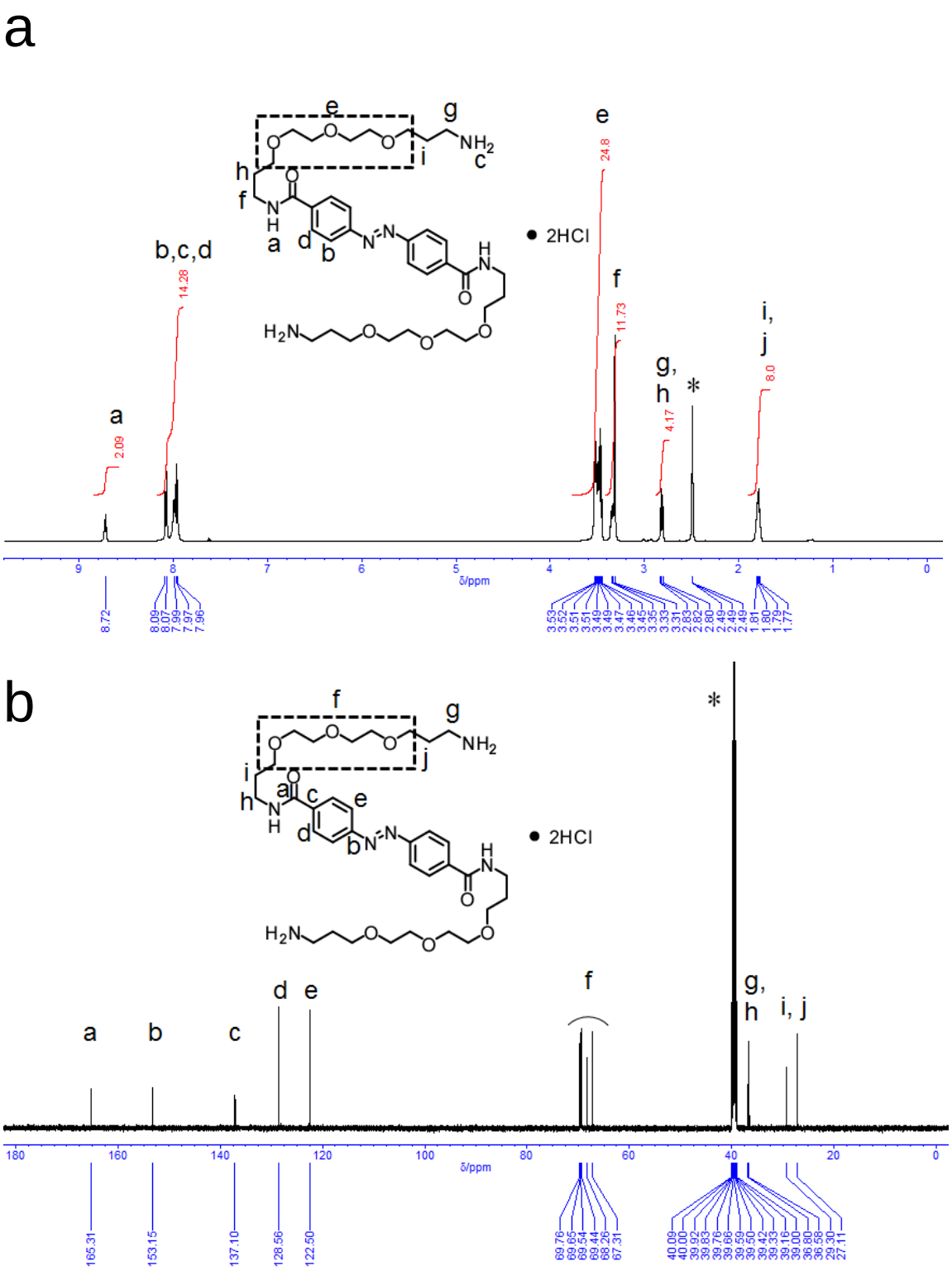

Figure 3-24. **a)** 500 MHz ^{1}H and **b)** 125 MHz ^{13}C NMR spectra of Am-DEG-Azo-DEG-Am in DMSO-d_6. "*" denotes the signals due to the solvent used.

Preparation of a [c2]AzoCD$_2$ hydrogel

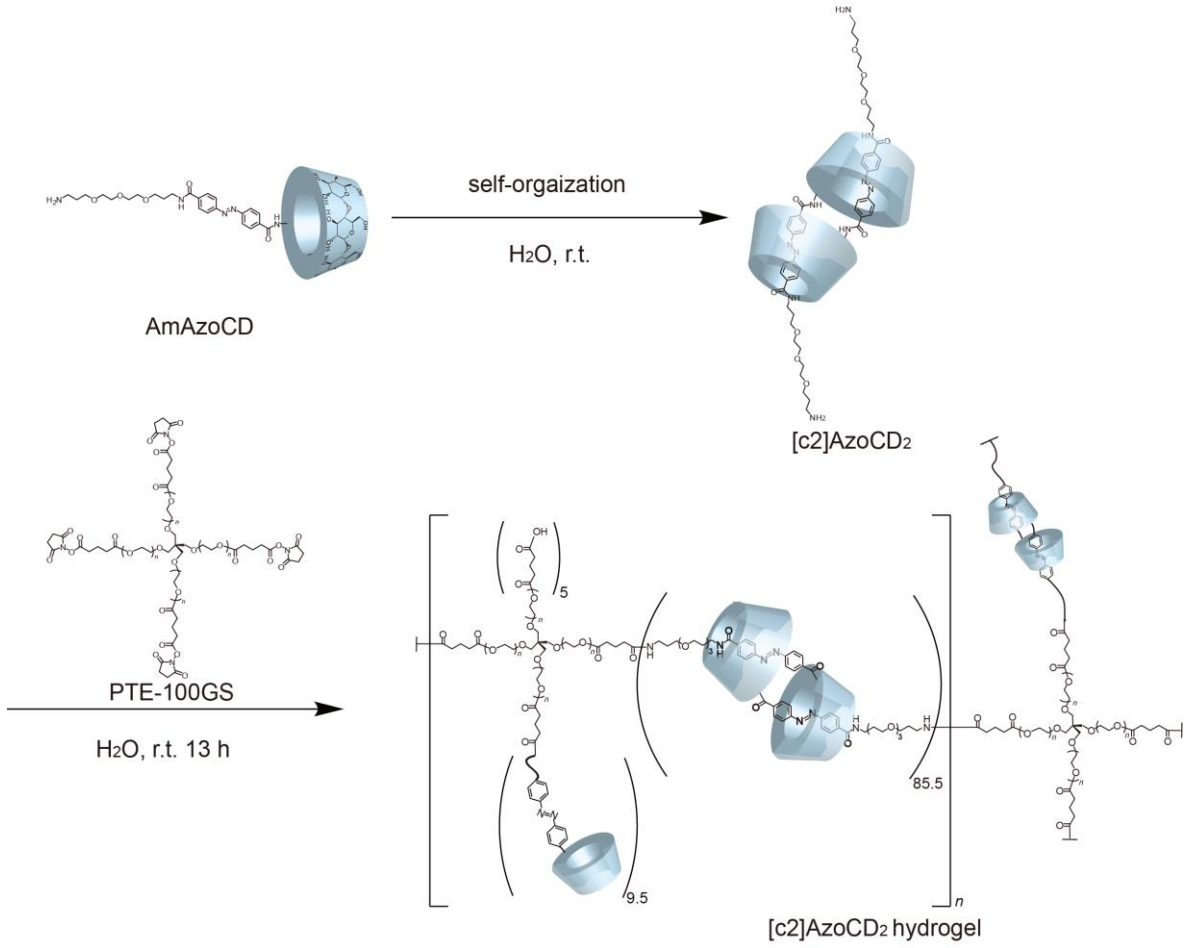

Scheme 3-2. Preparation of the [c2]AzoCD$_2$ hydrogel.

PTE-100GS (100 mg, 10 μmol) was dissolved in water (706 μL). An aqueous solution (706 μL) of AmAzoCD (57 mg, 40 μmol) was added to the aqueous solution of PTE-100GS at 0 ^{o}C. After stirring for an hour, the mixture was warmed to room temperature. After stirring for 13 hours, the obtained hydrogel was washed with DMSO and water several times to give a red-colored [c2]AzoCD$_2$ hydrogel.

^{1}H FGMAS NMR (400 MHz, D$_2$O): δ (ppm) 8.59 (d, J = 32 Hz, 2H), 8.40 (d, J = 32 Hz, 2H), 8.20 (d, J = 32 Hz, 2H), 8.14 (br, 0.8H), 8.05 (d, J = 32 Hz, 2H), 5.31–2.91 (m, overlaps with H$_2$O), 2.57–2.54 (m, 2H), 242–2.38 (m, 2H), 2.10–1.88(m, 6H).

Preparation of an Azo hydrogel

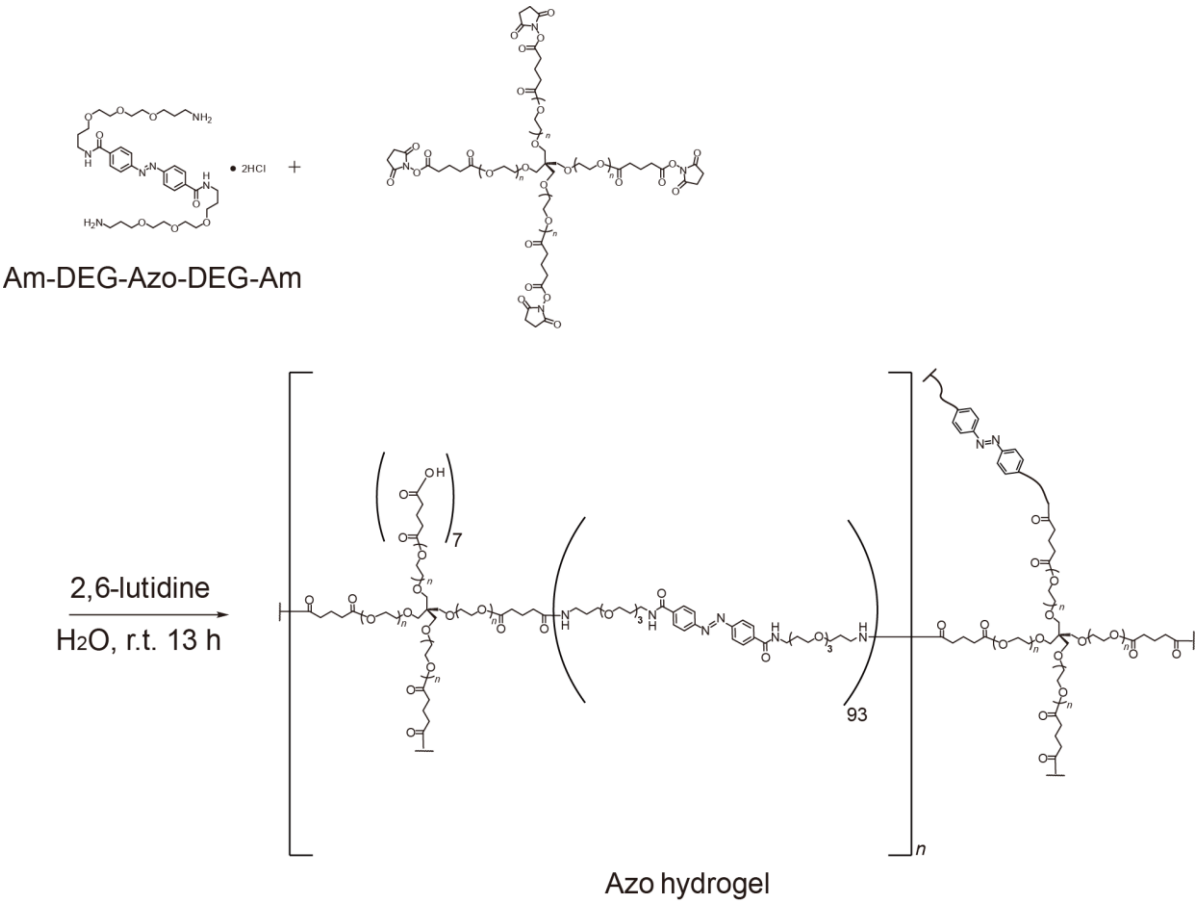

Scheme 3-3. Preparation of the Azo hydrogel.

PTE-100GS (100 mg, 10 μmol) was dissolved in water (515 μL). An aqueous solution (515 μL) of Am-DEG-Azo-DEG-Am (15 mg, 20 μmol) and 2,6-lutidine were added to the aqueous solution of PTE-100GS at room temperature After stirring for 13 hours, the obtained hydrogel was washed with DMSO and water several times to give a red-colored Azo hydrogel.

^{1}H FGMAS NMR (400 MHz, D_2O): δ (ppm) 7.91 (br, 4H), 4.94–3.22 (m, overlaps with H_2O), 2.40(br, 2H), 2.23 (br, 2H), 1.92–1.76(m, 6H).

Preparation of a PEG hydrogel

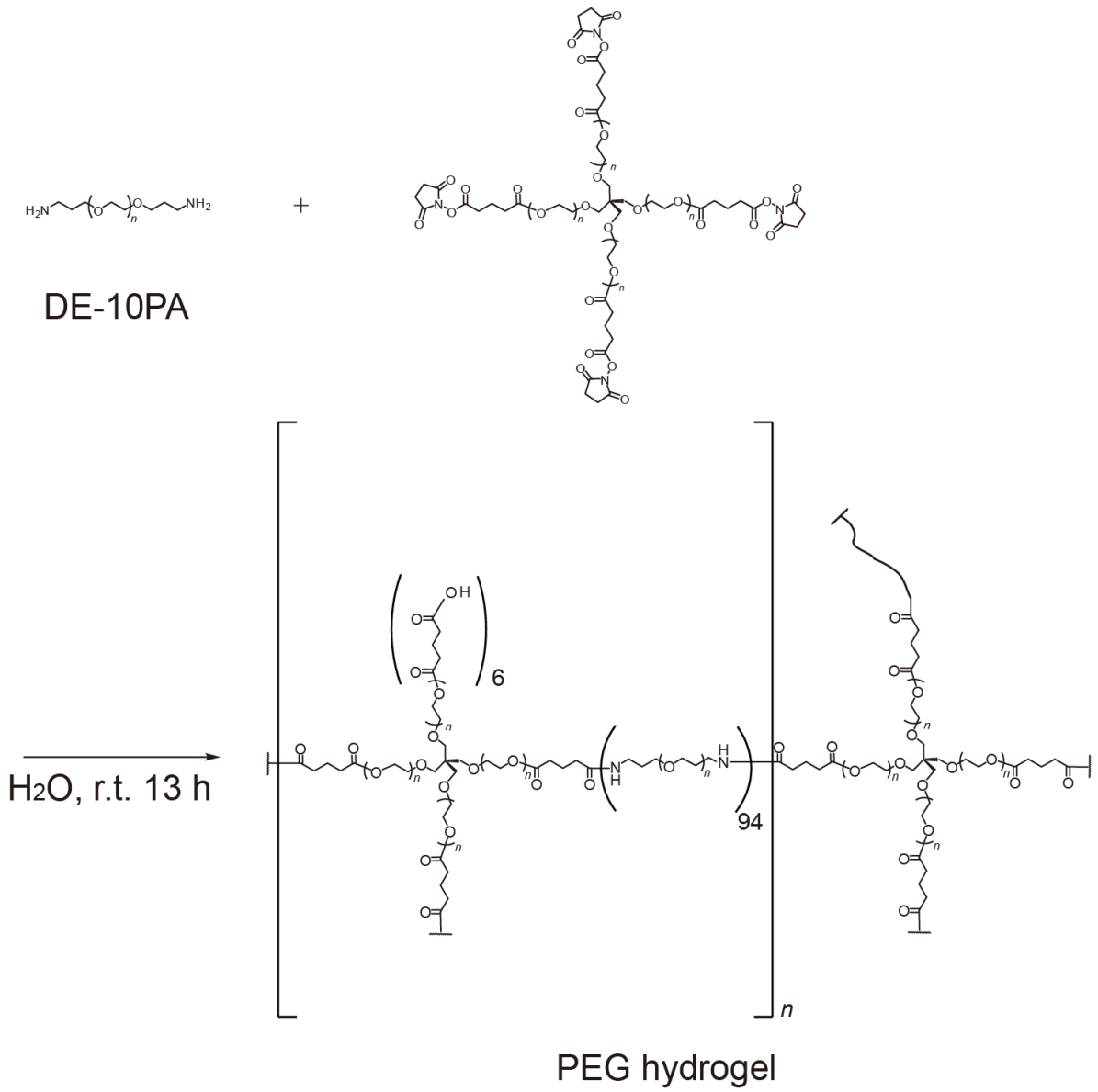

Scheme 3-4. Preparation of the PEG hydrogel.

PTE-100GS (100 mg, 10 μmol) was dissolved in water (540 μL). An aqueous solution (540 μL) of DE-10PA (20 mg, 20 μmol) was added to the aqueous solution of PTE-100GS at room temperature After stirring for 13 hours, the obtained hydrogel was washed with DMSO and water several times to give a colorless PEG hydrogel.

^{1}H FGMAS NMR (400 MHz, D_2O): δ (ppm) 4.94–3.36 (m, overlaps with H_2O), 2.57(t, J = 8 Hz, 2H), 2.41 (t, J = 8 Hz, 2H), 2.03 (quintet, J = 4 Hz, 2H), 1.91 (quintet, J = 8 Hz, 2H).

References

1 Alberts, B.; Johnson, A.; Lewis, J.; Raff, M.; Roberts, K.; Walter, P. *Molecular Biology of the Cell*, 5th ed.; Garland Science: New York, (2008).

2 Yin, H. *et al.* Transcription Against an Applied Force. *Science* **270**, 1653-1657 (1995).

3 Hirokawa, N. Kinesin and Dynein Superfamily Proteins and the Mechanism of Organelle Transport. *Science* **279**, 519–526 (1998).

4 Vale, R. D., Milligan, R. A. The Way Things Move: Looking Under the Hood of Molecular Motor Proteins. *Science* **288**, 88–95 (2000).

5 Schill, G. *Catenanes, Rotaxanes, and Knots*; Academic Press: New York, (1971).

6 Dietrich-Buchecker, C. O., Sauvage, J. P. Interlocking of molecular threads: from the statistical approach to the templated synthesis of catenands. *Chem. Rev.* **87**, 795–810 (1987).

7 Amabilino, D. B. Stoddart, J. F. Interlocked and Intertwined Structures and Superstructures. *Chem. Rev.* **95**, 2725–2828 (1995).

8 Niess, F. *et al.* Molecular Muscles: From Species in Solution to Materials and Devices. *Chem. Lett.* **43**, 964-974 (2014).

9 Ashton, P. R. *et al.* Supramolecular Daisy Chains. *Angew. Chem. Int. Ed.* **37**, 1294–1297 (1998).

10 Kay, E. R., Leigh, D. A. Zerbetto, F. Synthetic Molecular Motors and Mechanical Machines. *Angew. Chem. Int. Ed.* **46**, 72–191 (2007).

11 Coskun, A., Banaszak, M., Astumian, R. D., Stoddart, J. F. Grzybowski, B. A. Great expectations: can artificial molecular machines deliver on their promise? *Chem. Soc. Rev.* **41**, 19-30 (2012).

12 Rotzler, J., Mayor, M. Molecular daisy chains. *Chem. Soc. Rev.* **42**, 44-62 (2013).

13 Jiménez, M. C., Dietrich-Buchecker, C., Sauvage, J.-P. Towards Synthetic Molecular Muscles: Contraction and Stretching of a Linear Rotaxane Dimer. *Angew. Chem. Int. Ed.* **39**, 3284–3287 (2000).

14 Jimenez-Molero, M. C., Dietrich-Buchecker, C., Sauvage, J.-P. Chemically Induced Contraction and Stretching of a Linear Rotaxane Dimer. *Chem. Eur. J.* **8**, 1456–1466 (2002).

15 Jimenez-Molero, M. C., Dietrich-Buchecker, C., Sauvage, J.-P. Towards artificial muscles at the nanometric level. *Chem. Commun.* 1613–1616 (2003).

16 Collin, J.-P., Dietrich-Buchecker, C., Gaviña, P., Jimenez-Molero, M. C., Sauvage, J.-P. Shuttles and Muscles: Linear Molecular Machines Based on Transition Metals. *Acc. Chem. Res.* **34**, 477–487 (2001).

17 Tsukagoshi, S., Miyawaki, A., Takashima, Y., Yamaguchi, H., Harada, A. Contraction of Supramolecular Double-Threaded Dimer Formed by α-Cyclodextrin with a Long Alkyl Chain. *Org. Lett.* **9**, 1053–1055 (2007).

18 Wu, J., Leung, K. C. F., Benítez, D., Han, J. Y., Cantrill, S. J., Fang, L., Stoddart, J. F. An Acid–Base-Controllable [c2]Daisy Chain. *Angew. Chem. Int. Ed.* **47**, 7470–7474 (2008).

19 Romuald, C., Busseron, E., Coutrot, F. Very Contracted to Extended co-Conformations with or without Oscillations in Two- and Three-Station [c2]Daisy Chains. *J. Org. Chem.* **75**, 6516–6531 (2010).

20 Bruns, C., J. Li, J., Frasconi, M., Schneebeli, S. T., Lehl, J., Rouville, H. P. J., Stupp, S. I., Voth, G. A., Stoddart, J. F. An Electrochemically and Thermally Switchable Donor–Acceptor [c2]Daisy Chain Rotaxane. *Angew. Chem. Int. Ed.* **53**, 1953–1958 (2014).

21 Dawson, R. E., Lincoln, S. F., Easton, C. J. The foundation of a light driven molecular muscle based on stilbene and [small alpha]-cyclodextrin. *Chem. Commun.*, 3980–3982 (2008).

22 Yamauchi, K., Takashima, Y., Hashidzume, A., Yamaguchi, H., Harada, A. Switching between Supramolecular Dimer and Nonthreaded Supramolecular Self-Assembly of Stilbene Amide-α-Cyclodextrin by Photoirradiation. *J. Am. Chem. Soc.* **130**, 5024–5025 (2008).

23 Li, S., Taura, D., Hashidzume, A., Harada, A. Light-Switchable Janus [2]Rotaxanes Based on α-Cyclodextrin Derivatives Bearing Two Recognition Sites Linked with Oligo(ethylene glycol). *Chem. Asian J.* **5**, 2281–2289 (2010).

24 Liu, Y. *et al.* Linear Artificial Molecular Muscles. *J. Am. Chem. Soc.* **127**, 9745-9759 (2005).

25 Fang, L. Hmadeh, M., Wu, J., Olson, M. A., Spruell, J. M., Trabolsi, A., Yang, Y. W., Elhabiri, M., Gray, A. M. A., Stoddart, J. F., Acid−Base Actuation of [c2]Daisy Chains. *J. Am. Chem. Soc.* **131**, 7126–7134 (2009).

26 Hmadeh, M. *et al.* On the thermodynamic and kinetic investigations of a [c2]daisy chain polymer. *J. Mater. Chem.* **20**, 3422–3430 (2010).

27 Du, G., Moulin, E., Jouault, N., Buhler, E., Giuseppone, N. Muscle-like Supramolecular Polymers: Integrated Motion from Thousands of Molecular Machines. *Angew. Chem. Int. Ed.* **51**, 12504–12508 (2012).

28 Bruns, C. J., Stoddart, J. F. Supramolecular polymers: Molecular machines muscle up. *Nat. Nanotechnol.* **8**, 9–10 (2013).

29 Clark, P. G., Day, M. W. Grubbs, R. H. Switching and Extension of a [c2]Daisy-Chain Dimer Polymer. *J. Am. Chem. Soc.* **131**, 13631−13633 (2009).

30 Harada, A., Kobayashi, R., Takashima, Y., Hashidzume, A., Yamaguchi, H. Macroscopic self-assembly through molecular recognition. *Nat. Chem.* **3**, 34–37 (2011).

31 Nakahata, M., Takashima, Y., Yamaguchi, H., Harada, A. Redox-responsive self-healing materials formed from host–guest polymers. *Nat. Commun.* **2**, 511 (2011).

32 Kakuta, T., Takashima, Y., Nakahata, M., Otsubo, M., Yamaguchi, H., Harada, A. Preorganized Hydrogel: Self-Healing Properties of Supramolecular Hydrogels Formed by Polymerization of Host–Guest-Monomers that Contain Cyclodextrins and Hydrophobic Guest Groups. *Adv. Mater.* **25**, 2849–2853 (2013).

33 Takashima, Y., Hatanaka, S., Otsubo, M., Nakahata, M., Kakuta, T., Hashidzume, A., Yamaguchi, H., Harada, A. Expansion–contraction of photoresponsive artificial muscle regulated by host–guest interactions. *Nat. Commun.* **3**, 1270 (2012).

Chapter 4

Dry artificial muscle materials with [c2]daisy chains.

Introduction

The construction of artificial muscle actuators is an important target in medical physics, and materials science. A research topic to realize muscle-like movements in actuators are consuming input energies (electric, thermal, change, photo energies) into demonstrated movements (deformation, transformation, pressure, etc.). There are many attempts to realize actuators using organic, inorganic, electrostrictive, and piezoelectric materials. Stimuli-responsive polymeric materials have attracted attentions due to the active-control of the functional properties and biological compatibility. Hydro- or organogels are very useful materials for stimuli-responsive actuators. The absorption and desorption of solvents as driving principles affect polymeric gels with the contraction and expansion properties. However, the swelled gels have low mechanical strengths and the other reason is slow response speed using gel actuators because the rate determining step of gel actuators is absorption and desorption of solvent from gels.

Previously, stimuli-responsive actuators prepared from acrylic polymer,[1-5] polymer brush,[6] and poly pyrole,[7] etc. Ikeda *et al.* prepared azobenzene-based liquid crystalline films, which exhibit rotating motions under dry state.[8] However, supramolecular actuators consisting of [c2]daisy chains in macroscopic scale is still a challenging subject not only in chemistry but also in materials science especially under dry conditions. In this Chapter, the author realizes a dry polymeric actuators with photo-responsive [c2]daisy chains (Figure 4-1a). In the previous chapter, a symmetric polymer network cross-linked with [c2]daisy chains demonstrated a responsive efficient molecular actuator responsive to UV and Vis light irradiation under wet conditions. The author chooses a four-arm poly(ethylene glycol)

(TetraPEG) cross-linked into a symmetric polymer network (Figure 4-1b). Herein, we prepare a supramolecular xerogel containing of CD-based [c2]daisy chains as cross-linkers. Irradiating with UV light under dry conditions induces a flexion in the supramolecular xerogel. More importantly, the response speed of the [c2]daisy chain xerogel is very fast. Although the hydrogel takes requires 3 hours to bend 7 degrees, whereas the xerogel only required 1 s. The response speed of the xerogel is over more than 10,800 times faster than that of the hydrogel.

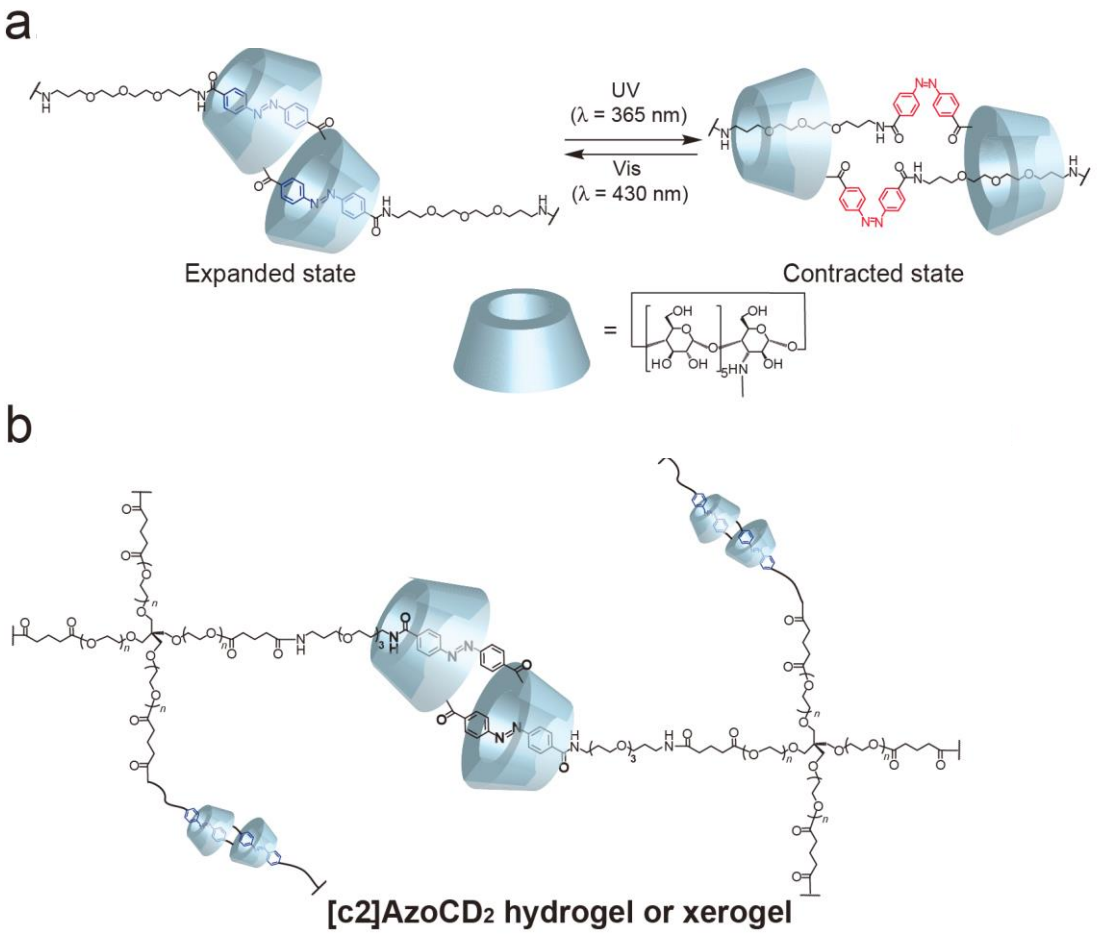

Figure 4-1. **a)** Chemical structure and photo-isomerization scheme of an αCD-based [c2]daisy chain with an azobenzene derivative as the axis. **b)** Chemical structure of a [c2]AzoCD$_2$ xerogel consisting of TetraPEG.

Photo-responsive actuation of the [c2]AzoCD$_2$ xerogel

The [c2]AzoCD$_2$ hydrogel or the Azo hydrogel was slowly frozen on an ice plate. Then, the frozen hydrogels were slowly lyophilized to afford the [c2]AzoCD$_2$ xerogel or the Azo xerogel. To avoid the thermal expansion effect, a 1 W- light-emitting diode (LED) lamp was used to generate UV light (λ = 365 nm). The [c2]AzoCD$_2$ xerogel immediately responded to the UV light irradiation in the dry state and bends toward the light source. Approximately 3.6 s was required to reach a 52 degrees bending angle, which is ca. 30 times faster than that of the [c2]AzoCD$_2$ hydrogel (Figure 4-2). More importantly, the response speed of the [c2]AzoCD$_2$ xerogel is faster than that of the [c2]AzoCD$_2$ hydrogel. Although the [c2]AzoCD$_2$ hydrogel requires ca. 3 hours to bend 7.2 degrees, the [c2]AzoCD$_2$ xerogel requires only 1 s to bend, thus resulting in a response speed that is more than 10,800 times faster than that of the [c2]AzoCD$_2$ hydrogel. Continuous irradiation with Vis light (λ = 430 nm) from the same side of the [c2]AzoCD$_2$ xerogel does not restore the initial form because the hydrophobic interaction (the CD unit / the *trans*-Azo unit) and the swelling pressure fail to function in the dry state. However, irradiation of the opposite side with UV light restores the initial position. The size is reduced by the sequence of right and left UV light irradiation.

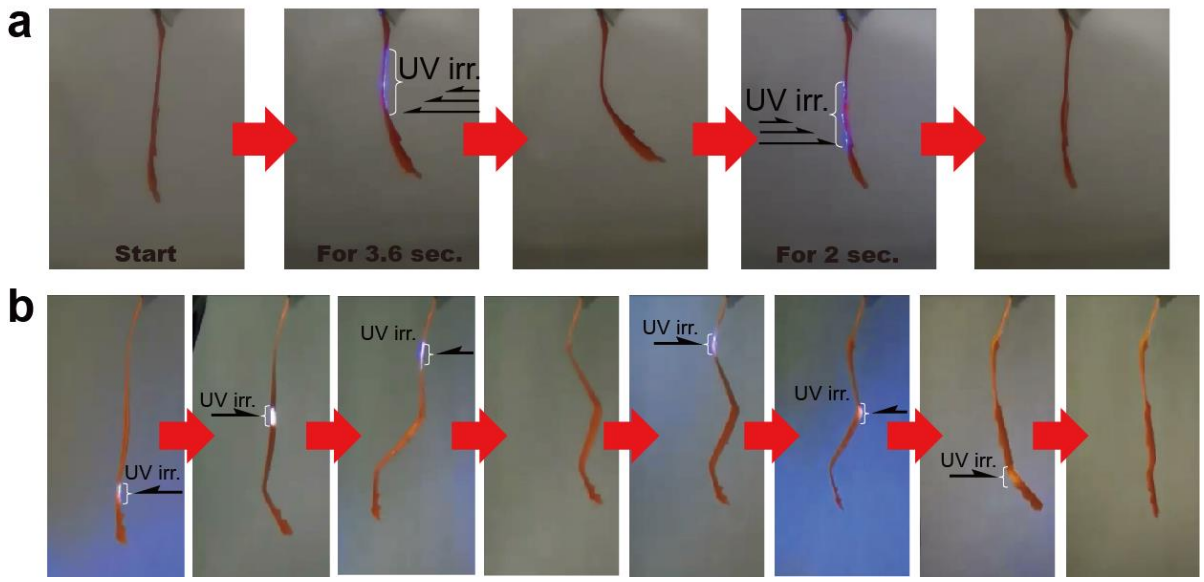

Figure 4-2. Photo-responsive xerogel actuators under dry conditions. **a)** Photographs of the [c2]AzoCD$_2$ xerogel irradiated with UV light from the right side. The [c2]AzoCD$_2$ xerogel bends to the right but continuous UV light irradiation from the left side restores the initial form. **b)** Photographs of the [c2]AzoCD$_2$ xerogel, which was alternately irradiated with UV light from the right and left sides resulting in the formation of a zigzag conformation.

Figures 4-3 and 4-4 show the relation between the flexion angle (θ) of the xerogel irradiated with UV light and the irradiation time. The bending angle immediately increased and does not decay against its own weight. However, the Azo xerogel does not exhibit a photo-responsive properties under dry conditions. The bending mechanism of the [c2]AzoCD$_2$ xerogel involves the sliding motion of [c2]AzoCD$_2$ unit, which shrinks the end-to-end distance of the [c2]daisy chain and reduces the form of xerogel (Figure 4-3). However, Vis light irradiation does not restore the initial form even when the Azo unit isomerizes from the *cis*- to the *trans*-form because swelling and hydrophobic interactions do not occur under dry conditions. The *cis*-Azo exists outside the αCD cavity because the low affinity of cis-Azo and αCD after UV light irradiation. However, after subsequent Vis light irradiation, the CD unit on the PEG unit does not recognize the *trans*-Azo unit due to the weak hydrophobic interaction in the dry state.

To compare the bending speed (V_0) of the [c2]AzoCD$_2$ hydrogel and Azo hydrogel, V_0 was determined based on the results in Figure 4-4. V_0 of the Azo hydrogel (V_0= 1.7×10^{-2} deg s^{-1}) is faster than that of the [c2]AzoCD$_2$ hydrogel (V_0= 1.7×10^{-3} deg s^{-1}). The [c2]AzoCD$_2$ hydrogel and the Azo hydrogel have different contraction–expansion mechanisms.

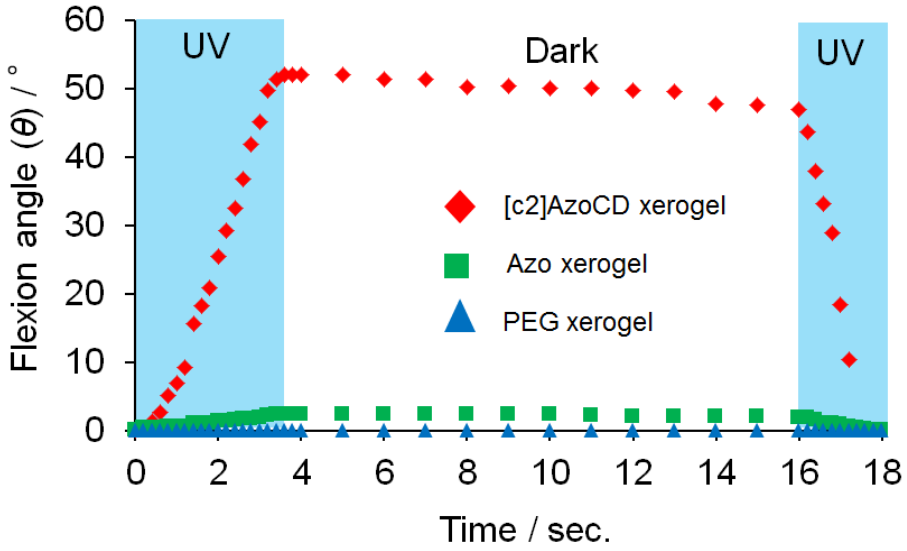

Figure 4-3. Plots of the flexion angle (θ) as a function of the irradiation time of the [c2]AzoCD$_2$ xerogel. The blue areas denote UV irradiation. The white area indicates no irradiation under dry conditions.

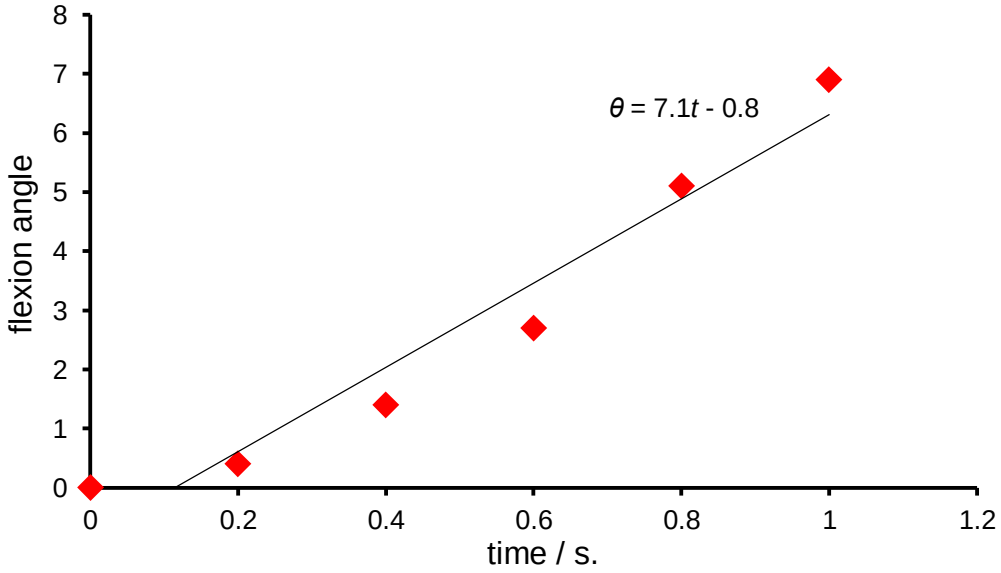

Figure 4-4. Plot of the flexion angle versus irradiation time in the case of the [c2]AzoCD$_2$ xerogel The initial velocity (V_0) was calculated from slope of lines. The initial velocity of [c2]AzoCD$_2$ xerogel was 7.1 (deg s^{-1})

Mechanical properties of the [c2]AzoCD$_2$ xerogel before and after UV light irradiation

Stress–strain measurements were used to evaluate the mechanical property of the [c2]AzoCD$_2$ xerogel in response to photo-stimuli. In general, the Young's modulus is correlated with the cross-link density of materials. Photo-irradiation does not change the rupture stress of the [c2]AzoCD$_2$ xerogel because a number of the covalent cross-link points are not fundamentally influenced by photo-irradiation. However, the rupture strain value of the [c2]AzoCD$_2$ xerogel increased after irradiation with UV light irradiation. Before UV light irradiation, the rupture strain value of the [c2]AzoCD$_2$ xerogel is significantly low (30%) because the αCD unit have no space to slide on the axis molecule. After UV light irradiation, the *cis*-Azo unit dethreads from the cavity of αCD, which increases the sliding mobility of the AmAzoCD unit and leads to an increased rupture strain (1140%) (Figure 4-5a) and a decreased Young's modulus (decreasing cross-link density) because the [c2]daisy chain unit functions as a dynamic interpenetrated cross-linker. However, the rupture stress of the [c2]AzoCD$_2$ xerogel does not change due to the number of covalent cross-link points remaining the same. However, the order of the Young's modulus of the Azo xerogel does not change before or after UV irradiation (Figure 4-5b).

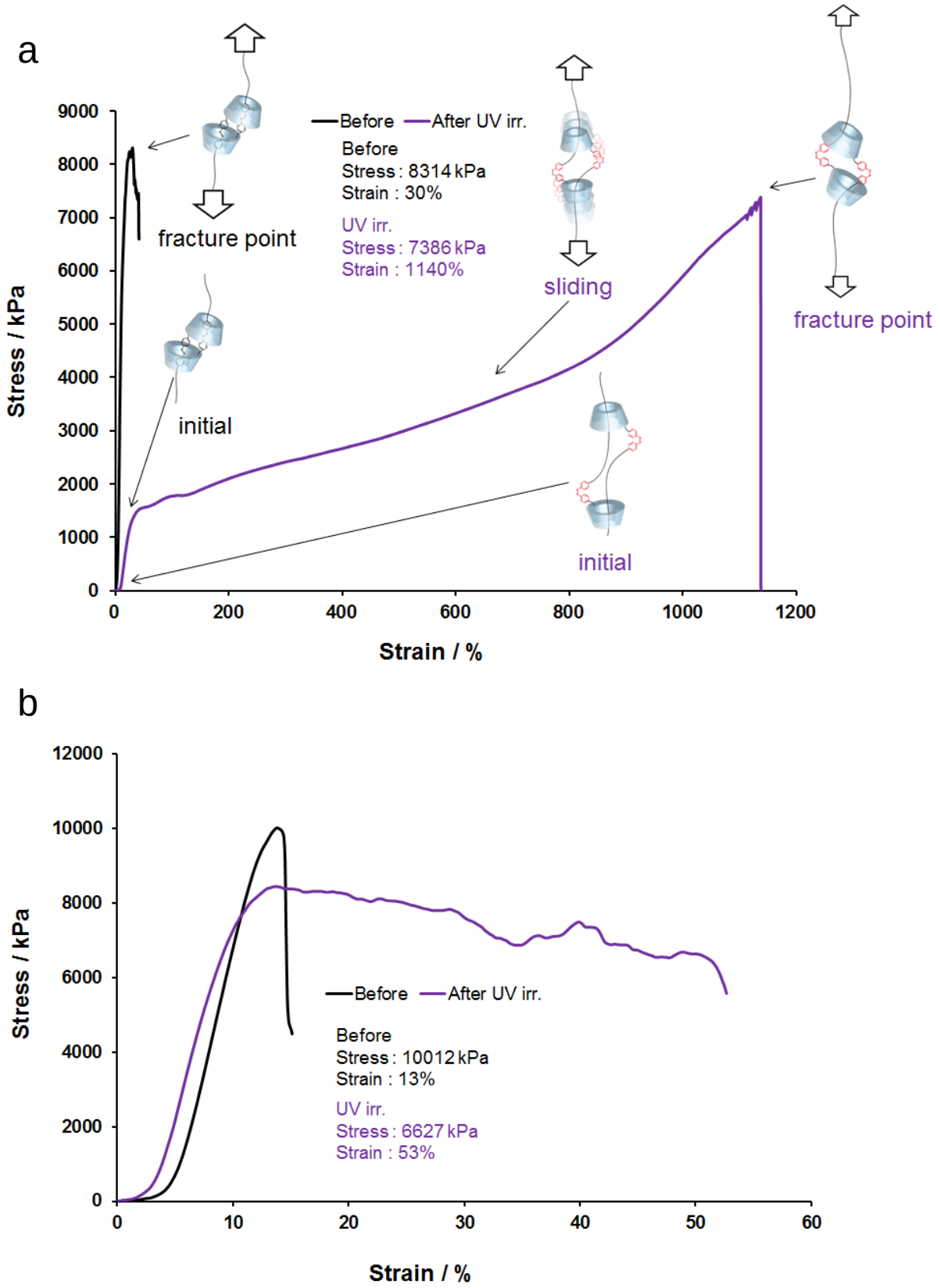

Figure 4-5. Stress–strain curves of the **a)** [c2]AzoCD$_2$ and **b)** Azo xerogel. Before UV irradiation (—) and after UV (λ = 365 nm) irradiation for 20 s.(—).

SEM images of [c2]AzoCD$_2$ and Azo xerogels

Figure 4-6 shows that the SEM image of the [c2]AzoCD$_2$ xerogel show clear fine mesh network before UV light irradiation. After UV irradiation for 10 s, the network structure of [c2]AzoCD$_2$ xerogels disappeared (Figures 4-6 a and b). In contrast, the structure of Azo xerogel did not change (Figures 4-6 c and d). These results indicate that only [c2]AzoCD$_2$ xerogel offer a response to UV light.

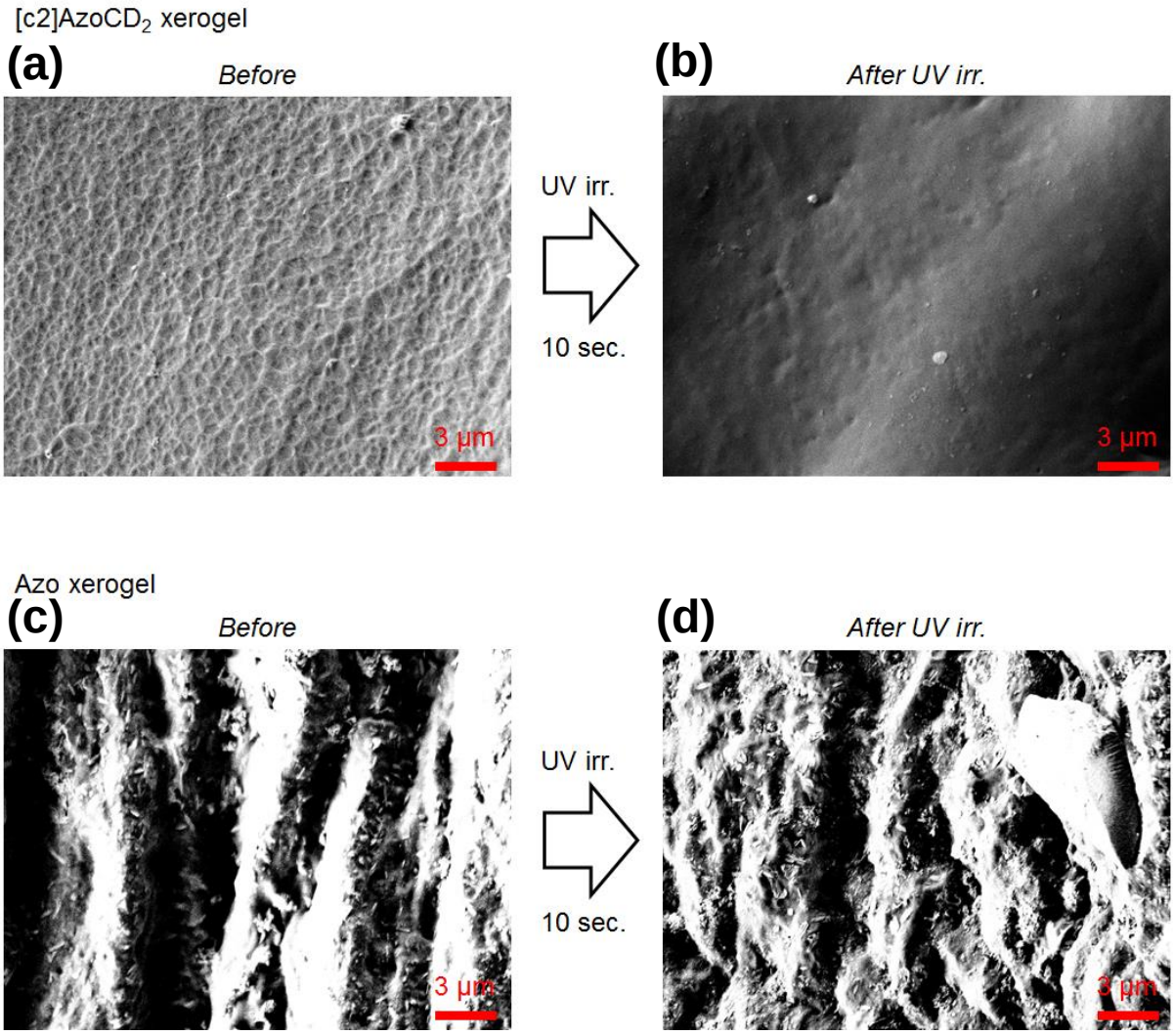

Figure 4-6. SEM images of [c2]AzoCD$_2$ xerogel **a)** before and **b)** after UV irradiation (λ = 365 nm) for 10 s. **c)** and **d)** show the SEM images of the Azo xerogel before and after UV irradiation for 10 s.

Thermal properties of the [c2]AzoCD$_2$ xerogel

The thermal properties of the [c2]AzoCD$_2$ xerogel as well as Azo xerogel by DSC. Melting point (T_m), the T_m and of xerogels were observed. All xerogels were heated from 25 ^oC to 140 ^oC and quenched by liquid nitrogen for -50 ^oC. The cooling ratio is 30 ^oC / min. The glass transition temperature (T_g) was observed by the slow heating (10 ^oC / min.) of cooled xerogel. As a result the T_g and T_m of the [c2]AzoCD$_2$ xerogel were determined to be 6.6 ^oC and T_m was 32.6 ^oC respectively (Figure 4-7a). On the other hand, T_g and T_m of Azo xerogel were determined to be 4.1 ^oC and 43.6 ^oC, respectively (Figure 4-7b). In the both cases, T_m values are significantly higher than the measurement temperature (i.e., room temperature). These results indicate that bending of the [c2]AzoCD$_2$ xerogel is not caused by the melting.

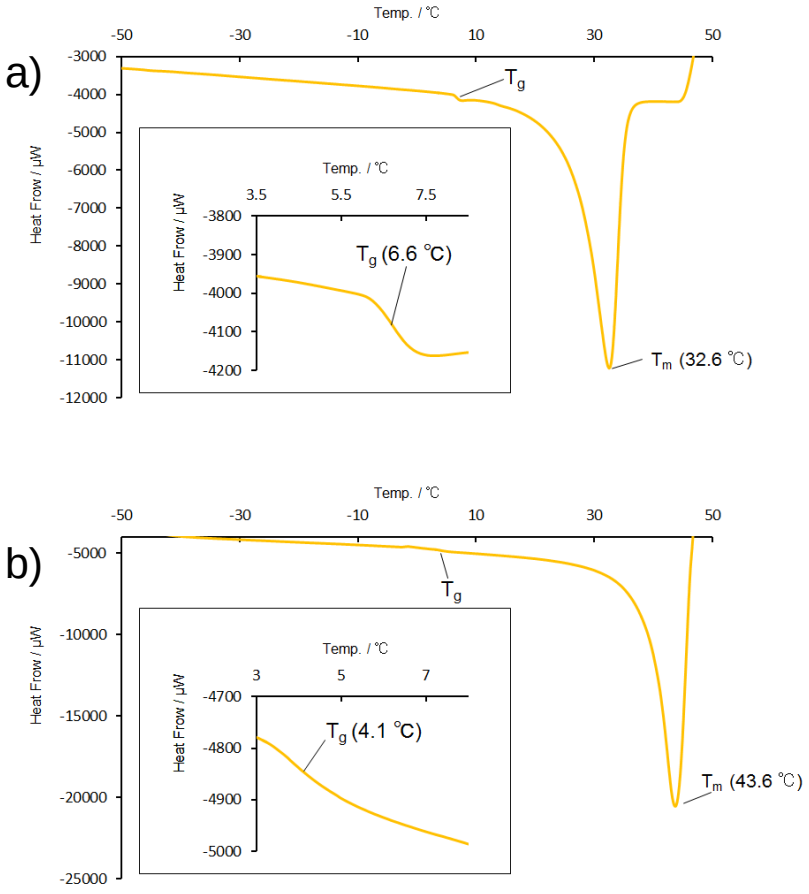

Figure 4-7. T_g and T_m measurements of **a)** the [c2]AzoCD$_2$ and **b)** the Azo xerogel.

Mechanical works of [c2]AzoCD$_2$ xerogel

A weight (37.8 mg) was attached to the bottom of a rectangular xerogel (size: 10×5×1 mm^3). UV light irradiation results in the contraction of the xerogel, lifting the weight (Figure 4-8). Figure 4-9 shows the position of the weight as a function of irradiation time. During UV light irradiation, the weight undergoes mechanical work (W), which is determined by $W = (m\text{-}\rho V)gx$ (m: mass of the weight, g: acceleration of gravity, x: length of the weight that is lifted). The mechanical work of the [c2]AzoCD$_2$ hydrogel and xerogel was estimated to be ca. 0.12 μJ.

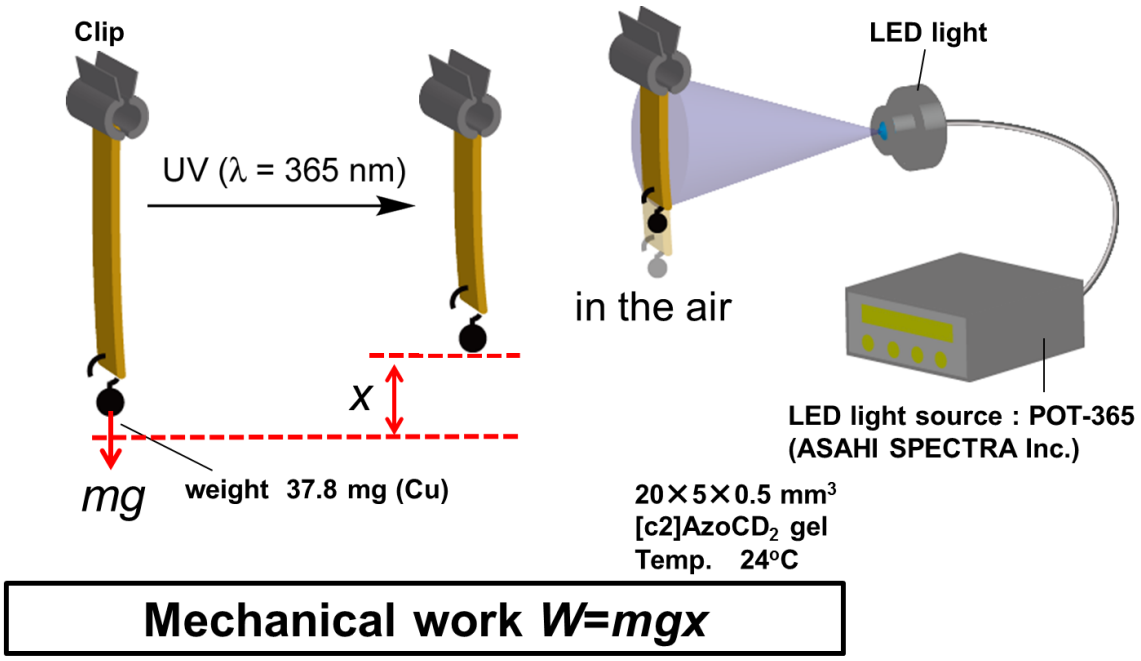

Figure 4-8. Experimental setup of the [c2]AzoCD$_2$ xerogel actuator in response to photo-stimuli. After UV light irradiation, the length of the xerogel shorten and the weight became up. Subsequent Vis light irradiation restored the weight to the original position. Here m, g and x denotes the mass of weight, the gravitational acceleration and the difference in height of the weight, respectively.

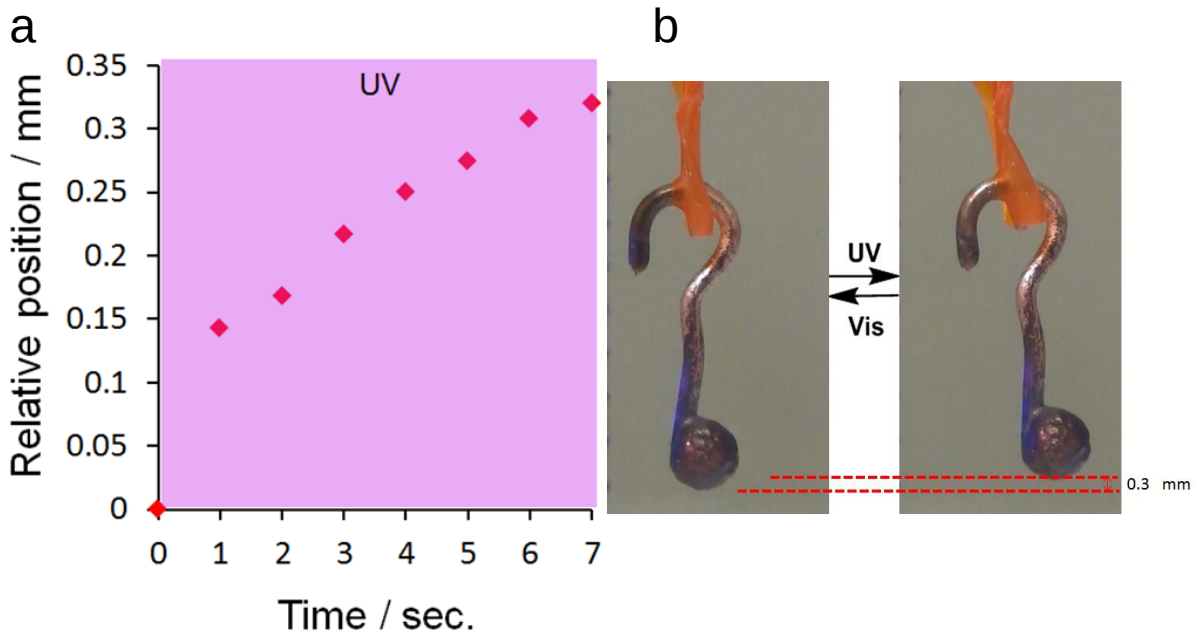

Figure 4-9. **a)** Plot of the relative position of the weight versus irradiation time in the case of the [c2]AzoCD$_2$ xerogel with a weight (37.8 mg). The mechanical work of the [c2]AzoCD$_2$ xerogel was estimated to be ca. 0.12 μJ. The energy density was 12 μW/ cm^2. **b)** Photographs of before UV and after UV irradiated [c2]AzoCD$_2$ gel attached copper weight.

Finally, we conducted a lifting experiment using a match and the [c2]AzoCD$_2$ xerogel. Figure 4-10a shows the setup, which consists of a hand with stimuli-responsive fingers ([c2]AzoCD$_2$ xerogel) and an iron plate. When reaching the hand position, the xerogel was irradiated to grip the match. The hand successfully pinches and lifts up the object, confirming that the fingers of the [c2]AzoCD$_2$ xerogel have sufficient stiffness to provide weight resistance for a match of 107.8 mg (Figure 4-10b).

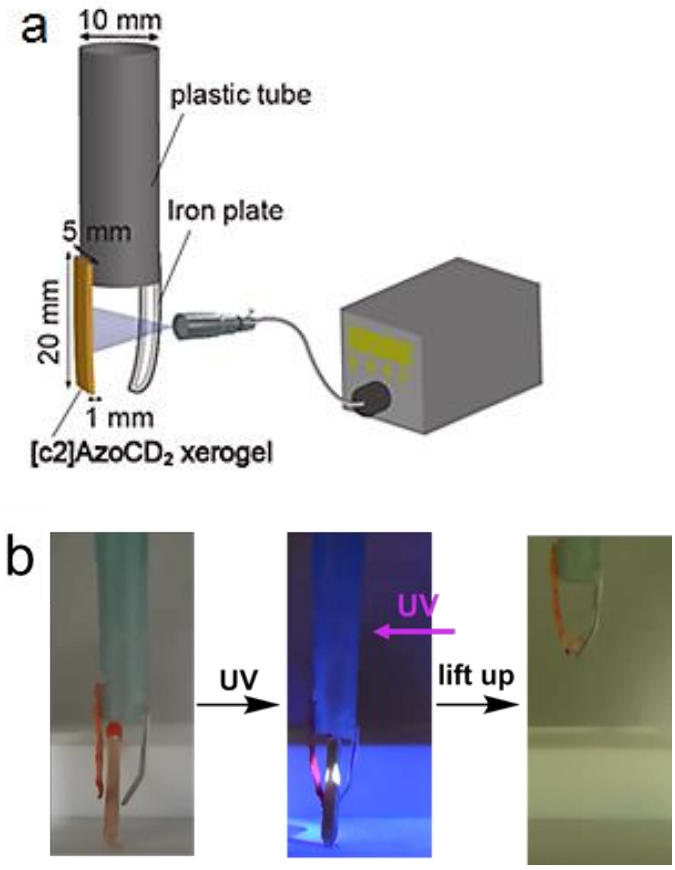

Figure 4-10. **a)** Schematic of the experimental setup. **b)** Photograph of a hand with stimuli-responsive fingers (the [c2]AzoCD$_2$ xerogel) and an iron plate. After UV light irradiation, the clipped object is not dropped.

Experimental

Measurements

Photo-isomerization. The distance between the sample cell and the lamp was fixed at 10 cm. The bending experiment of [c2]AzoCD$_2$ xerogel irradiated with UV light (λ = 365 nm) was carried out by a 1 W LED lamp (Asahi spectra POT365).

Mechanical properties measurements.

Mechanical properties of hydro- and xerogels were measured by a rupture tensing system (Creep meter, RE-33005B, Yamaden Ltd. and Autograph AG-X plus, Shimadzu).

References

1 Yu, Y., Nakano, M., Ikeda, T. Photomechanics: directed bending of a polymer film by light. *Nature* **425**, 145–145 (2003).

2 Ikeda, T., Nakano, M., Yu, Y., Tsutsumi, O., Kanazawa, A. Anisotropic bending and unbending behavior of azobenzene liquid-crystalline gels by light exposure. *Adv. Mater.* **15,** 201–205 (2003).

3 Nakano, M., Yu, Y., Shishido, A., Tsutsumi, O., Kanazawa, A., Shiono, T., Ikeda, T. Photoresponsive behavior of azobenzene liquid-crystalline gels. *Mol. Cryst. Liq. Cryst.* **398,** 1–9 (2003).

4 Ikeda, T. Photomodulation of liquid crystal orientations for photonic applications. *J. Mater. Chem.* **13,** 2037–2057 (2003).

5 Barrett, C. J., Mamiya, J. I., Yager, K. G., Ikeda, T. Photo-mechanical effects in azobenzene-containing soft materials. *Soft Matter*, **3,** 1249–1261 (2007).

6 Yamada, M., Kondo, M., Mamiya, J. I., Yu, Y., Kinoshita, M., Barrett, C. J., Ikeda, T. Photomobile polymer materials: towards light-driven plastic motors. *Angew. Chem. Int. Ed.* **47,** 4986–4988 (2008).

7 Hosono, N., Kajitani, T., Fukushima, T., Ito, K., Sasaki, S., Takata, M., Aida, T. Large-area three-dimensional molecular ordering of a polymer brush by one-step processing. *Science* **330,** 808–811 (2010).

8 Ma, M., Guo, L., Anderson, D. G., Langer, R. Bio-inspired polymer composite actuator and generator driven by water gradients. *Science* **339,** 186–189 (2013).

Chapter 5

Conclusions.

In this study, various stimuli responsive supramolecular materials composed of C_2-symmetric double threaded rotaxanes ([c2]daisy chains) have been prepared utilizing recognition characteristics of host–guest complexes.

In Chapter 2, the author prepared photo-responsive reversible contraction–expansion molecular muscles consisting of αCD and Azo ([c2]DMTAzoCD$_2$). The [c2]DMTAzoCD$_2$ shows the sliding behaviour in water and DMSO. When, the aqueous solution of [c2]DMTAzoCD$_2$ was irradiated by UV (λ=365 nm) light, [c2]DMTAzoCD$_2$ was contracted. Whereas continuous Vis (λ=430 nm) light irradiation, the formation was restored to initial form.

In Chapter 3, the author prepared photo-responsive reversible expansion–contraction hydrogel actuators. The design and motion of the [c2]AzoCD$_2$ gels are reminiscent of a natural muscle fibril system. The author hypothesized that polymer chains cross-linked with [c2]daisy chains would realize a novel supramolecular actuator whose volume contracts upon UV light irradiation but expands upon visible (Vis) light irradiation. This contraction would bend the flat plate actuator toward the incident UV light because UV irradiation causes the shrinkage of the end-to-end distance of the [c2]daisy chain to shrink polymeric materials due to desorption of the solvent on the exposed surface.

In Chapter 4, although the [c2]AzoCD$_2$ hydrogel exhibits a photo-stimuli-induced back and forth motion, photo-responsive actuation in a [c2]AzoCD$_2$ xerogel was thought to been difficult. In this Chapter the author demonstrated that photo-responsive actuation was possible. The author hypothesized that both the structure of TetraPEG and the flexible property of PEG chains play important roles in achieving photo-responsive actuation in the

dry state. Although the [c2]AzoCD$_2$ xerogel does not achieve reversible deformation control and cycling by UV light irradiation, the ability to slide is important for the photo-driven movement of a xerogel on a macroscopic scale in the dry state.

A List of Publication

[Publication related to the thesis]

1. “Fast Response Dry-type Supramolecular Artificial Muscles with [c2]Daisy Chains”

Kazuhisa, Iwaso., Yoshinori, Takashima., Akira, Harada.

Nat. Chem. Accepted.

(Corresponding to Chapter 2–4)

[Publication not related to the thesis]

1. “Preparation of Tris (spiroorthocarbonate) Cyclophanes as Back to Back Ditopic Hosts”

Hiroshi, Danjo., Kazuhisa, Iwaso., Masatoshi, Kawahata., Kazuaki, Ohara., Toshifumi, Miyazawa., Kentaro, Yamaguchi.

Org. Lett. **15,** 2164–2167 (2013).

2. “刺激に応じて形態の変化する超分子ゲルアクチュエータ”

原田 明, 高島 義徳, 中畑 雅樹, 岩曽 一恭, 畠中 省吾.

精密工学会誌, **80(8),** 722 (2014).

3. “シクロデキストリンによるホスト-ゲスト相互作用を用いた自己修復ポリマーの開発”

原田 明, 高島 義徳, 中畑 雅樹, 岩曽 一恭, 畠中 省吾.

月刊ファインケミカル, 12 月号 (2014).